5-2013

ADAPTIVE MODEL BASED COMBUSTION PHASING CONTROL FOR MULTI FUEL SPARK IGNITION ENGINES

Baitao Xiao
Clemson University, bxiao@clemson.edu

ADAPTIVE MODEL BASED COMBUSTION PHASING CONTROL FOR MULTI FUEL SPARK IGNITION ENGINES

A Dissertation
Presented to
the Graduate School of
Clemson University

In Partial Fulfillment
of the Requirements for the degree of
Doctor of Philosophy
Automotive Engineering

---

by
Baitao Xiao
May 2013

Accepted by:
Dr. Robert G. Prucka, Committee Chair
Dr. Beshah Ayalew
Dr. Paul Venhovens
Dr. Zoran Filipi

ABSTRACT

This research describes a physics-based control-oriented feed-forward model, combined with cylinder pressure feedback, to regulate combustion phasing in a spark-ignition engine operating on an unknown mix of fuels. This research may help enable internal combustion engines that are capable of on-the-fly adaptation to a wide range of fuels. These engines could; (1) facilitate a reduction in bio-fuel processing, (2) encourage locally-appropriate bio-fuels to reduce transportation, (3) allow new fuel formulations to enter the market with minimal infrastructure, and (4) enable engine adaptation to pump-to-pump fuel variations. These outcomes will help make bio-fuels cost-competitive with other transportation fuels, lessen dependence on traditional sources of energy, and reduce greenhouse gas emissions from automobiles; all of which are pivotal societal issues.

Spark-ignition engines are equipped with a large number of control actuators to satisfy fuel economy targets and maintain regulated emissions compliance. The increased control flexibility also allows for adaptability to a wide range of fuel compositions, while maintaining efficient operation when input fuel is altered. Ignition timing control is of particular interest because it is the last control parameter prior to the combustion event, and significantly influences engine efficiency and emissions. Although Map-based ignition timing control and calibration routines are state of art, they become cumbersome when the number of control degrees of freedom increases are used in the engine. The increased system complexity motivates the use of model-based methods to minimize

product development time and ensure calibration flexibility when the engine is altered during the design process.

A closed loop model based ignition timing control algorithm is formulated with: 1) a feed forward fuel type sensitive combustion model to predict combustion duration from spark to 50% mass burned; 2) two virtual fuel property observers for octane number and laminar flame speed feedback; 3) an adaptive combustion phasing target model that is able to self-calibrate for wide range of fuel sources input. The proposed closed loop algorithm is experimentally validated in real time on the dynamometer. Satisfactory results are observed and conclusions are made that the closed loop approach is able to regulate combustion phasing for multi fuel adaptive SI engines.

ACKNOWLEDGMENTS

It is impossible to recognize all of the people who have made significant contributions to my research. I would like to acknowledge Dr Robert G. Prucka of Clemson University. His guidance and support throughout my 5 years study for my PhD degree has significantly enhanced my life, both personally and professionally. I am truly thankful that he provided me with the opportunity to continue my engineering education. I would like to thank Dr. Thomas Kurfess, Dr. Zoran Filipi, Dr. Paul Venhovens, Dr. Beshah Ayalew, Frank Webb, David Mann and Gary Mathis for their precious time in helping with my research and dissertation.

Thanks to all my dear friends Marshall Saunders, Emanuele Fadini, David Wafer, Chan Wong, Jen Lackey, Zhizhen He, Shu Wang, Shuonan Xu, Qilun Zhu, Yujie Chen and my entire fellow school-mates at CU-ICAR. They have made my life in the US very enjoyable and unique with their support and encouragement. For my family, especially my grandfather Detao Wang, this dissertation signifies their tremendous mentoring and selfless devotion to every aspect of my life. Finally, I am extremely grateful to my wife Ping Wei for her unconditional support and understanding throughout the entire relationship.

TABLE OF CONTENTS

Page

LIST OF TABLES

LIST OF FIGURES

LIST OF DEFINTIONS

A_{flame} : Flame front area

BVF: Burned volume fraction

BMF: Burned mass fraction

C_1, C_2, C_3, C_4, C_5: Empirical constants for a given fuel, equivalence ratio, and residual gas fraction

L: Instantaneous chamber height

lm : Taylor microscale

L_0 : Chamber height at ignition

$m_{entrained}$: Mass entrained

m_{burned} : Mass burned

MFB : Mass fraction burned

N: Engine speed

p_{comp} : In-cylinder pressure at compression

p_{cyl} : In-cylinder pressure

Pe: Exhaust manifold pressure

$p_{\exp}$: In-cylinder pressure at expansion

Pi: Intake manifold pressure

P_0 : Reference in-cylinder pressure

$r_{c:}$ Compression ratio

S_L : Laminar flame speed

$S_{L,O}$: Laminar flame speed at reference temperature and pressure

TDC: Top dead centre

T_0 : Reference unburned gas temperature

T_u : Unburned gas temperature

$u^{'}$: Turbulent intensity

V_{comp} : Cylinder volume at compression

V_{cyl} : Cylinder volume

$V_{\exp}$: Cylinder volume at expansion

V_{TDC} : Cylinder volume at TDC

$V_{unburned}$: Unburned volume

x_d : Residual gas fraction

γ : Polytropic exponents

γ_{comp} : Polytropic exponents of compression

$\gamma_{\exp}$: Polytropic exponents of expansion

ϕ : Air/fuel ratio

$\rho_{unburned}$: Unburned density

$\rho_{unburned,0}$: Unburned density at ignition

θ : Crank angle

ν: Kinematic viscosity

ξ : constant that equal to 1, assumption made by Tabaczynski, Ferguson and Radhakrishnan (1977)

I INTRODUCTION

I.1 PROBLEM STATEMENT

I.1.1 THE COMBUSTION PHASING CONTROL CHALLENGE

The combustion process is normally described by the percentage of mass burned as a function of crank angle, as shown in the Figure I.4. There are several critical combustion phasing locations that are of interest, but CA50 (the 50% mass burned location in crank angles) is of primary interest combustion phasing analysis and control. CA50 can be understood as the 'center line' of the combustion process. By controlling the spark timing, the combustion event can be phased to a given target.

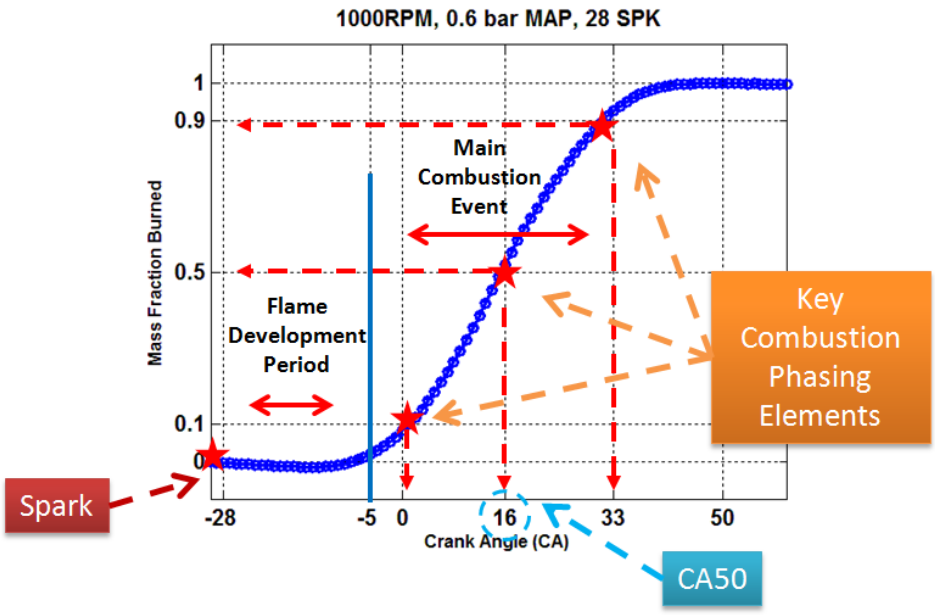

Figure I.1 Combustion phasing control description

Combustion phasing directly influences engine efficiency as shown in the Figure I.2, which is an IMEP vs CA50 plot for a spark sweep under steady state operating conditions. There is one optimum location for CA50 that can generate the highest

efficiency, called maximum brake torque (MBT) timing. It can also be observed that efficiency lost around MBT timing is smaller than when combustion phasing is further away from MBT. This can be used as a cost function or performance requirement for spark timing control. Figure I.2 also shows the natural combustion variation. Each cloud of the data points in one color represents CA50 of 500 consecutive cycles at single spark timing. Large of variation can be observed, and this can limit the performance of spark timing control systems.

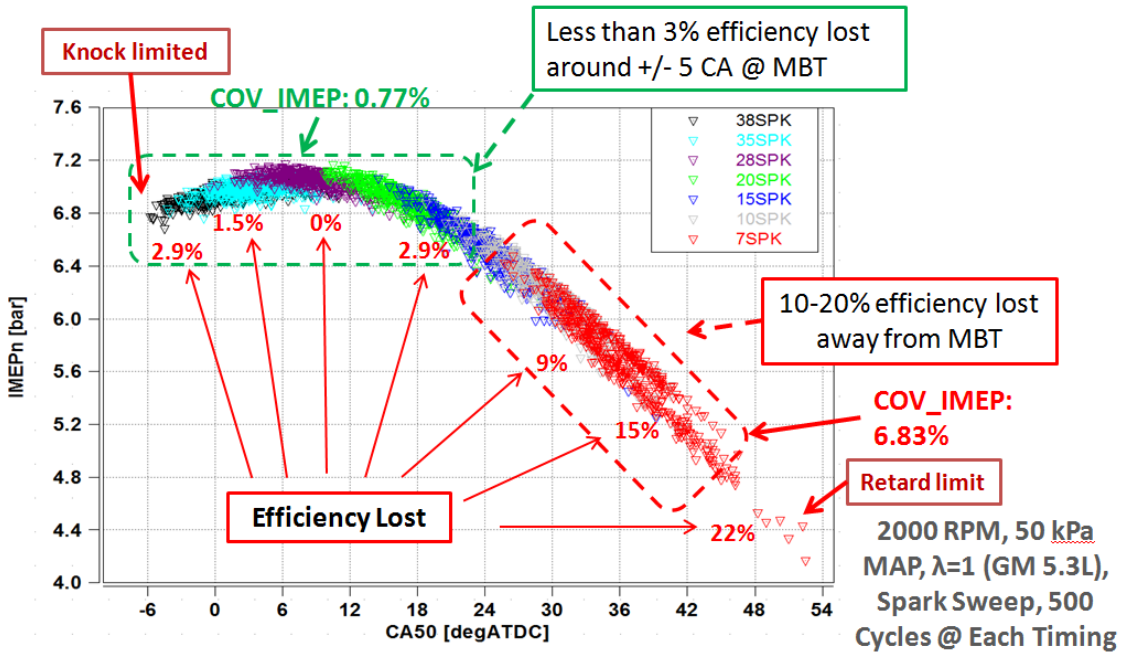

Figure I.2 Combustion phasing control challenge

Figure I.3 shows how different fuel sources may affect the combustion process. Figure I.3 (a) indicates that burn rates are different for gasoline and E85 under similar operating conditions. Figure I.3 (b) illustrates the knock intensity of gasoline and E85 during a spark sweep for similar operating conditions. It is clear from the plot that these

fuels have vastly different knock behavior under certain conditions, and the best achievable CA50 will be limited by the fuel source. An adaptive combustion phasing target algorithm should adapt to both of these differentiating aspects of fuel behavior.

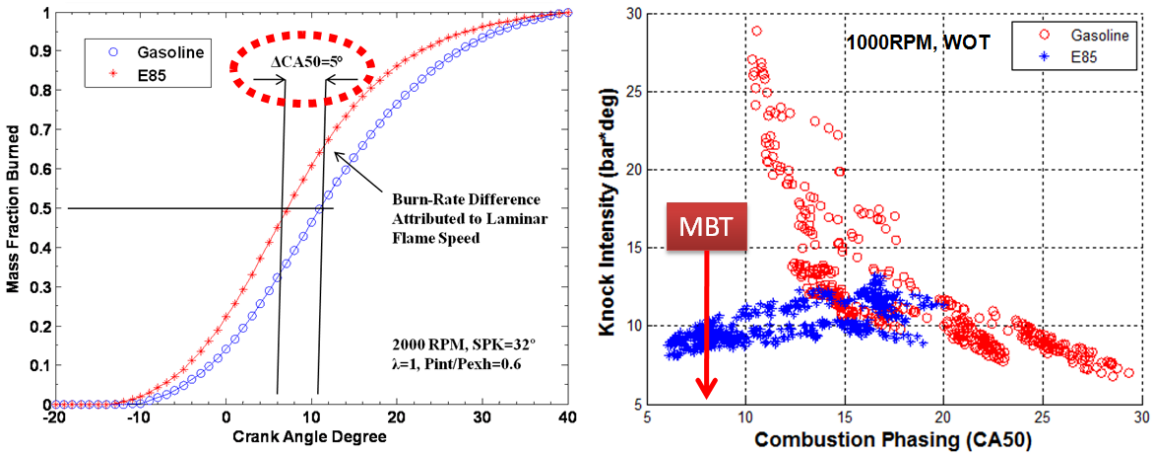

(a) (b)

Figure I.3 Fuel behaviors are different for gasoline and E85

Ignition timing is the last control actuator setting selected at a given operating point because it is a strong function of all other actuator positions. Proper ignition timing is extremely critical for fuel economy and emissions it is important to develop fast prediction models that can be used in conjunction with algorithms developed for the remaining actuators. Figure I.4 shows the relative efficiency, defined as normalized Indicated Mean Effective Pressure (IMEP) value compared to the best available IMEP at Minimum spark advance for Best Torque (MBT), for one engine speed and load (2250 RPM and 0.5 bar MAP). The spark timing to achieve best engine efficiency for gasoline and E85 (85% ethanol blend with 15% gasoline) requires a 9 Crank Angle (CA) degree

difference. If the spark timing were held unchanged for these two fuels, engine efficiency loss at this operating condition would have been 2%. Moreover, this efficiency margin will increase up to 15% under some knock limited operating conditions, because the octane number of the two fuels differs significantly. Having the ability to detect different fuel properties and optimize the control algorithm to maintain the highest engine efficiency is a necessity.

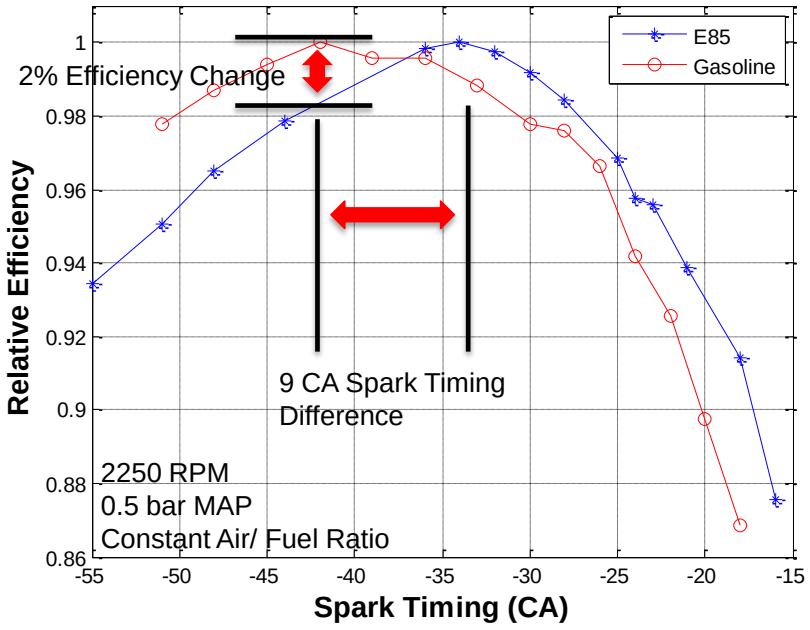

Figure I.4: Engine efficiency decrease if spark timing unchanged with different fuel type input.

I.1.2 MOTIVATION FOR MODEL-BASED CONTROL ALGORITHM RESEARCH

This research hypothesizes that a closed loop model based spark timing control algorithm can be used to regulate combustion phasing in a Spark-Ignition (SI) engine that

is operating on an unknown blend of input fuels. Success of this research will help enable a new generation of internal combustion engines that are capable of on-the-fly adaptation to a wide range of fuels. The introduction of multi-fuel-adaptive engines would; (1) facilitate a reduction in automotive bio-fuel processing prior to vehicle use, (2) allow the use of fuels containing varying levels of water content, (3) encourage locally-appropriate bio-fuel production to reduce fuel transportation, (4) allow new fuel formulations to enter the market with minimal infrastructure impediment, and (5) enable the engine to adapt to pump-to-pump fuel variations and maintain peak fuel efficiency. These outcomes will make the production of bio-fuels cost-competitive with other transportation fuels, lessen dependence on foreign sources of energy, and reduce life-cycle greenhouse gas emissions from automotive transportation; all of which are pivotal societal issues.

There are a number of technical challenges that require research prior to implementation of multi-fuel-adaptive engines. Ultimately, highly flexible engines that contain a large number of control actuators will allow the greatest adaptation to new fuel types. Control actuators that influence fundamental engine operation will be most desirable in such engines. The primary control areas pertain to gas exchange, mixture preparation, in-cylinder charge motion, and combustion, along with compression and expansion ratios. Acceptable fuel properties for SI engines, material selection, fuel systems, and emissions control devices are a few of the other technical aspects of multi-fuel-adaptive engines that must be addressed prior to realization. Control algorithms that can sense and adapt to changing fuel conditions are the focus of the proposed research.

In the current market, the number of control actuators available (cam timings, charge motion control valves, turbo charging, load, etc.) on spark-ignition engines is rapidly increasing to meet demand for improved fuel economy and reduced exhaust emissions. These designs increase operational flexibility, but the added complexity greatly complicates control strategy development because there can be a wide range of potential actuator settings at each engine operating condition. Traditional map-based actuator calibration becomes challenging as the number of control degrees of freedom expand significantly, driving the need for model-based control approaches. Map based control requires minimum computational power; however intensive labor and advanced calibration methods are needed for high degree of freedom engines. Once the maps are generated, the control performance will be very stable and able to meet the expected accuracy when inside the map region.

Figure I.5 shows the ignition timing map for the test engine determined by the conventional full factorial experimental populated method. The test engine was not equipped with extra control actuators (besides engine speed and load) that will require separate calibration for spark timing. Therefore, only around 200 data points are required to populate the entire ignition timing map.

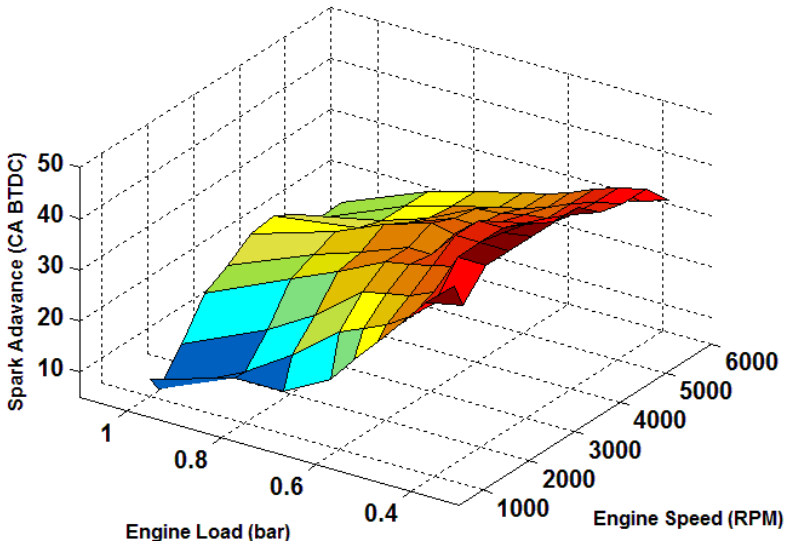

Figure I.5 Conventional full factorial experimental populated maps for the test engine

The calibration time increases exponentially when extra degrees of freedom are introduced. For example, multi-fuel adaptive ability, the possible blends between available fuel sources will result in an ultra high degree of freedom mapping problem. Advanced and fully automated engine testing systems have allowed the automotive industry to successfully adopt model-based calibration and design of experiments (DoE) technology [8][9][10] to reduce the calibration time, as shown in Figure I.6. These methods represent the current 'state-of-the-art' in the industry, and offer a robust final calibration that utilizes a relatively simple control structure (relative to model-based control techniques) within the engine controller.

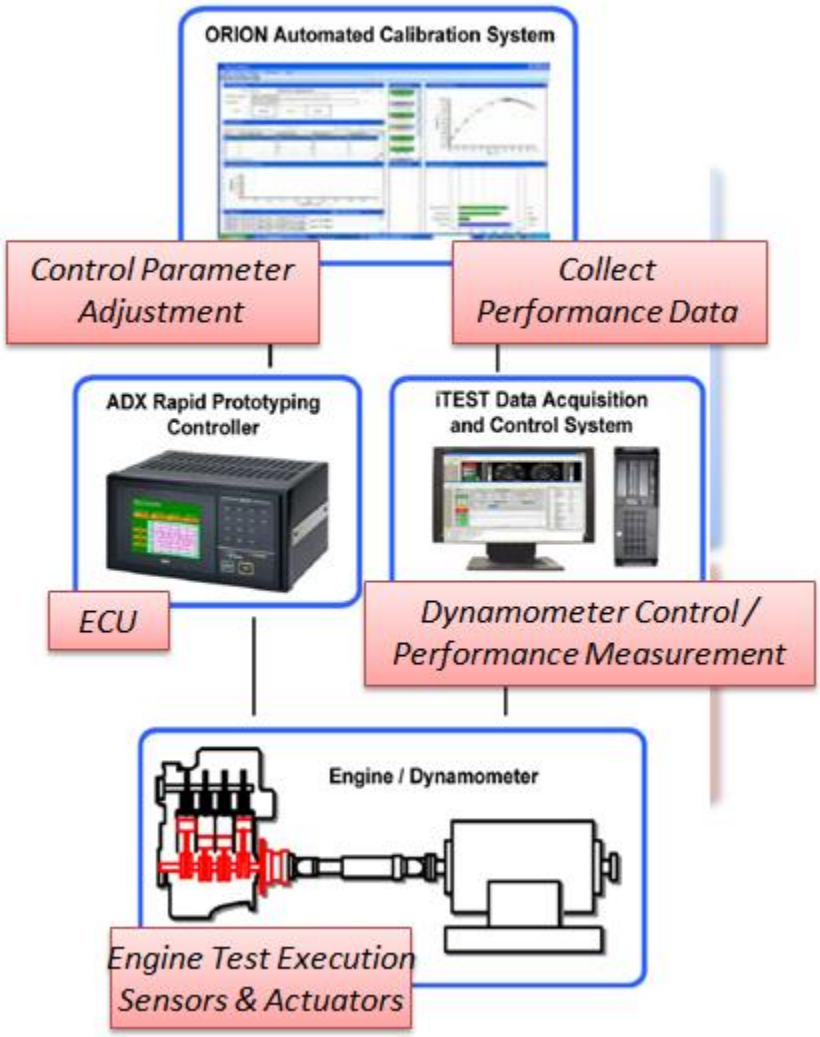

Figure I.6 Model based calibration (Design of experiments) method illustration

In contrast map-based methods, model based control requires an upfront effort of model development that hinges upon the comprehensive knowledge about the underlying phenomenon. Model based controls do require increased computational power for real time actuation and provides higher adaptive ability and predictiveness, therefore enabling novel approaches to high degree of freedom engine controls. Consequently, a tradeoff between model accuracy and computation power requirements is very important.

Selection between factorial populated maps and physical models depends on the application as shown in Figure I.7. It is important to note that actual spark timing prediction accuracy is not as primary factor influencing the use of model-based methods. It is expected that model-based control systems may suffer from slightly lower prediction accuracy than a map-based, but model-based methods offer the potential to significantly simplify the calibration process, and add flexibility to the control system.

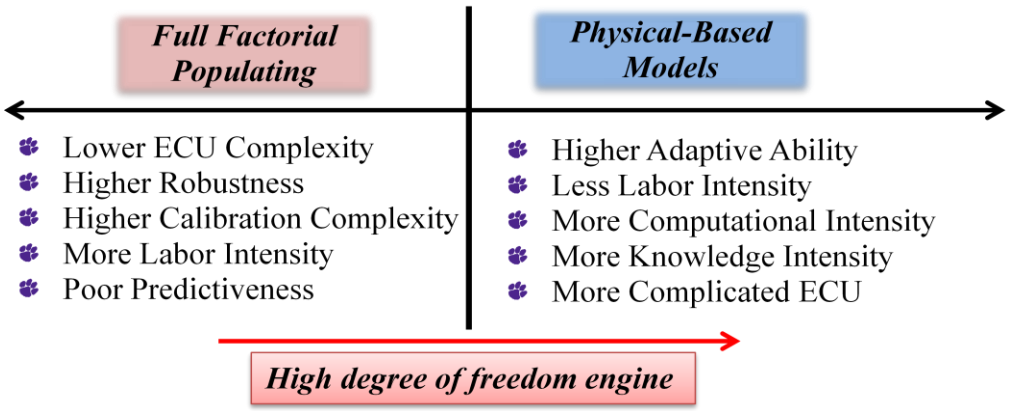

Figure I.7 Comparison between map based control and physical model based control methods

I.1.3 MOTIVATION FOR MULTI-FUEL ADAPTIVE ENGINES

The International Energy Agency (IEA) world energy outlook projects by 2035 there will be nearly a 50% energy gap with current available known fuel sources, meaning a large portion of unknown energy sources will need to be found or developed to sustain usage predictions, as shown in Figure I.8. The United States Energy Policy Act in 2005 [2] and the Energy Independence and Security Act in 2007 [3] mandated significant increases in the production and use of bio-fuels in 2012 and 2020 respectively.

This legislation requires a wide range of bio-fuel development and is spurring renewed interest and development of flexible fuel vehicles.

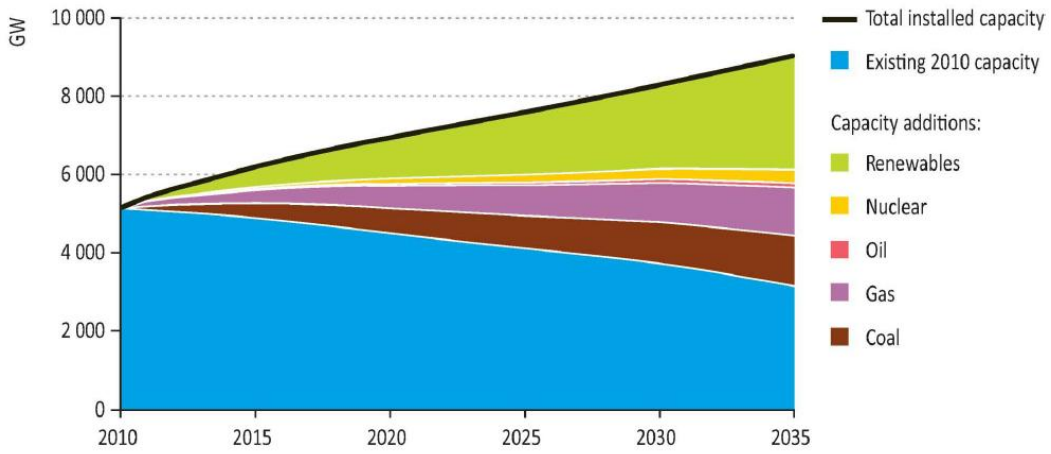

Figure I.8: International Energy Agency (IEA) world energy outlook showing the 50% unknown energy need to be found or developed to sustain humanity development [1].

The U.S. Energy Information Administration (EIA) projects that number of transportation vehicles will continue increasing over next 30 years, as shown in Figure I.9. A large majority of these vehicles will use liquid fuels.

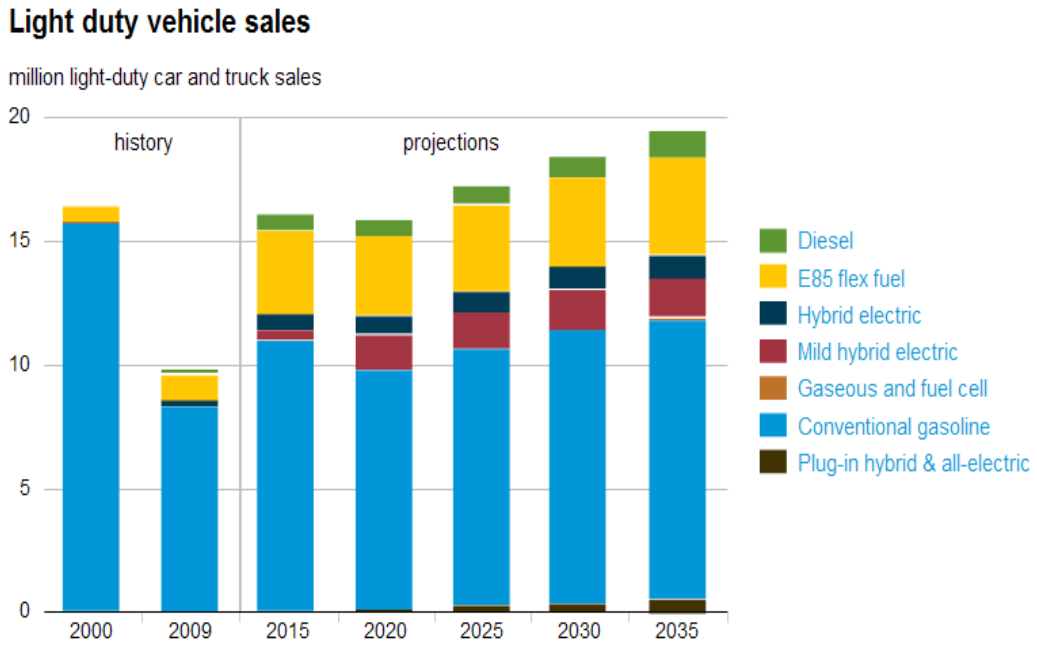

Figure I.9: U.S. Energy Information Administration (EIA) projects vehicle demand for transportation will increase over the next 30 years [2].

Different ways of addressing the energy crisis for transportation have been studied for years [4], as shown in Figure I.10. Non-conventional liquid fuel sources are still considered an important alternative energy over the near future to sustain the vehicles on the road. However, several limitations that constrain the development of this alternative energy are: 1) the vehicle fleet has a significant single-fuel legacy, discouraging the introduction of new fuel types; 2) current processing techniques for production of bio-fuel sources for current engines reduces the 'well-to-wheel' efficiency of the system; 3) fuel feedstocks vary by geographic location; 4) future fuel sources are evolving and unknown; 5) engines are becoming more complex to meet fuel economy and emissions regulations, and are generally designed around a single fuel.

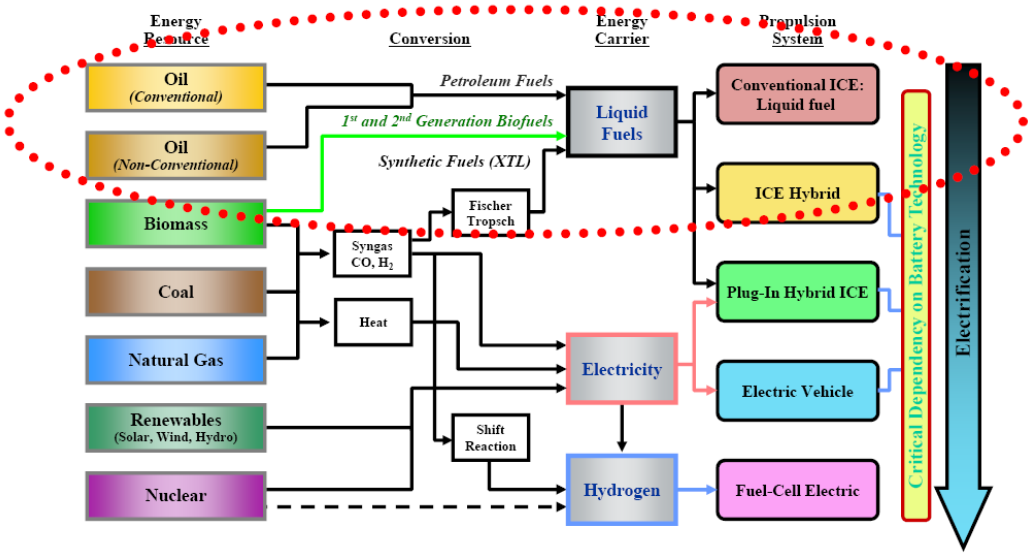

Figure I.10: Energy solutions for transportation [4].

Future engines should not be optimized for only one or two types of known fuels to allow flexibility for the introduction of new fuel to the marketplace. Blends of several fuels in the storage tank over time may result in decreased fuel efficiency if the engine does not have a flexible control structure. Therefore, a control algorithm able to not only optimize the modern high-degree of freedom engine efficiency, but also adapt to a reasonable range of unknown fuel sources is highly desirable. The main goal of this research is to develop such an algorithm.

I.2 RESEARCH BACKGROUND

I.2.1 SI COMBUSTION MODELING

Fuel properties such as stoichiometric air-to-fuel ratio, laminar flame speed, and octane number (among others) influence engine calibration, in particular injection duration and spark timing. Air and fuel mixture preparation processes and the associated physics are better understood [6] than combustion for the purposes of engine control. Feed forward models combined with cost effective oxygen sensor feedback are already used in production engines for flex-fuel (E85 and gasoline) injection control [7]. On the other hand, ignition timing is the last control step that depends on set points for all other engine actuators. The actuator set points translate into in-cylinder physical conditions, such as turbulence intensity, pressure, temperature, and recirculated exhaust gas content of the unburned gases. Since different fuel sources might lead to different burn rates (through laminar flame speed), spark timing requires adjustment for individual fuel sources to achieve optimal fuel efficiency (i.e. MBT timing).

Combustion models are used to represent the mixture reaction rates in the cylinder, predict the formation of emissions, and capture abnormal combustion phenomenon (i.e. knock). Different classes of combustion models have been implemented into engine simulations. They could be categorized as 0D, quasi-D, 1D and 3D combustion models based on their computational power requirements and model predictiveness, as shown in Figure I.11.

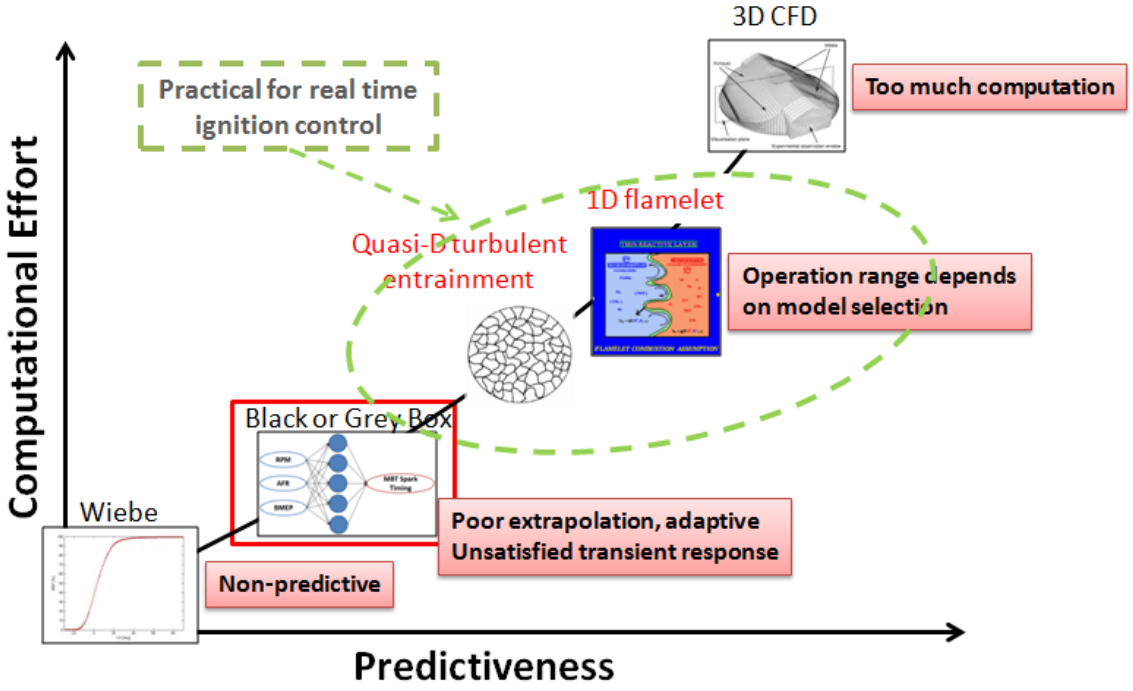

Figure I.11 Combustion models background

The Wiebe function [11][12] can be seen as a 0D combustion model. It uses specific parameters during the combustion process, like start of combustion, burning duration, etc., and experiment based fitting coefficients to set up an equation that represents the mass burn rate during engine combustion process. It is the simplest combustion model and can be implemented into the 0-D engine simulation with time as the only independent variable, but predictiveness is extremely limited due to a semi-empirical nature of the model.. To reduce the need for large set of calibration data, researchers proposed a method to predict parameters in Wiebe function based on the existing correlations of laminar burning velocity. The parameter changes in Wiebe function could be predicted by comparing with the relative change of the estimated laminar burning velocity at spark timing [13]. However, for a Wiebe function, it is totally empirical based combustion model and without physical meaning, so it cannot be used to

predict engine combustion process. Another kind of fully empirical based combustion model is Neural Network (NN) or Black Box based combustion model. NNs are trained on the experiment data to build the relationships between inputs and outputs. The predicted outputs of the NN combustion model could be combustion duration [14][15], emissions [16][17] and etc. The nature of NN to other methods using complex equation fitting do not allow flexibility to make adjustments to a single aspect without completely retraining the model. To improve this situation, semi-physical neural networks or grey box based combustion models have been proposed [18][19]. In these models, physical models and neural networks (or black box) are combined to try to increase the adaptive ability of the combustion models.

For the quasi-dimensional combustion model, the well-known approach to SI combustion is the turbulent flame entrainment combustion model, which is firstly proposed by Keck [10][20].This model subsequently assumes that fresh gas eddies are entrained in a spherical flame front and burn in a characteristic time [21]-[24]. During the turbulent entrainment process, the mass entrainment rate is affected by unburned gas density, flame front area, turbulence intensity and laminar flame speed. The burn-up rate within the reaction zone is influenced by entrained and burned gas mass, Taylor micro-scale and laminar flame speed. This quasi-dimensional combustion model incorporates mixture flow parameters and geometric aspects of the flame front interaction with the combustion chamber within the 0-D framework. It aims to fulfill the real-time calculation and the accuracy and adaptive ability of the model depends on the sub-models.

In [25], a simplified turbulence model for the prediction of the in-cylinder turbulence parameter during combustion for SI engines is proposed. It simplified from the K-ϵ model, ignores the squish and swirl influence, and assumes that the turbulence is in equilibrium. This sub-model is easy to code in thermodynamic models. For the stratified SI engine combustion modeling, a new quasi-dimensional calculation is developed [26]. It is based on the two-zone entrainment model. However, due to the insufficient of two-zone treatment to describe the inhomogeneous air/fuel composition, the four unburned zones are defined. There are a rich zone, a stoichiometric zone, a lean zone and a remaining air zone. Similar to the existing method, a burned zone is defined and these zones are connected to each other by the mixture model calculated mass flow rates. The mixture model puts the current geometry of the zones into consideration and the flame propagation was developed to fulfill the stratified combustion process. In [27], to predict the mass burning rates, a quasi-dimensional combustion model is proposed, which is based on flame stretch concepts and turbulent entrainment theory. The flame stretch sub-model assesses the flame response to combined effects of curvature, non-unity Lewis number mixture and turbulent strain. This model can simulate the development of early flame, flame propagation and flame termination periods. It neglects the spark ignition processes and does not consider flame kernel formation. In order to better capture the detailed flame front shape, a 1D coherent flame model (CFM) combustion model is proposed [28]. This is a 1D physical combustion model for gasoline engine transient application used to replace the traditional empirical models. This CFM-1D model is simplified from the 3D extended coherent flame model (ECFM) for gasoline combustion [29]. For this model, there are two zones in the combustion chamber: burned

and unburned zones. Two zones are separated by a premixed turbulent flame modeled by using a 1D adaptation of the 3D flame surface density method. The chemical reactions of fuel oxidation happen in a very thin layer which is called the flamelet. For the simplification of the 1D CFM model from 3D model, there are some assumptions: mixture is homogenous, mixture is perfect gases (fresh air, fuel vapor and burned gases), stoichiometric combustion, no dependency on different variables space and the cylindrical combustion chamber.

Some three-dimensional combustion modeling examples are shown below. In [27][37], an improved DPIK model and G-equation combustion model are proposed. The flame kernel position is tracked by particles and the turbulent flow effects on the turbulent flame during velocity are concerned. The G-equation combustion model was modified and implemented into KIVA-3V. Using the G-equations (level set method) can track the propagation of the mean turbulent flame. To model the chemical reaction within the cells which contains the mean turbulent flame, the flame surface density and the turbulent burning velocity are considered. The detailed turbulent flame brush is ignored and species in cells in the burnt gas behind the mean flame front location are assumed to be chemical equilibrium. In order to reducing the computing time, the fine numerical resolution is not needed and the narrow band concept of Chopp [38] was applied. In [39], a universal engine combustion model called the GAMUT (G-equation for All Mixtures. A Universal Turbulent) is developed here. The methodology can be applied to partially premixed, premixed and non-premixed combustion regimes. The level set method (G-equation) is a very powerful numerical technology which can be applied to analyze and

compute interface motions. The application examples are the crystal growth calculation, shape recovery, two-phase flow, image processing and combustion [40]. In 1985, Williams introduced the method to describe the flame propagation for a premixed air-fuel mixture. In this model, G-equations are used to track the premixed turbulent flame propagation (e. g., for premixed and partially premixed combustion). The diffusion combustion that happens behind the premixed flame branched was modeled with a modified characteristic time scale model. When combined with the Shell auto-ignition model, this model can be used to simulate premixed and diffusion combustion processes in diesel combustion. A new three-zone combustion model was developed to provide better correspondence of the numerical calculated results to the experimental data in a wide range of operation parameters for engines with different geometry [41]. The additional third zone is used to simulate the processes in the flame kernel volume inside the spark plug gap. It captures detailed mechanism of chemical and thermal ionization chemical interaction, heat transfer between electrodes and combustion products and the mass exchange between in-cylinder combustion products and third zone. This three-zone model looks more adequate to simulate the real process of SI engine combustion. Chemical kinetics method to the simulation of combustion and behavior of combustion products in all zones gives a chance to carefully analyze the ionization process and confirm the two peaks of ion current.

Among all the available SI combustion modeling options, quasi-dimensional turbulent flame entrainment model and 1D CFM are agreed to be most practical models for real time control purposes. They do not require intensive computing time but still able

to capture most of the physical fundamentals of SI combustion, as shown in Figure I.12. Fidelity and computational power requirements can be balanced based on the specific applications. Framework of this research will base on the quasi-dimensional turbulent flame entrainment model.

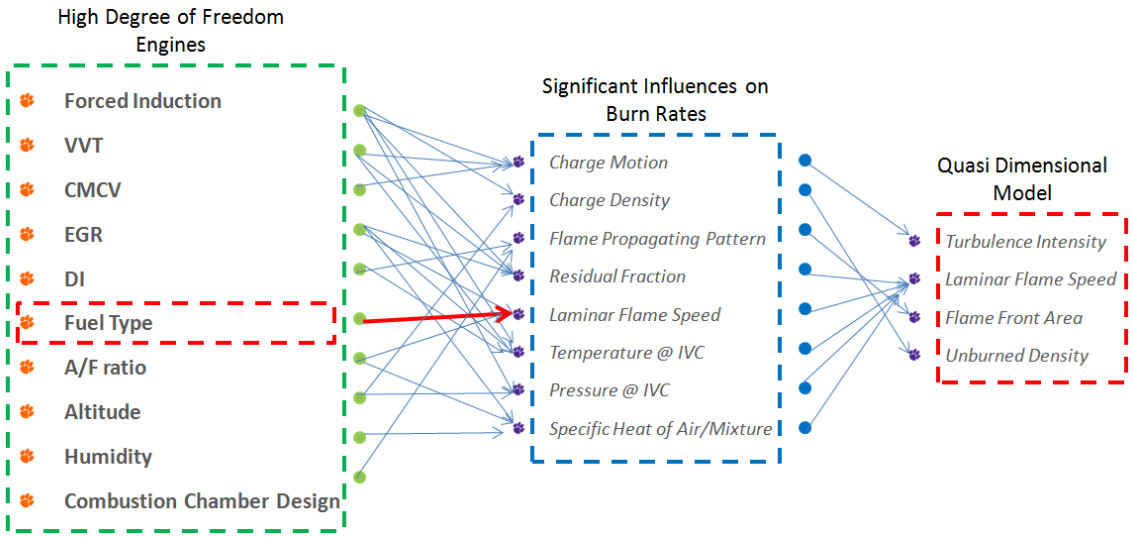

Figure I.12 Quasi dimensional turbulent flame entrainment model is able to capture most of the physical fundamentals of SI combustion process

I.2.2 ARTIFICIAL NEURAL NETWORK BACKGROUND

Fidelity of physical combustion models strongly depends on sub input model development. There are several input models found to be problematic which will be explained in Chapter 3. Moreover, physical combustion models are generally crank angle resolution equations which contain more than necessary information for spark timing control. Therefore an approach that utilize a neural network to eliminate the problematic input models and covert the discrete time domain combustion model to mean value model will be implemented, as shown in Figure I.13.

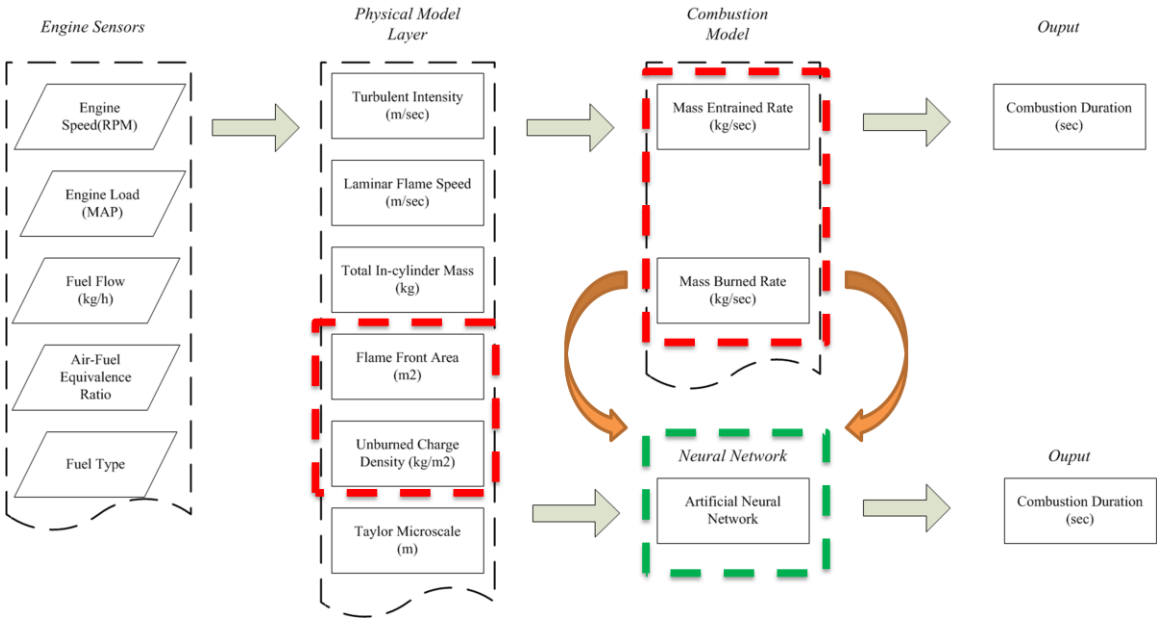

Figure I.13 A semi physical neural network is used to eliminate problematic sub input models and convert combustion model to a mean value model

Artificial Neural network (ANN) approach is based on the biological neural network to model the interconnection of the neuron in the nervous systems of the human brain and other organisms. ANN as a non-linear processing system can be applied to a wide range of areas, especially where the algorithms are too complex or unclear. However, a suitable manner for the organization of the processing units to accomplish a given pattern recognition task is critical for artificial neural network to be useful. Artificial neural network are organized into processing units layers where the connections can be interlayer or intralayer or both. Feedforward and feedback manners could be used to organize the connections across the layers and among the units within a layer. The basic structures of artificial neural networks includes: instar and outstar, which have fan-in and fan-out geometries respectively [52]; group of instars/outstars, which is a heteroassociation network; bidirectional associative memory, where either of the layers

can be used as input/output; autoassociative memory, where each unit is connected to both itself and every other unit.

In 1943, Warren McCulloch and Walter Pitts brought out McCulloch-Pitts neuron, a model of computing element, which performs the inputs' weighted sum to the element followed by a threshold logic operation [42]. However, the weights for this model of computing are fixed and hence the model could not learn from examples. In 1949, Donald Hebb proposed a learning scheme which based on pre- and post-synaptic values of the variables to adjust a connection weight [43]. In neural network literature, Hebb's law has been seen as a fundamental learning rule. Marvin Minsky developed a learning machine in 1954 and it could automatically adapt the connection strengths [44]. In 1958, Rosenblatt proposed the perceptron model which applies perceptron learning law to adjust weights [45]. The learning law was converged for linearly separable pattern classification problem. A multilayer perceptron, other than a single layer of perceptrons, could be used to perform any pattern classification. But the lack of systematic learning algorithm to adjust the weights made the classification task difficult to realize. In 1969, Minsky and Papert used several illustrative examples to show the limitation of the perceptron model [46]. Until 1984, the development of neural network models for pattern recognition tasks had been severely hampered due to the lack of suitable learning law for a multilayer perceptron network for 15 years. In 1960s, Widrow and Hoff tried to adjust the weights of an Adaline model for a eomputing element by an LMS learning algorithm [47]. The convergence of the LMS algorithm was proven to be successful applied for adaptive signal processing situations. In early 1980s, two key developments brought back

the interest in artificial neural networks. They are energy analysis of feedback neural networks by John Hopfield [48][49] and the generalized delta rule (or error back-propagation learning law) which applies a systematic way to adjust the weights of a multilayer feedforward neural network [50]. About the same time, Ackley, Hinton and Sejnowski brought out a feedback neural network called Boltzmann machine which has stochastic neuron units [51]. Boltzmann machine has additional hidden units to make a given pattern storage problem representable in a feedback network.

Neuronal dynamics governs a neural network's operation. Normally, the neuronal dynamics consists of two parts: they are corresponding to dynamics of the activation state and dynamics of the synaptic weights, respectively. Learning laws are implementation models of synaptic dynamics. The basic learning laws are: Hebb's law, where the product of input data and the unit output signal have the proportional weight increment. This law has a representation of an unsupervised learning. Perceptron learning law, as a supervised law, it requires a desired output for each input. Delta learning law, it could be seen as a continuous perceptron law and can be generalized to the case of a feedforward network multilayers. For Wldrow and Hoff LMS learning law, also called the Least Mean Squared error learning law, the convergence of the weights for a given set of training data could be achieved by applying input-output pattern pairs data several times. Correlation learning law, which is a special case of the Hebbian learning law, it is a supervised learning. Instar (Winner-take-all) learning law, it is a case of unsupervised learning. Outstar learning, however is a supervised learning law, used with a network of instars to capture the characteristics of the input and output patterns for data compression.

There are two difference situations for the applications: one is where the known neural networks models and concepts could be used directly and the other is potential to use the neural networks ideas but still unclear how to evolve a suitable neural network architecture. For the direct application, there are: (1) pattern classification, which is the most direct among all neural networks applications. One example is the recognition of Olympic Games symbols [52]. (2) Associative memories, which is used to store a pattern or data for later recall or to store association between two patterns, has example applications like image pattern recall [53][54], content addressable memory [55], information retrieval [56][57][58]. (3) Optimization is one of the most successful applications of neural network [59]-[62]. There are examples such as Graph bipartition problem [63], Linear programming problem and Travelling salesman problem [64]. (4) Vector quantization: achieving a significant compression in the data representation by encoding a large sent of training data vectors into a small set of representative points [65][66]. (5) Control applications, includes robotic, process control, aerospace, industrial manufacturing and automotive engineering [67][68]. The main task of the neural networks in control is the generation of an appropriate input signal to the physical process (called plant) to get the desired feedback from the plant [69][70]. There are two types of plant control: open-loop control and close-loop feedback control. The controller includes cascade of a system and the inverse of the plant in an open-loop control system. The system aims to achieve a desired response for the input. This means the controller will generate a control signal to the actuators to get the desired response output. In the process, the plant's inverse transfer function is needed and the characteristic of the plant should not change during the process. Multilayer feedforward networks have the ability

to capture characteristics of the plant transfer function and the plant's inverse transfer function. Then, the controller could be designed by using the neural network [71][72].

From 1980s, Ford Motor Company, as one of the pioneers, started the research and development of Neural networks in automotive engineering [73][74]. The growth of the emphasis on model based development helps to push mature elements of neural network into the mainstream. Although neural network can be used for both on-board and outside of the vehicle applications, the available computational ability limits the on-board application. Three main roles of neural network in automotive engineering are discussed below. They are models, virtual sensors and controllers. The neural networks have broad applications in modeling, like vehicle dynamics modeling [75][76][77], driver behavior [78][79][80], engine combustion [81][18] [82], emissions [83][84], hybrid vehicle energy storage system [16] and so on. Virtual sensors are often ' Black Box ' like neural network. They are especially suitable for the situation that the physical is complex or uncertain while there are plenty of data. Virtual sensors could be an air-fuel ratio estimator [86][87], an emission calculator [88][89] or an air flow mass/rate estimator [90][91]. Neural network used as controller has been known for a long time [92]-[96]. In the automotive applications, there are examples such as vehicle electric actuators and system controller [97][98][99], engine operation controller [100][101][102] and vehicle handling controller [103][104].

I.2.3 ENGINE SYSTEM CONTROL FRAMEWORK

Feed forward model-based control requires a target combustion phasing for proper calibration that is generally based on the crank angle location where fifty percent of the air/fuel mixture is burned (CA50). The best CA50 location (MBT timing) will phase the combustion to a best efficiency range that is a balance between early combustion (heat transfer loss) and late combustion (expansion loss). For control strategies with variable octane fuels, the best CA50 location may be limited by abnormal combustion (or knock), as shown in Figure **I.14**.

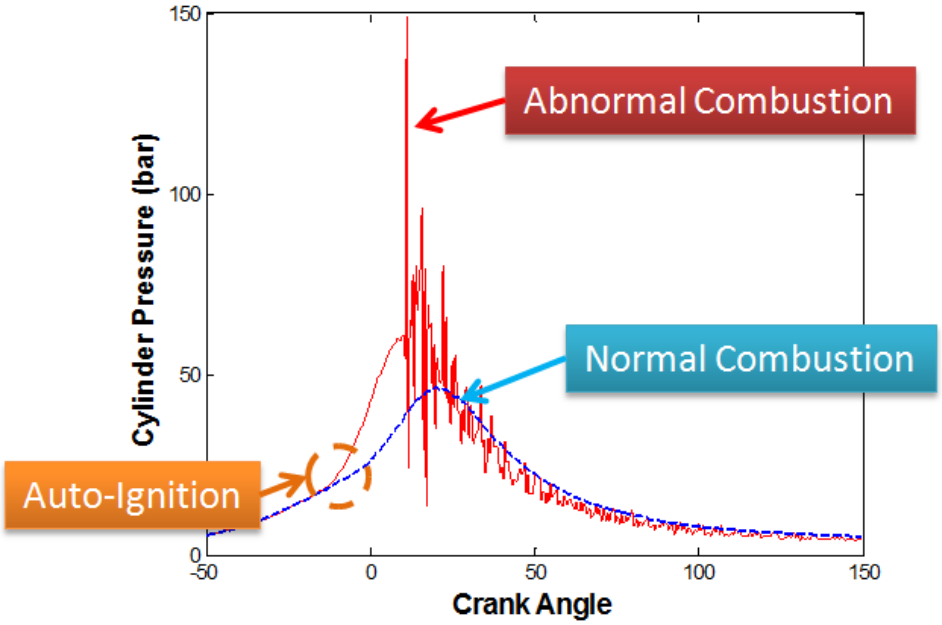

Figure I.14 SI engine knock phenomenon

Based on compression ratio or boost level, the desired combustion phasing will be determined by the calibrator for a particular engine with a known fuel source input. However, when fuel type is altered engine will be subjected to different characteristics of

knock and then require an update for the desired CA50 in the 'knock region' to avoid mechanical damaged or maintain high thermal efficiency.

Traditionally, knock feedback control utilizes a structure-mounted accelerometer as an observer [105], spark plug ionization signal [106], or in-cylinder pressure sensor [107]. The sensor will accumulate several knock events and constantly adjust spark advance using an adaptive map until knock is eliminated. The spark timing delivered to the engine is the sum of the base ignition map, spark advance adjustment and the adaptive map. Drawbacks of such feedback approach are: 1) The engine will experience large amount of knock events until the adaptive map has been created; 2) The learning process is relatively slow because the algorithm requires input from all the possible operating conditions (speed/load points). In an example given by the Kiencke [105], the adaptation map required 50km of vehicle operation for 50:50 blending of 87 and 93 octane fuel sources.

To speed up this process a feed-forward knock prediction algorithm is desired in the multi-fuel adaptive engines because of the possible wide range of fuel source inputs. Spark knock is the consequence of auto-ignition in the unburned end-gas ahead of the propagating spark ignited flame front. The auto-ignition characteristic therefore is greatly related to the octane rating of the fuel source and governed by kinetics chemical reactions under the time history of temperature and pressure of the unburned end gas. Auto-ignition models [108]-[111] are available with a wide variety of fidelity options. Two other fuel properties are also of particular interest to knock control; 1) laminar flame speed that describes the potential mass burn rate which can reduce the time scale of the end-gas

exposure prior to combustion, and 2) fuel heat of vaporization which alters charge cooling effects and unburned mixture temperatures.

Existing flex-fuel engines have known boundaries of their input fuels (0% to 85% ethanol) so it is possible calibrate the engine prior to production with all possible blend ratios. Fuel type/blend detection is a critical aspect of multi-fuel engines so that calibration can be adjusted to optimize fuel efficiency at all times. Fuel blend ratio can be detected directly by measuring known chemical differences between liquid-phase gasoline and ethanol [112]. Less expensive 'sensorless' strategies have also been employed by inferring blend ratio from existing exhaust oxygen sensors and fuel injection parameters [113],[114]. Sensorless methods exploit differences in stoichiometric air-to-fuel ratios between fuels of different and known chemical compositions (i.e. carbon/hydrogen and carbon/oxygen ratios). Cylinder pressure during compression has also been successfully used to determine blend ratios of gasoline and ethanol [115]. All of these fuel type sensing routines are based on known fuels, so their boundary conditions are well defined. Ultimately, fuel behavior, not type, within the engine is the most important aspect influencing calibration and control of multi-fuel-adaptive engines because it is assumed that future fuel compositions are not known at the time of initial calibration. A task within the proposed research is to develop a fuel 'behavior' sensing routine based on cylinder pressure.

Combustion phasing feedback have been studied for closed loop ignition control by linking various modeling approaches with either engine speed, torque [116][117], cylinder pressure [118][119][120], or ionization detectors [121]-[127]. While these

methods are well-suited for use on high degree of freedom engines they have seen somewhat limited use in production because of low accuracy, poor durability, and high cost. Additionally, most control strategies based around these concepts do not properly account for the difference between normal cycle-to-cycle variability and actual combustion phasing differences that need to be corrected. Large sample sets are required to have high confidence in decision making, limiting use in a highly transient engine. The proposed task of this research is to use cylinder pressure feedback combined with statistical data analysis to update fuel properties with small data sets.

I.3 RESEARCH OBJECTIVES

A model based ignition control algorithm for multi-fuel adaptive engines is proposed in this research, including a feed forward spark timing prediction, utilizing a quasi-dimensional turbulent flame entrainment model as well as a reduced detailed mean value model using a semi-physical neural network for predicting the combustion duration. Two virtual fuel properties observers for sensing the laminar flame speed and octane number of fuel sources are used for the purpose of multi-fuel adaptation. The feed-forward spark timing prediction is then be determined based on the combustion duration prediction and a desired combustion phasing (CA50). This desired combustion phasing is first determined by the calibration engineer for a particular engine taking into consideration combustion stability, emissions, performance, etc. Then the "best achievable" combustion phasing in the knock region will be updated based on the current fuel source input. The illustration of the overall closed-loop algorithm is shown in Figure I.15. Six proposed tasks to achieve this objective are listed below and each of the technical details will be presented in the following chapters.

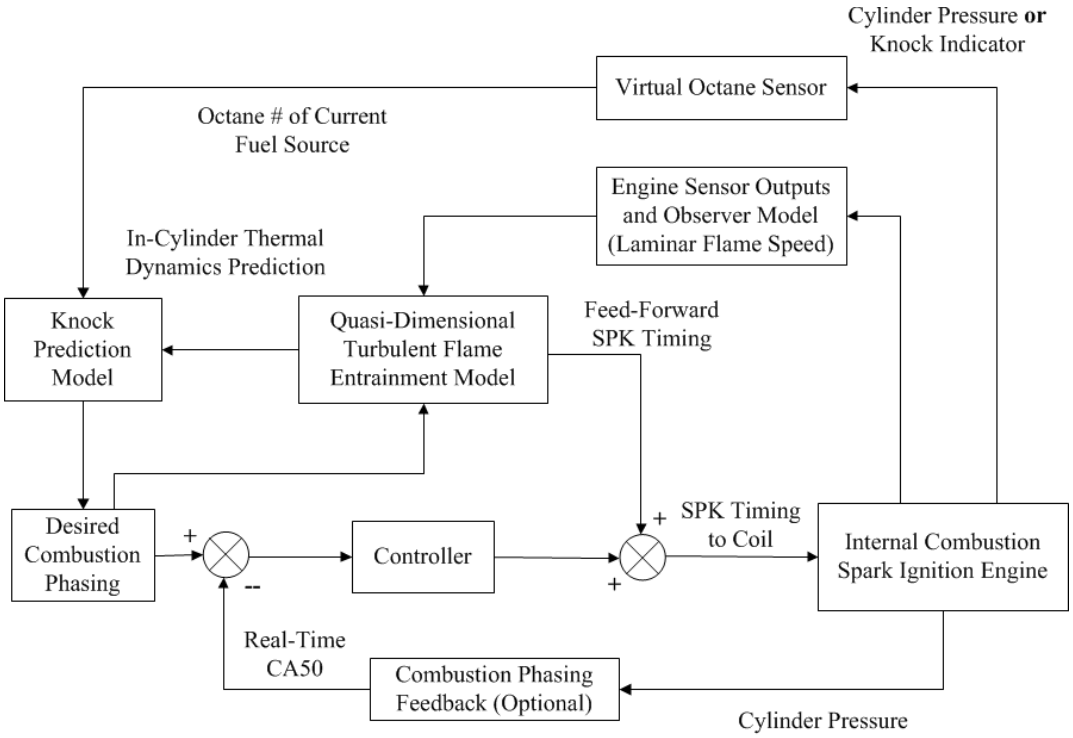

Figure I.15. Proposed multi-fuel adaptive model based spark timing control algorithm.

Task 1. Setup a test engine including 1) installation and calibration of all the sensors for research grade combustion analysis and engine control purposes. These sensors include in-cylinder and manifold pressure acquisition, temperature measurement from critical locations and boundary conditions (mass flow and oxygen measurement etc.); 2) access the control of the test cell and test engine environment including inlet air temperature, inlet fuel pressure and temperature, engine coolant temperature and oil temperature etc. for data consistency and results repeatability; 3) prepare a rapid-prototype engine controller with a

Graphic User Interface (GUI) that can quickly test the newly developed control algorithm and dial in the control parameters real time; 4) build and validate a 1D engine simulation model that will be used offline for combustion model development.

Task 2. Record and document detailed experimental combustion data from the test engine using gasoline and E85 fuels over a wide range of normal engine operating conditions. Check the data quality and repeatability by doing several repeated tests. Each data point is constructed with 500 consecutive cycles for quality evaluation. Import the experimental data into the validated 1D engine simulation model for generating physical combustion related data, such as residual gas fraction, turbulence intensity etc.

Task 3. Formulate preliminary physical input models for residual gas fraction, turbulence intensity and laminar flame speed, that are capable of accurately representing the influence of all engine control actuators on combustion and can run in real-time.

Task 4. Derive a real-time combustion model that will provide a feed-forward prediction of ignition timing during transient conditions based on the desired combustion phasing. The predicted spark timing accuracy should be within 2-3 Crank Angle Degree (CAD) of the calibrated ideal spark timing. Executed time for the prediction model should be in the 0.01 second range with a reasonable computing processor.

Task 5. Develop a virtual fuel behavior sensing feedback strategy using cylinder pressure that accounts for real cycle-to-cycle variations in combustion phasing. Observe only the fuel behavior, rather than actual fuel type, by understanding how the fuel affects combustion such as burn rate, knock etc.

Task 6. Design a methodology to update the desired combustion phasing location based on fuel behavior throughout the engine operating range. This model will focus mainly on knock performance of each fuel, for example the knock limited low engine speed and high load operating conditions. By observing the fuel behavior and self-calibrating the closed loop engine spark timing control model. It will be possible to maintain highest available engine efficiency.

Task 7. Experimentally validate the proposed real time closed loop control strategy using a rapid-prototype engine controller with Hardware In the Loop (HIL) testing including 1) steady-state performance for spark timing prediction accuracy assessment; 2) predictable transient engine operating condition testing (e.g. step or ramp change in engine RPM and load), and evaluation of the spark timing prediction performance.

I.4 BOARDER IMPACTS

The transportation accounts for 72% of petroleum usage in the United States, about half of which is imported [5]. In the near future (20 years) internal combustion (IC)

engines will continue to be a key element of the automobile powertrain due to their low cost, high power density, fast refueling, and allowable driving range. A critical aspect of reducing the US's dependency on foreign oil is the use of alternative fuels in IC engines. The ability to efficiently utilize a variety of bio-fuel feedstocks without generating significant emissions must be enabled. Of the roughly 250 million registered vehicles in use today in the United States [146], only around 8 million (3.2%) are flex-fuel capable [147]. With the median age of the fleet at roughly 9.4 years [146] and most vehicles having a service life of well over 10 years, there will continue to be a significant single-fuel legacy in the United States for many years to come. Fleet dependence on a single fuel generates a large barrier to market penetration for future bio-fuel formulations, and presents a large national security risk if fuel supply sources are interrupted. Engines capable of on-the-fly adaptation to fuel types that may be non-existent when the vehicle is sold could address these issues, and such engine concepts have not been thoroughly studied.

This research proposes focus on a new generation of multi-fuel-adaptable engines that can burn a wide range of fuels, including those that are not be available at the time the engine is produced. This concept could shift the current direction of bio-fuel processing, where a common fuel (i.e. ethanol) is produced, to a strategy where feed stocks are minimally processed and left in a form closer to their initial composition. If engines could adapt to a wide range of fuels, there would be potential to reduce fuel processing upstream of the vehicle and save energy from a well-to-tank perspective. One could imagine different fuel types sold throughout the nation that are produced from

locally-appropriate feedstocks, minimizing both processing and transportation energy losses. Fuel processing and distribution accounts for approximately 22% of the total well-to-wheel energy usage for a gasoline vehicle with a conventional powertrain [148], so even small reductions in well-to-tank energy usage could provide massive energy savings.

I.5 DISTINCTIVENESS OF THIS RESEARCH

The proposed approach is unique because it attempts to incorporate a significant amount of physics with the artificial neural network into the control model for adaptation to new fuel types that may not be available at the time of initial calibration. Additionally, the physics-based methodology allows universal application to a wide range of SI engines, allowing incorporation with new engine platforms with simple re-parameterization. The virtual fuel behavior sensor strategy is also unique because it provides feedback of a physical parameter and allows for ignition timing control for fuels with unknown chemical composition. All of these areas are important to the implementation of multi-fuel-adaptive engines, and have not been thoroughly researched previously.

II RESEARCH SETUP AND COMBUSTION BEHAVIOR

II.1 TEST ENGINE DESCRIPTION

A GM 5.3 liter 90 ° V8 was used to acquire experimental data for this project. Engine specifications are given in Table II.1, Table II.2and Table II.3. It is a push rod engine equips with hydraulic lifter which performs variable displacement function using cylinder deactivation technology. The aluminum cylinder head has a pent-roof combustion chamber with 2 valves (1 intake valve and 1 exhaust valve) per cylinder layout and a center mounted sparkplug. Flat top aluminum pistons have machined recesses for the intake and exhaust valves. Engine load is controlled by an electronic throttle plate. Fuel is injected into the intake port by a single fuel injector located at each intake runner.

The engine has a cross-plane crankshaft design which means the first and fourth crank pins are 180 ° out of phase, and the inner two crank pins are 180 ° apart from each other, and 90 ° apart from the crank pins on each end. Therefore it has a cross-plane firing order: 1-8-7-2-6-5-4-3. The cross-plane V8 would have a first-order imbalance problem, but can be easier solve with the use of full-weight counterweights. An H type balance exhaust pipe is used to equalize the large pressure difference between each bank of the engine.

Table II.1 GM 5.3 Liter V8 Engine Specifications

Configuration	V-8 Gasoline
Firing Order	1-8-7-2-6-5-4-3
Total Displacement	325 CI (5300cm3)
Compression Ratio	9.95:1
Bore and Stroke	96mm x 92mm (3.78” x 3.63”)
Bore/Stroke	1.04 (over-square)
Connecting Rod Length	155.1 mm (6.1”)
Valve Configuration	2 OHV per cylinder, 1 Cam-in-Block
Injection System	Port Fuel Injection (PFI)
Aspiration	Neutrally Aspirated
Rated Power	216 kW (296 hp) at 5000 RPM
Rated Torque	447 N-m (330 ft-lb) at 4200 RPM

The test engine is equipped with variable displacement technology which deactivate cylinder though hydraulic lifter deactivation. Normally, the hydraulic lifters will have pressurized oil inside, and can be treated as a solid lifter when activated. Since there is no oil pressure inside the lifter when engine is not in operation condition, it is going to generate error in measurement of the valve lift profile due to the bleed down of the lifter. Hence, the accurate valve lift profile can be obtained by: 1) calculate from direct measurement from camshaft and known rocker arm ratio; 2) Make the lifter solid with special washer installed.

Table II.2 GM 5.3 Liter V8 Engine Intake Valve Parameters

Number of Intake Valves	1
Intake Valve Head Diameter	44.5mm
Maximum Intake Valve Lift	12.15mm
Intake Duration (@ 0.15mm lift)	-10 CAD – 266 CAD (276 CAD)
Intake Opening (@0.15mm lift)	-10 CAD – 115 CAD
Intake Closing (@0.15mm lift)	115 CAD – 266 CAD

Table II.3 GM 5.3 Liter V8 Engine Exhaust Valve Parameters

Number of Exhaust Valves	1
Exhaust Valve Head Diameter	50.7mm
Maximum Exhaust Valve Lift	12.62mm
Exhaust Duration (@ 0.15mm lift)	-240 CAD – 35 CAD (275 CAD)
Exhaust Opening (@0.15mm lift)	-240 CAD – -112 CAD
Exhaust Closing (@0.15mm lift)	-112 CAD – 35 CAD

The test engine does not equip with any variable valve phasing mechanism, so the valve lift profile (Figure II.1) is set for all the operating condition as shown below:

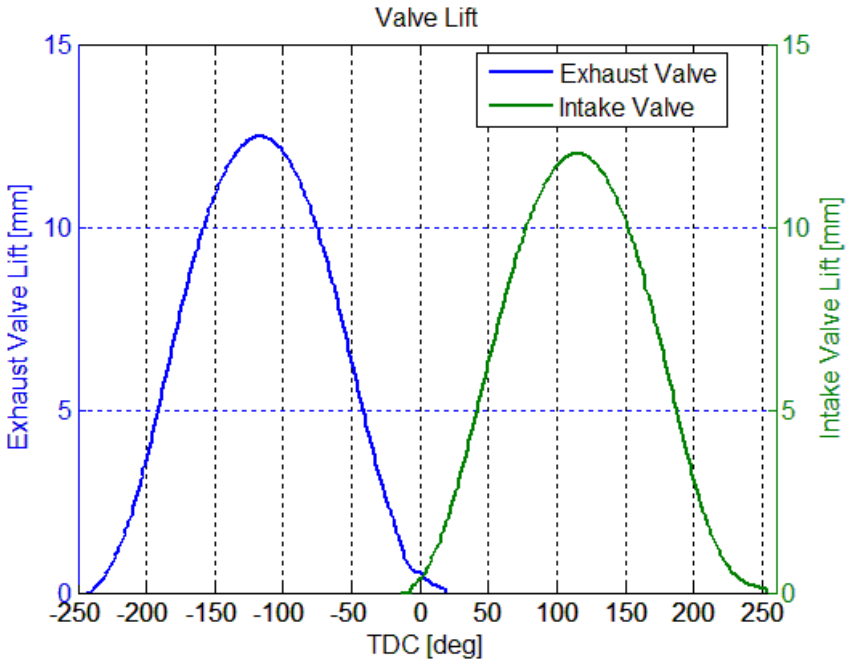

Figure II.1: GM 5.3 Liter V8 Engine Valve Lift Profile

II.2 TEST CELL SETUP

The test engine is installed into a FEV Engine Test Cell located at the Clemson University – International Center for Automotive Research (Figure II.2). A low-inertia 430KW (~580HP) AC dynamometer which is capable to simulate realistic transient engine operation is used to absorb power and regulate engine speed. Engine torque is measured from a torque flange on the dynamometer side driveshaft. Special driveshaft for V8 engine is used to ensure on oscillation arising from the engine-dynamometer coupling natural frequency.

FEV Fuel-Con system is used for fuel conditioning. The Fuel-Con controls the fuel temperature and pressure supply to the test engine. Fuel flow rate is measured with a SIEMENS Sitrans 2100 mass flow meter. Mass flow meter can compensate different fuel

density and output an accurate fuel flow measurement. Existing multi-fuel testing capabilities will also be used for this research. FEV Cool-Con system is used to control the engine coolant and oil temperature. Cool-Con set temperature can be programmed to any reasonable temperature. Target temperature control can be set to engine coolant inlet or outlet. Oil temperature is controlled through a heat exchanger using coolant from engine coolant outlet.

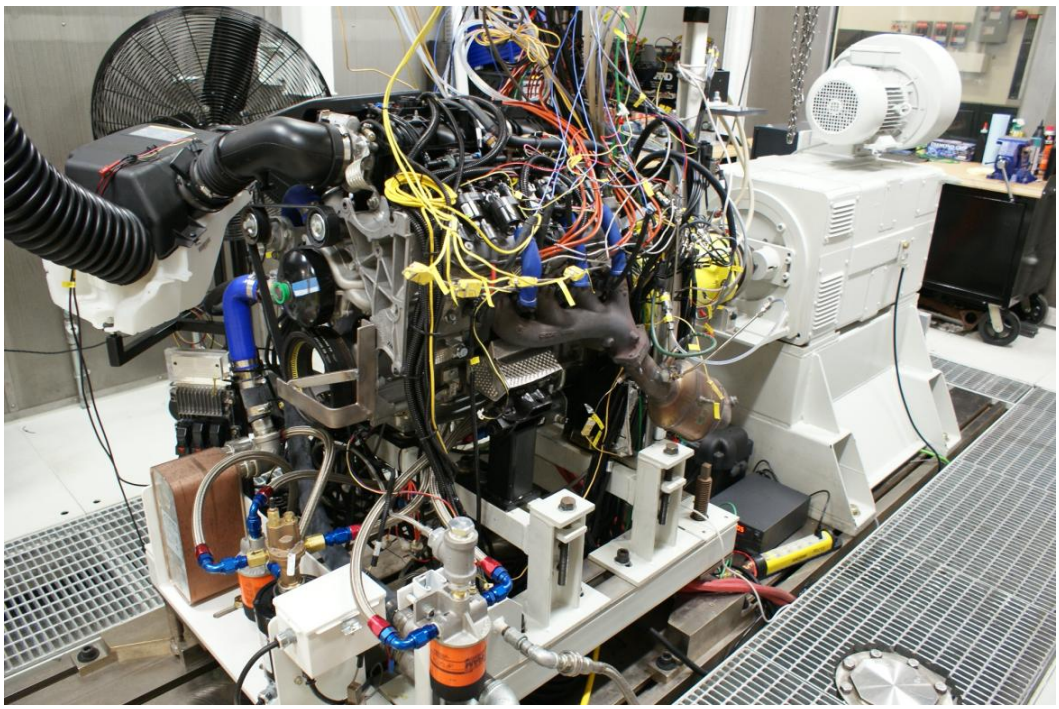

Figure II.2: the engine dynamometer facility at the Clemson University - International Center for Automotive Research

II.3 DATA COLLECTION AND PROCESSING

Each cylinder of one engine bank instrumented with passage-mounted AVL GH12D piezoelectric cylinder pressure sensors. The sensors were located in the cylinder head to maximize accuracy according to Patterson and Davis [128], and were equipped with flame guards to nearly eliminate thermal shock errors. Piezoresistive Kulite sensors were used for both intake and exhaust pressure measurements. The exhaust sensors were water cooled to minimize signal drift when exposed to high temperatures. Cylinder and manifold pressure measurements were recorded using an AVL-671 crank-angle resolved data acquisition system with a $0.5\,^{\circ}$ CA resolution. AVL Concerto software is used to process the high volume of data that is acquired during each experiment. Bosch lambda sensors, driven by Fuel Air Spark Technology (FAST) wide-band modules, were used to record air-to-fuel ratio for each cylinder.

II.4 GAS EXCHANGE AND COMBUSTION SIMULATION

AVL Gas Exchange and Combustion Analysis (GCA) 1D engine simulation software is used to calculate several important gas exchange parameters that is non-measureable in the test cell, for example residual gas fraction, and turbulent intensity. GCA uses the experimentally measured intake and exhaust pressures as boundary conditions for a gas dynamic model and experimentally measured cylinder pressure curve in order to determine the rate of heat release and other combustion characteristics such as unburned gas temperature and mass fraction burned curve etc. Various other operating-point-dependent characteristic values are also required from the DAQ measurement

imported for simulation. Engine construction is built in the gas exchange and cycle simulation code BOOST and integrated together with GCA for complete engine simulation. The simulated engine mode has been validated against the experimental engine data to ensure the simulation results accuracy, including energy balance validation, gas exchange and most importantly the combustion curve validation which is shown in Figure II.3. Various speed and load points were also studied and the GCA simulation is confirmed to produce satisfactory results across a wide range of engine operating conditions.

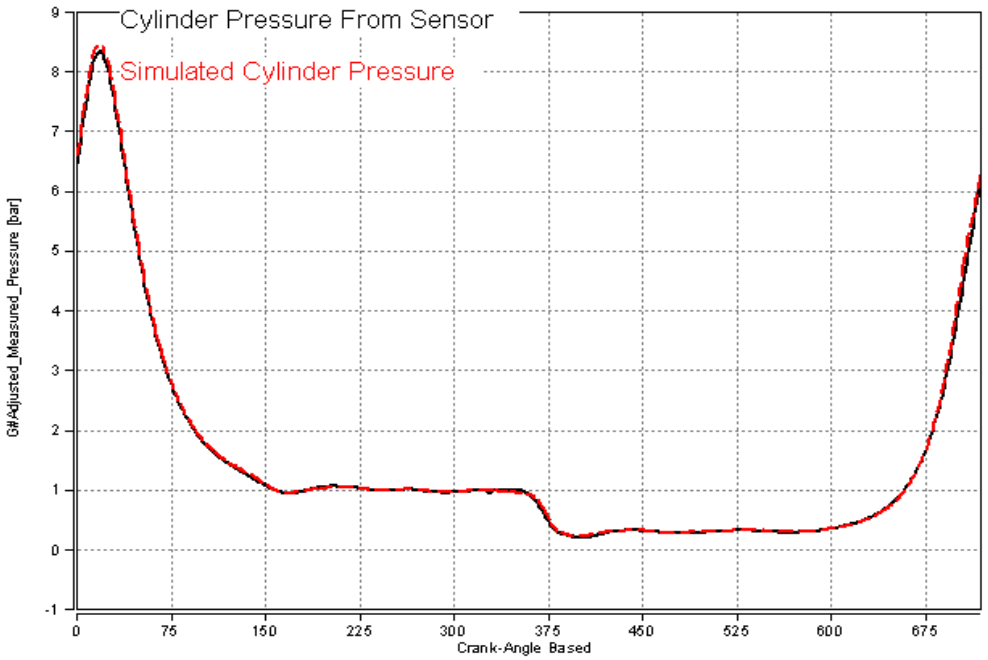

Figure II.3: GCA simulation results validation

II.5 VIRTUAL ENGINE SIMULATION

The 1-D engine model was developed based on the test engine geometry and configuration as shown in Figure II.4, using the market leading engine simulation software GT-POWER. A predictive combustion model is implemented that utilizes a quasi-dimensional flame propagation process. A 3-D combustion chamber shape model is used to calculate flame propagation area. Predicted cylinder pressures from the GT-POWER simulation were compared with experimental results under the similar operating conditions for validation. Areas of particular focus for model validation were cylinder pressure during gas exchange and combustion to evaluate both the performance of the intake and exhaust system as well as the predictive combustion model.

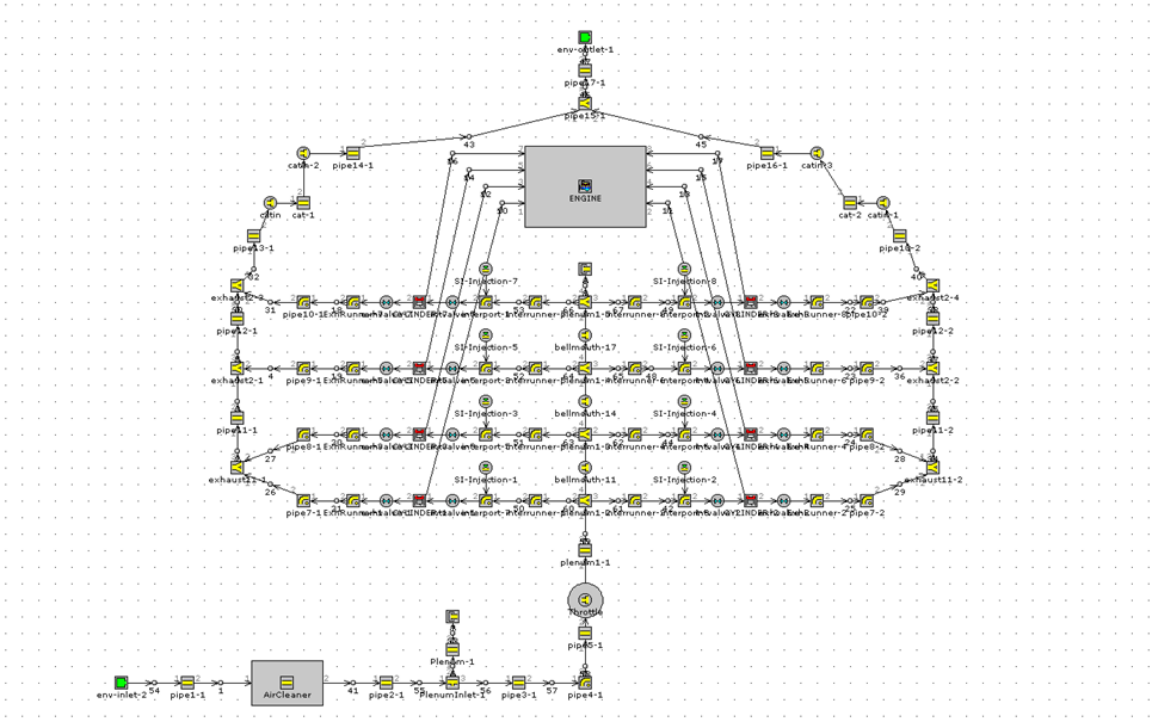

Figure II.4. GT-POWER virtual engine model structure

The combustion process is modeled using a quasi-dimensional flame propagation model. Geometry of intake and exhaust system components are measured and convert in 1D coordinate representation, measurements also include flow coefficients and operating environment. Combustion chamber shape was created with a 3D scanner and imported into GT-POWER for SI engine combustion flame propagation area calculations. Predicted cylinder pressure from the virtual engine simulation is compared with experimental results under similar operating conditions to evaluate the model accuracy. Examination of pressure traces during gas exchange and combustion processes were used evaluate the performance of the intake and exhaust system as well as the predictive combustion model. The entire range of engine speed and load was examined to ensure the developed model was globally accurate. Validation processes were carried out for both gasoline and E85. Adjustments on the combustion model multiplier are 0.69 for turbulent flame speed, 0.55 for dilution exponents and 0.2 for kernel growth. Only 1 set of multipliers are used for all engine operating conditions.

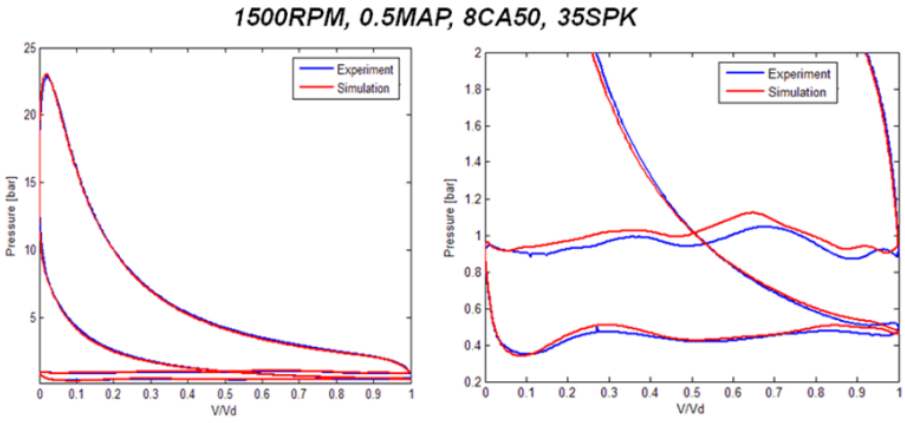

Figure II.5. Simulated cylinder pressure from GT-POWER compared to the experimental data.

II.6 PROTOTYPE REAL TIME ENGINE CONTROLLER

The test engine was controlled using an A&D Technology, Inc. ADX rapid-prototype ECU system (AD5435) that allows for complete adjustment of all actuators and fast user defined function, control algorithm implementation. The AD5435 is a high-speed measurement and control system that can be customized for a wide variety of engine control applications. It addresses various systems requirements by combining multiple I/O boards and a CPU employing RTOS with excellent real-time performance through MATLAB/Simulink control models and A&D's GUI-generating and experimentation support tool, VirtualConsole, as shown in Figure II.6. ECU in the prototype engine controller has an Intel Celeron M 1.5 GHz processor and 512 RAM that is capable of executing a complete engine control code with a model based combustion model at a sampling time of 100Hz.

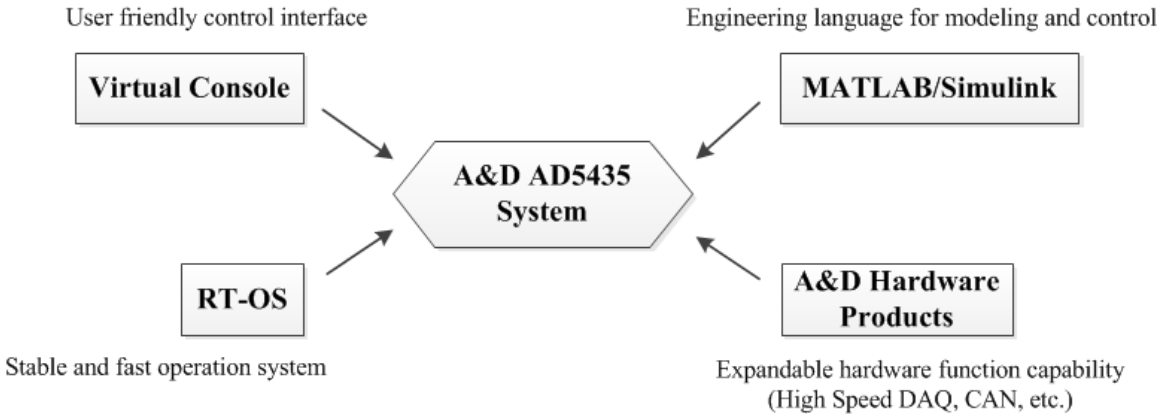

Figure II.6. A&D AD5435 engine control system

The structure of Simulink code for engine control is shown in Figure II.7. Standard engine sensors are used for engine control purposes. High speed cylinder pressure sensor data is also available for real time heat release analysis. Physical sub models take the

standard sensor signals and generate several combustion related parameters for model based spark timing control. Engine electronic throttle and injection are controlled using closed-loop PID based on the TPS and lambda feedback. Map based ignition control is also available utilizing a look up table which is pre-calibrated based on stock ECU.

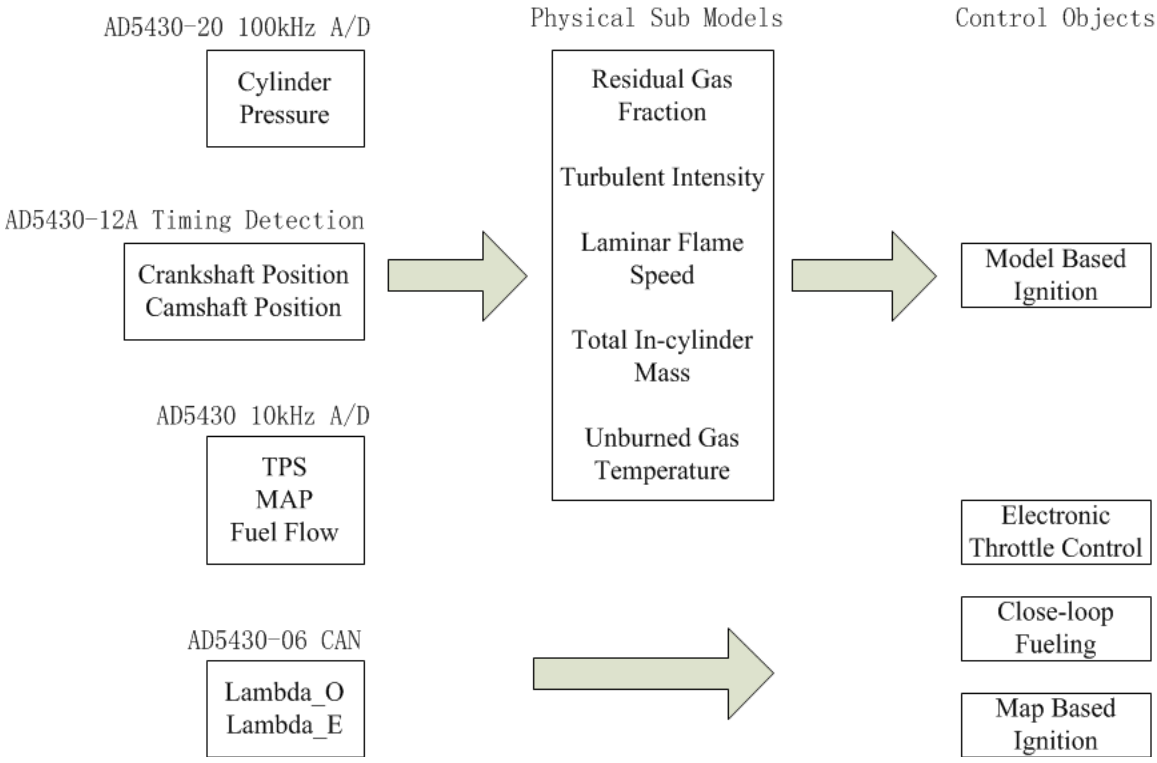

Figure II.7. Real time engine control Simulink program structure.

II.7 COMBUSTION BEHAVIOR

II.7.1 ENGINE PERFORMANCE PARAMETERS

Indicated mean effective pressure (IMEP)

Mean effective pressure (MEP) is normalized parameters which represent the practical engine performance index such as power, torque, and specific fuel consumption. MEP was defined to eliminate the effects of engine size that allows for comparison between engines having different displacement. Indicated mean effective pressure represent only the thermodynamic work available to the engine. It is the work produced per cycle divided by the displaced volume which can be calculated by the numerical integration of the pressure versus volume data.

Combustion phasing

Combustion process can be described by a heat release process of the unburned mixture. The energy release rate which is a function of in-cylinder pressure and temperature can be converted to a normalized integral form which represents the fraction of heat release from the total energy, called mass fraction burned curve, as shown in Figure II.8. It is clocked with engine crank angle which eliminates the absolute cycle times changing for different RPMs.

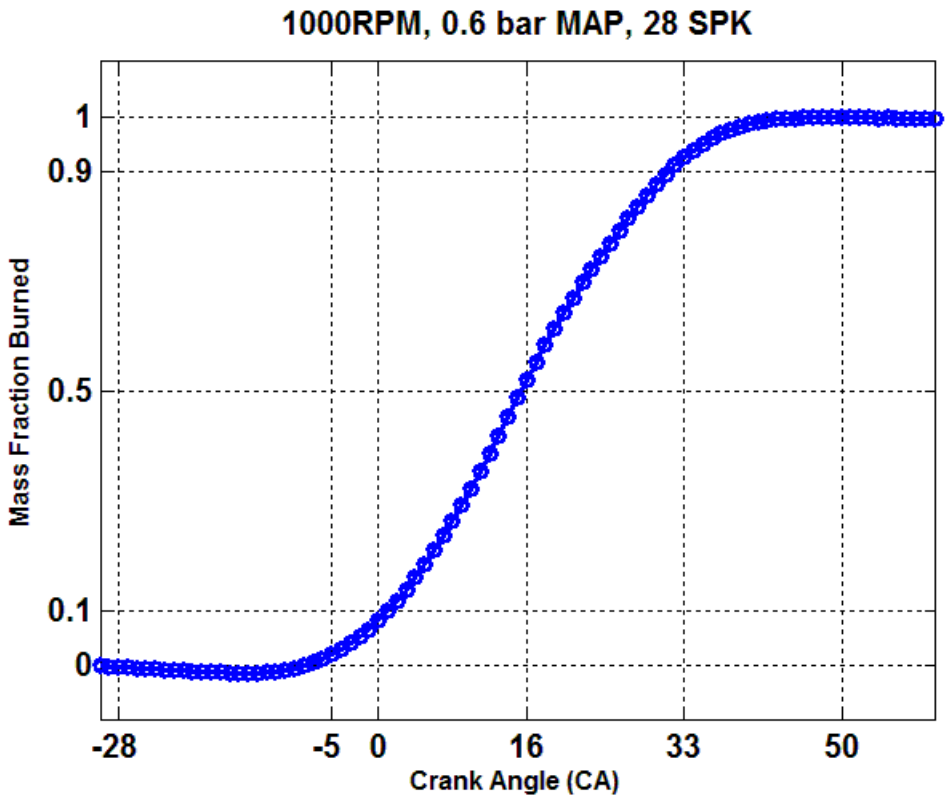

Figure II.8. Mass Fraction burned curve for a steady state engine operating conditions.

Several important index/locations are commonly used to describe the combustion phasing which in the forms of CA (percentage of mass burned). It represents the location when certain amount of mass is burned. Typical index are:1) CA00, the start of the combustion after initial flame development introduced by the spark energy; 2) CA10, the start point of rapid combustion when pressure and temperature developed into optimum environments for combustion; 3) CA50, the centerline of combustion which is used to represent the combustion phasing; 3) CA90, the end of rapid combustion, followed by relatively slow reactions of hydrocarbon oxidation when pressure and temperature is decreasing.

Maximum Brake Torque (MBT) timing

The optimum combustion phasing is defined as minimum spark advanced timing for best brake torque. For ideal thermodynamics cycle, the combustion happed at constant volume which will results in the maximum efficiency. However, combustion is a relatively slow event compared to the time period in the high speed SI engines. The excitation spark has to happen during the compression stroke to give time for combustion. This introduced the problem for proper phasing the combustion event. Early combustion will generate larger heat transfer losses and late combustion will results in expansion loss. Therefore, the optimum spark timing is a balanced between heat transfer loss and expansion loss. General rule of thumb for the MBT timing is 50% mass burned at around 8CA after top dead center if the engine is not knock limited. The optimum combustion phasing also will favorite more advanced during the high engine speed operation because of the reducing time for heat transfer.

II.7.2 COMBUSTION PHASING CHARACTERISTIC

Spark timing is the direct control parameters for combustion phasing. Retard and advance the spark timing will results in the same effects for combustion phasing as shown in Figure II.9. Spark and combustion phasing generally have a linear 1 to 1 relationship especially around the MBT timing which means retard 1 degree of spark timing will results in 1 degree retarded combustion phasing. Notice the difference between gasoline and E85, spark timing need to be advanced around 3CA to be able to achieve the same combustion phasing.

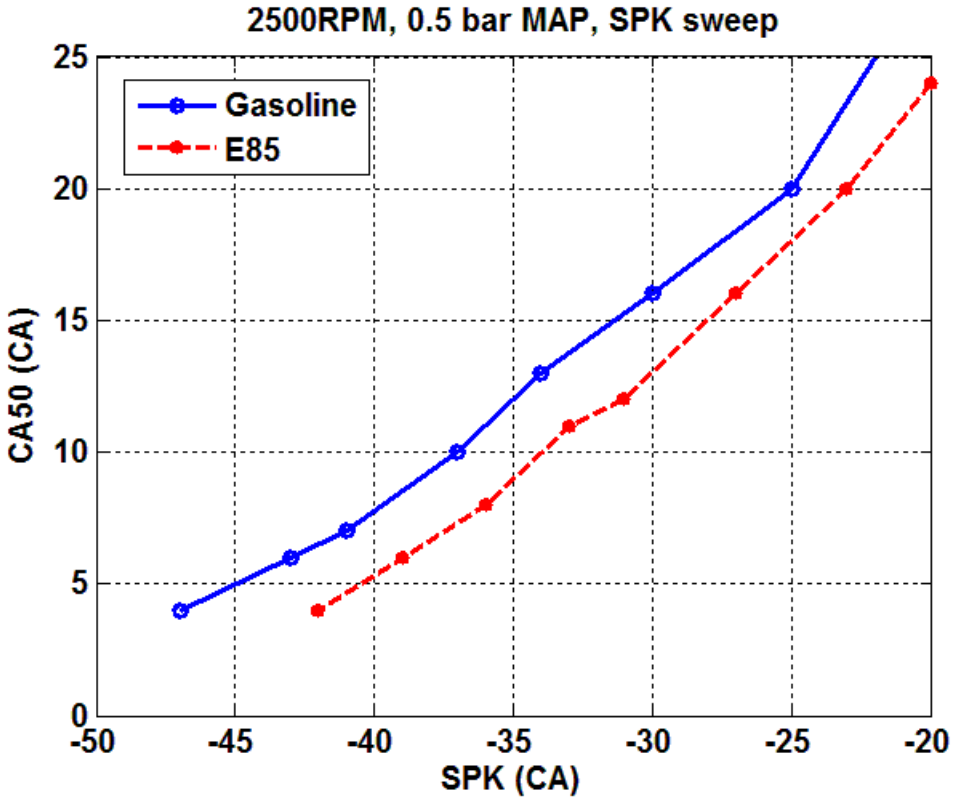

Figure II.9. Combustion phasing (CA50) results at 2500RPM and 0.5 bar MAP during spark sweeps.

Opposite trends can be observed for the flame development period. The duration from spark to CA5 is decreasing when retarding the spark timing, as can be seen from Figure II.10. This is because the in-cylinder pressure and temperature is higher when piston compressed the unburned mixture closer to the top dead center. E85 compared to gasoline is easier to evaporate and also the laminar flame speed is higher which in general will shorten the flame development period.

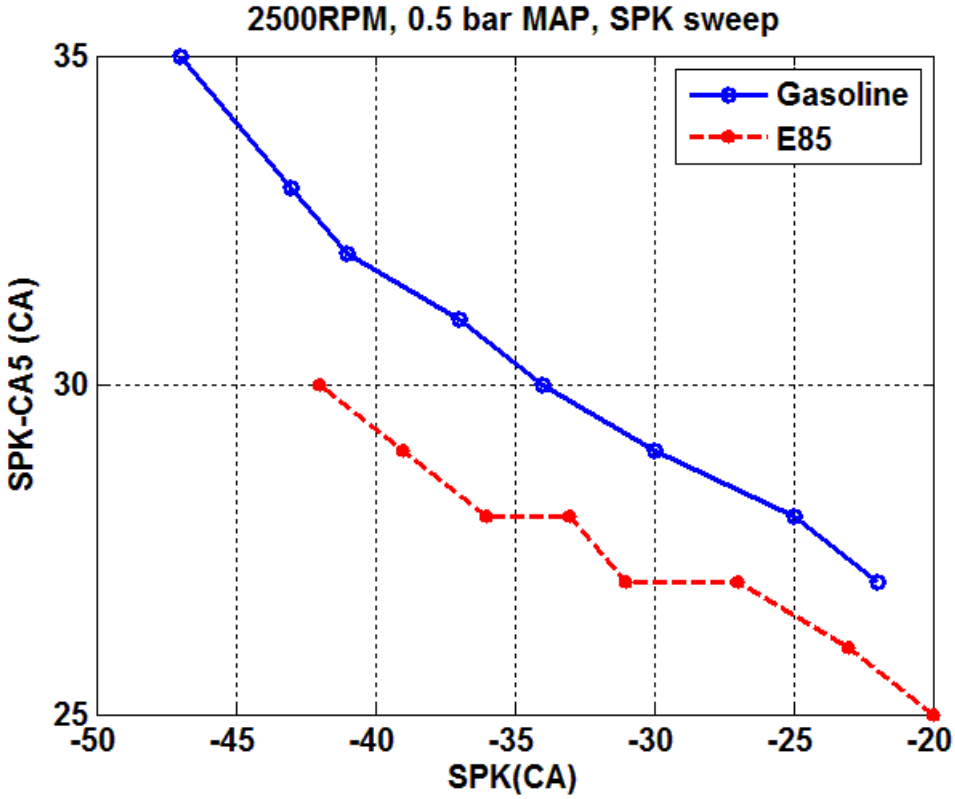

Figure II.10. Flame development period (SPK-CA5) results at 2500RPM and 0.5 bar MAP during spark sweeps

Generally speaking a shorter combustion event will results in better efficiency because it is closer to a constant volume ideal combustion. Less heat transfer and expansion loss will be generated when combustion duration is short. It can be also related to the MBT timing rule which is shown in Figure II.11. The MBT timing for the operating conditions is around 30 CA to 35 CA where the combustion durations are at the minimum locations.

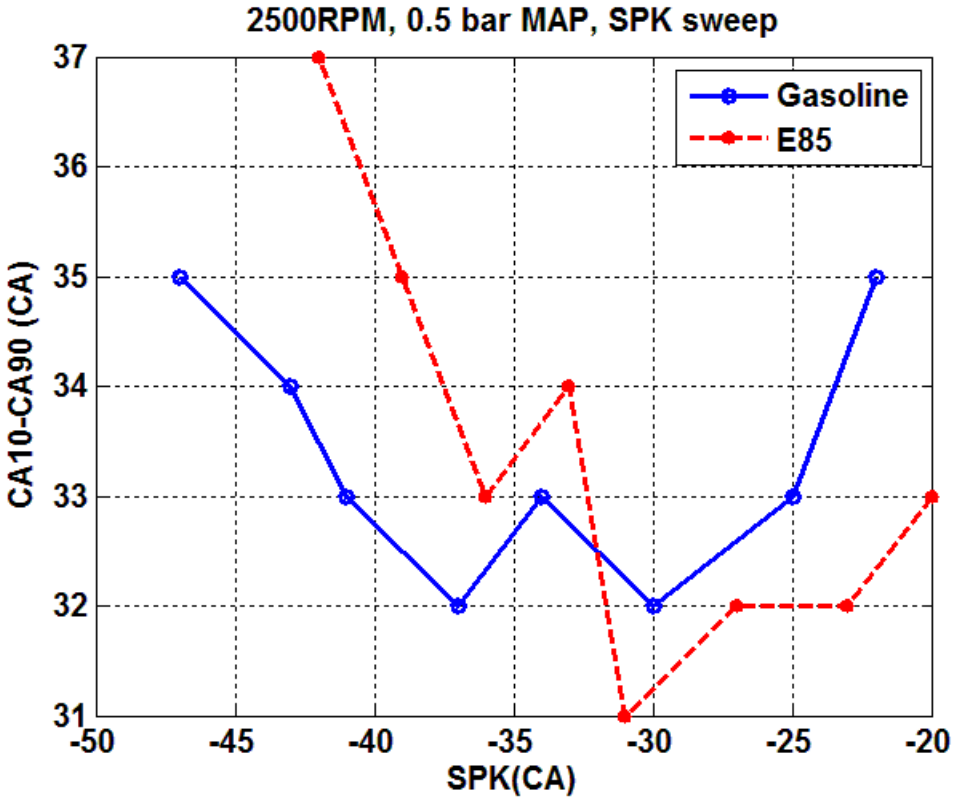

Figure II.11. Combustion duration (CA10-CA90) results at 2500RPM and 0.5 bar MAP during spark sweeps

II.8 TEST POINT SELECTION

Data was acquired over a large range of operating condition to ensure that the developed models were accurate and robust. Engine data is divided into two sets; one set for operating with gasoline fuel, and another for operating with E85 fuel. Experimental data was obtained at controlled coolant temperature and oil temperature for data consistency. Data selection plot, as shown in Figure II.12, was based on engine normal operation range, spark sweeps, load sweeps and RPM sweeps consist the overall matrix of the possible engine operating condition.

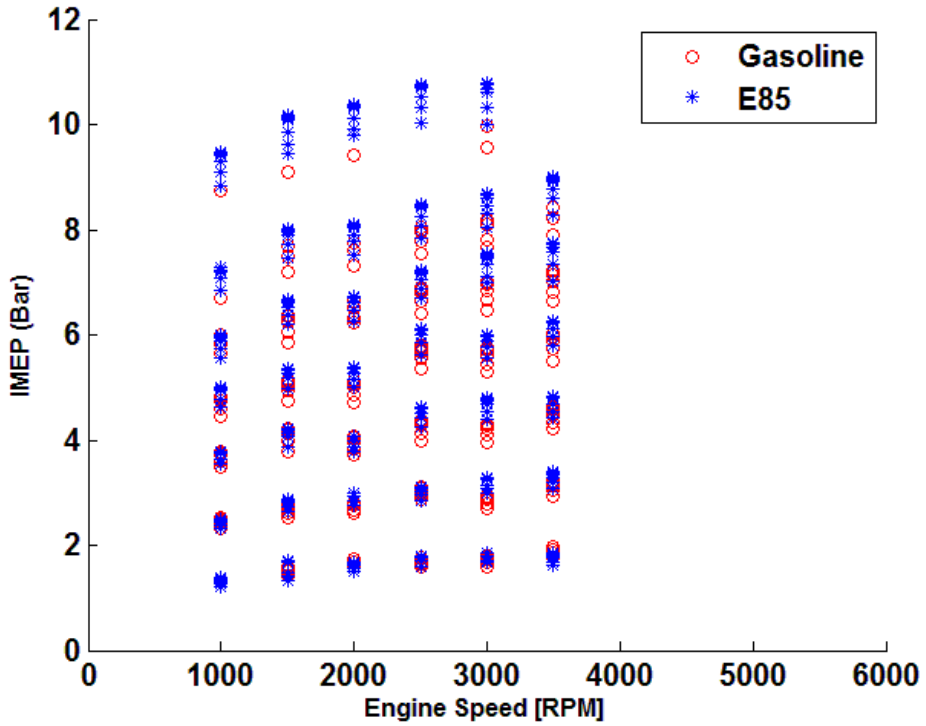

Figure II.12. Steady state operation data points only cover partial engine operating range; spark sweeps (7-24 °ATDC CA50), load sweeps (0.3-0.98 bar of MAP) and RPM sweeps (1000-3500 RPM) which contains total 440 data points for both gasoline and E85. Each data point is an average of 500 continuous cycles.

II.9 COMBUSTION STABILITY

The cyclic variability is usually attributed to the result of random fluctuations in equivalence ratio and flow field due to the turbulent nature of the flow in the cylinder Cycle-to-cycle variability is directly related to engine emission and drivability. For this reason, it is very important to quantify this cyclic variability for better engine control performance purpose.

II.9.1 COEFFICIENT OF VARIANCE OF IMEP

One of a common measurement of cycle-to-cycle variability is the coefficient of variance of IMEP which is defined as the standard deviation of an IMEP sample set divided by the average value of the same IMEP sample set. COV levels below 10% are generally considered acceptable. Figure II.13 shows the COV of IMEP of the GM 5.3 Liter V8 engine with each sampling data set contains 500 cycles. As can be observed, engine using gasoline fuel will have slight higher COV than using E85 especially in the knock limited and retard limited zone. 5% to 10% combustion cycle-to-cycle variability is observed as a nature of this test engine, therefore the spark timing prediction model will expect to have the same error tolerance.

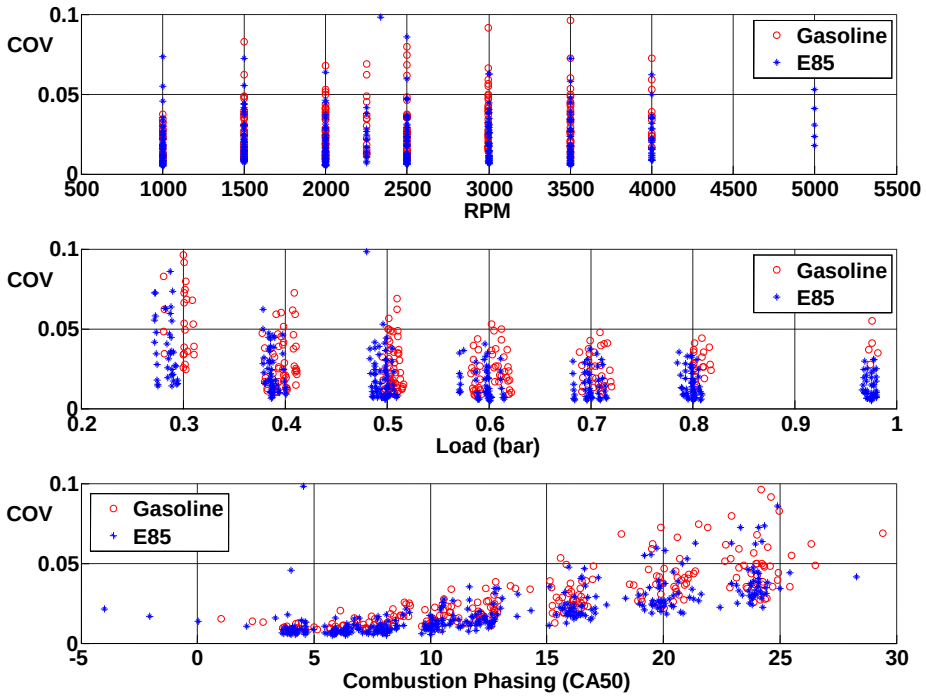

Figure II.13: GM 5.3 Liter V8 engine COV of IMEP

II.9.2 LOWEST NORMALIZED VALUE OF IMEP

Lowest normalized value (LNV) is used to evaluate the misfire tendency of an engine which is defined as the lowest value of an IMEP sample set divided by the average value of the same sample set. LNV correlates well with engine emissions and engine harshness. Figure II.14 shows the LNV of IMEP of the GM 5.3 Liter V8 engine with each sampling data set contains 500 cycles. LNV for engine using gasoline is also higher than with E85 especially at the knock limited and retard limited zone as shown in Figure II.14. There is no random nature misfire tendency of the test engine can be concluded from the LNV plot.

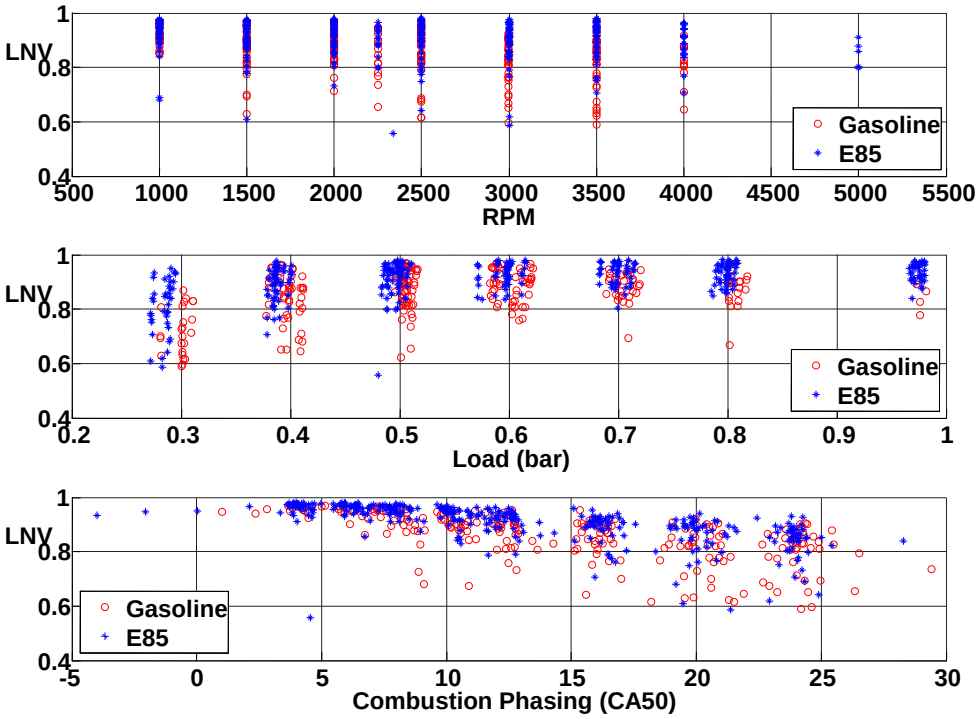

Figure II.14: GM 5.3 Liter V8 engine LNV of IMEP

II.9.3 INDEX OF COMBUSTION PHASING CONTROL PERFORMANCE

Combustion variance in this research is quantified by the standard deviation of CA50. Standard deviation of CA50 will be increased specially at higher RPM, lower engine load, or late combustion phasing, as shown in Figure II.15. To evaluate the real time combustion phasing control performance at each engine operating points, an empirical model is fitted for standard deviation of CA50, as shown in Equation (II.1). Since the test engine is not equipped with advanced control actuators, such as variable valve actuation, charge motion control system, external residual gas control system etc., and standard deviation of the combustion variability is mainly a function of RPM, load and CA50.

$$CA50_{Std.Dev.?} = f(RPM, LOAD, CA50) \tag{II.1}$$

Standard deviation is commonly used to measure confidence in statistical conclusions. In this research, the target performance of controlled combustion phasing (floating mean) is regulated to be less than +/- 0.7 the standard deviation based on the standard error of the mean (SEM) theory, as shown in Equation (II.2).

$$SE_{\bar{X}} = \frac{\sigma}{\sqrt{n}} \tag{II.2}$$

Because the combustion phasing (CA50) will randomly locate around the mean assuming normal distribution, if the SEM hold, the floating mean of CA50 results will share the same population mean of CA50 control target, in other word, the best the control system can do.

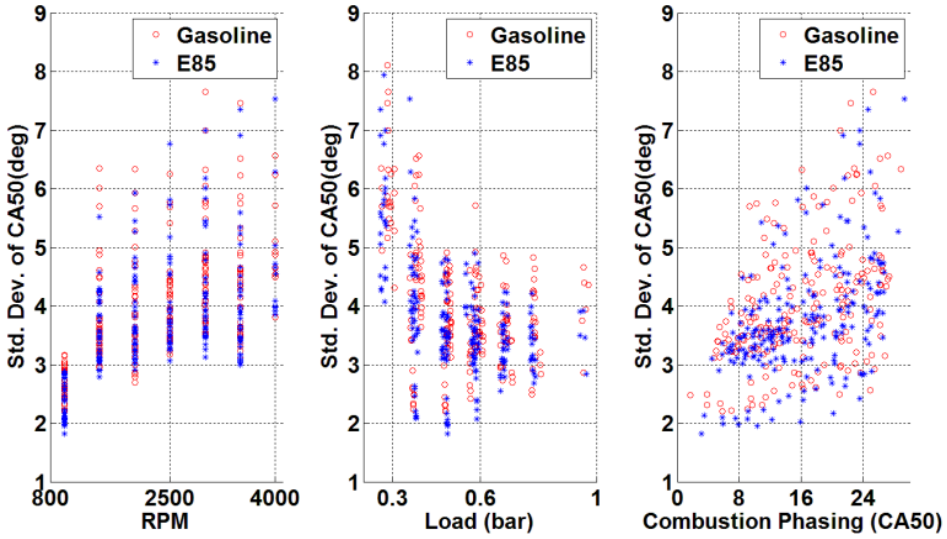

(a)

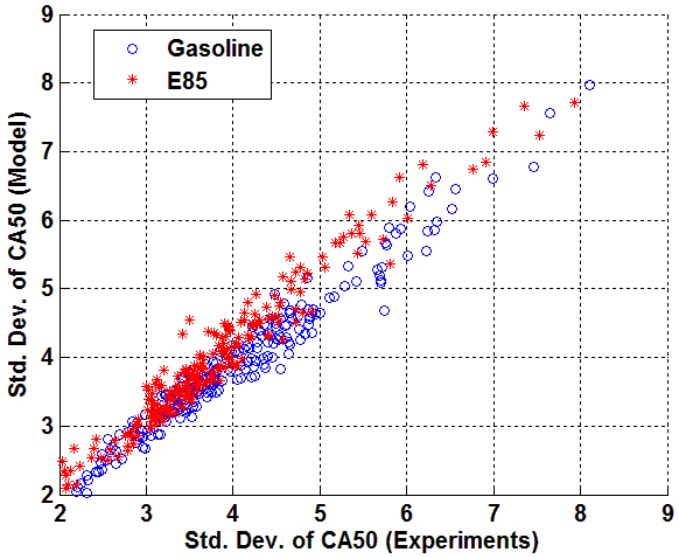

(b)

Figure II.15. (a) Standard deviation of CA50 (500 consecutive cycles sample) for different engine speed, load and combustion phasing, and (b) empirical model results of standard deviation of CA50 which are both used to evaluate the spark timing control performance.

III QUASI-DIMENSIONAL COMBUSTION MODEL DERIVATION

A simplified version of a well-proven quasi-dimensional turbulent flame entrainment model is used as the foundation of this research. Quasi-dimensional turbulent flame entrainment models can accurately predict spark-ignition engine performance for a wide range of designs and operating conditions [149], without the need to setup a complex CFD simulation. They do not capture the flow structure and flame propagation detail of multi-dimensional models; however, they offer physics-based results with low computational complexity making them good candidates for model-based control strategy development. This combustion model was originally introduced by Blizard and Keck [150] and refined by Tabaczynski et al. [151][152]. The model consistently provides good agreement with experimental data, making it a good representation of combustion processes [24]. Combustion is modeled using two steps; (1) pockets of the fresh air and fuel mixture are entrained by an advancing turbulent flame front, and (2) entrained pockets burn-up on the Taylor microscale level at the laminar flame speed of the mixture.

$$\frac{dm_{entrained}}{dt} = \rho_{unburned} A_{flame}(u' + S_L) \qquad \text{(III.1)} \qquad \frac{dm_{burned}}{dt} = \frac{m_{entrained} - m_{burned}}{l_m / S_L} \qquad \text{(III.2)}$$

Equation (III.1) describes the rate which unburned mass is entrained by the flame front. The flame is assumed to entrain the unburned charge along Kolmogorov-scale vortices entraining turbulent eddies. Entrainment velocity is defined by the sum of a diffusive component, laminar flame speed (SL), and a convective component, turbulence intensity (u'). Flame front area (Afl) is defined by the leading flame edge, not the total flame surface area enclosing the still unburned eddies. After turbulent flame entrainment,

mass burn-up rate can be described by Equation (III.2). Burn-up rate is proportional to the total unburned mass entrained behind the flame front. Entrained turbulent eddies are then assumed to burn-up at the laminar flame speed since the length scale is small. Eddy size is approximated as the Taylor microscale (λ , which is the assumed length scale over which laminar diffusion occurs; justifying the use of laminar flame speed in this case [151]. The overall process can be illustrated by Figure III.1.

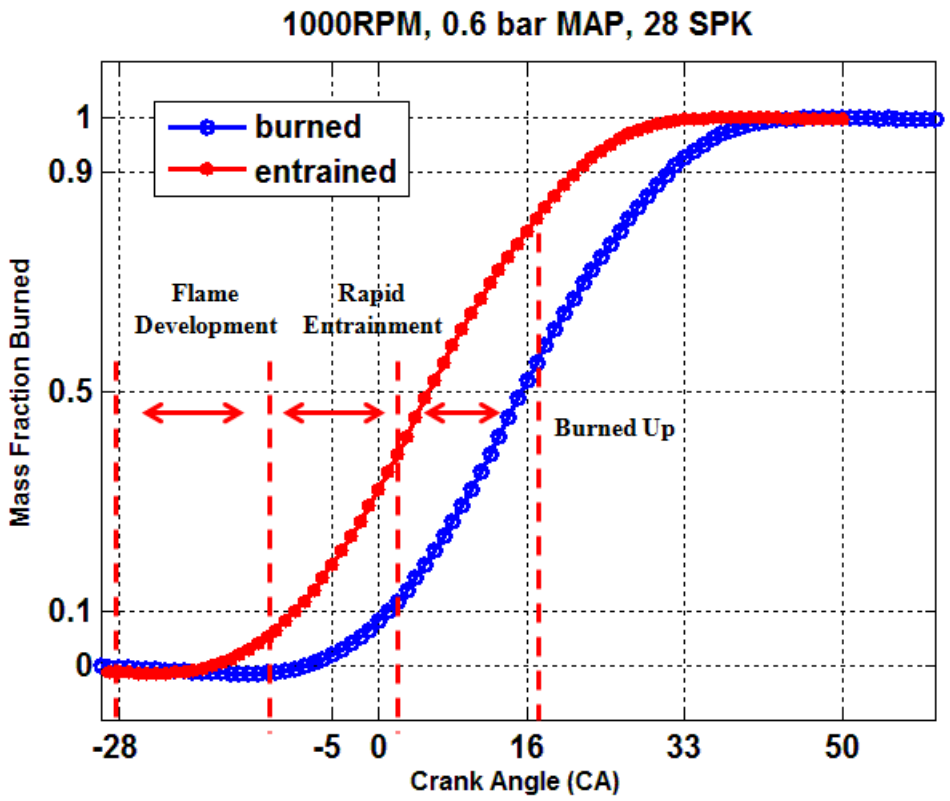

Figure III.1. Mass entrained and burned process of quasi-dimensional turbulent flame entrainment modeling

III.1 INPUTS CALCULATION

Inputs to the quasi-dimensional turbulent flame entrainment model can be described by Figure III.2. The model requires five inputs: (1) flame front area, (2) unburned charge density, (3) turbulence intensity, (4) Laminar flame speed, and (5) Taylor microscale of turbulence. Each of these inputs has specifically designed sub-models to predict their levels throughout the engine operating range in real-time. These sub-models can be constructed using results from a 1-D combustion simulation code for accuracy demonstration. For the real-time control purpose, the sub-models can be simplified and only take standard engine sensors as primary inputs such as mean piston speed, air/fuel ration, and intake manifold absolute pressure. Comparison between the two calculation methods will be shown in the following chapter.

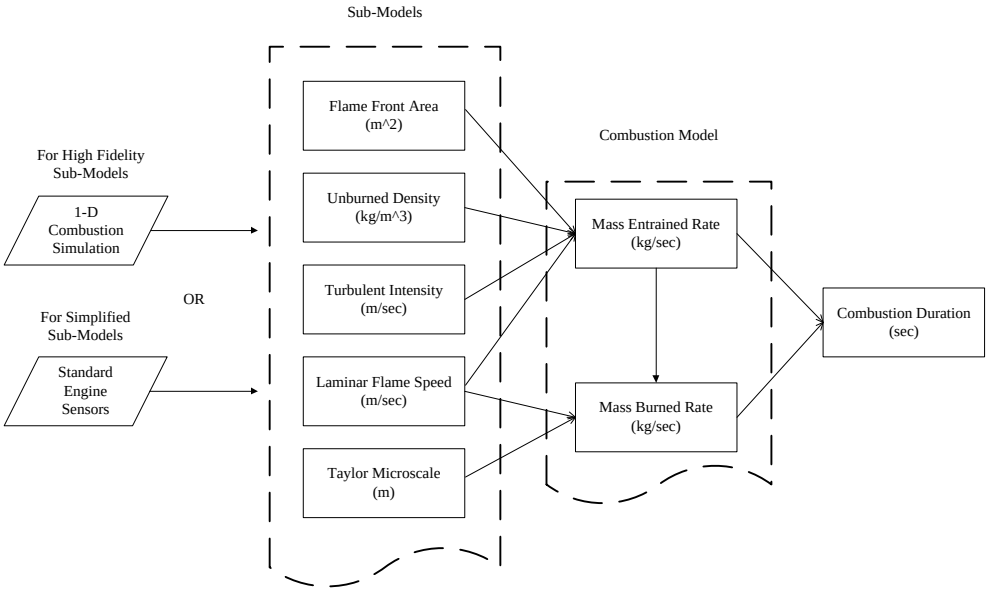

Figure III.2. Combustion model inputs structure with a comparison between high fidelity sub-models for accuracy demonstration and simplified sub-models for real-time control purpose.

III.1.1 RESIDUAL GAS FRACTION MODEL

Residual gas fraction serves as diluents to the combustion that can lower the in-cylinder temperature and decrease combustion burn rate by reducing the laminar flame speed of in-cylinder gas mixture. It is also used to calculate total in-cylinder mass together with the on-board mass air flow and lambda sensor. Since the test engine does not equip with any external EGR system, internal residual gas content can be calculated through pressure difference at the valve overlap period utilize the 1-D combustion simulation. A well-proven semi-empirical approach is used for real-time RGF prediction [28]. The model was rigorously validated against with the 1-D combustion simulation results. Empirical model constants were recalibrated for the test engine, as shown in Equation (III.3).

$$x_r = \frac{0.5484OF}{N}\left(\frac{P_I}{P_E}\right)^{-0.87}\sqrt{|P_E - P_I|} + 0.3221\phi\left(\frac{P_I}{P_E}\right)^{-0.74} / r_c \qquad \text{(III.3)}$$

III.1.2 UNBURNED CHARGE DENSITY

Initial unburned charge density (@ IVC) is calculated using the ideal gas law and the approximately known value of temperature, pressure and gas constant at intake valve closing.

$$\rho_{unburned,IVC} = \frac{m_{unburned,IVC}}{V_{unburned,IVC}} = \frac{P_{cyl,IVC}}{rT_{cyl,IVC}} \qquad \text{(III.4)}$$

Polytrophic compression is assumed and Equation (III.3) (III.4) can be used to calculate pressure and temperature. Temperature at intake valve closing (IVC) is estimated using the mass-weighted calculation assuming the specific heats of intake and exhaust gases are equal, as in Equation (7), residual gas temperature at IVC is assumed

equal exhaust temperature minus 100 degrees (K) to account for heat transfer during the gas exchange process.

$$P_{SPK,i} = P_{map}(\frac{V_{IVC}}{V_{SPK,i}})^{\gamma} \quad \text{(III.5)} \qquad T_{SPK,i} = T_{IVC}(\frac{V_{IVC}}{V_{SPK,i}})^{\gamma} \quad \text{(III.6)}$$

$$T_{IVC} = \frac{m_{RGF}(T_{EXH} - 100) + m_{fuel}T_{fuel} + m_{air}T_{air}}{m_{total}} \quad \text{(III.7)}$$

After ignition, unburned charge is compressed at a rate that the rapid distortion theory (RDT) is assumed valid (Wong [154]) which assuming that angular momentum within the turbulent field is conserved, and that there is no interaction between turbulent eddies. Rapid distortion theory defines the unburned charge density by Equation (III.8):

$$\rho_{unburned,i} = \rho_{unburned,IVC}(\frac{u'_i}{u'_{IVC}})^3 \quad \text{(III.8)}$$

III.1.3 FLAME FRONT AREA

Flame front area at each crank angle can be interpreted from a geometrically calculated table [24]. The flame area table is generated using engine-specific combustion chamber geometry. Alternative way of predicting the flame front area is used in this research which assuming a spherical flame pattern and used experimental data to generate the approximated results. The flame is assumed to start from the spark and propagate as a sphere-shaped front before it interfaces with the cylinder walls [155], for example the cylinder head, liner, and piston. Previous researchers [134]have shown this to be a reasonable assumption for the purpose of engine control during early combustion (before CA10). It is also assumed that flame thickness can be ignored which means the flame

volume is equal to burned volume. Flame area for early combustion is calculated using Equation (III.9).

$$A_{burned} = \sqrt[3]{36\pi} V_{burned}^{2/3} \tag{III.9}$$

A relationship between Burned Mass Fraction (BMF) and Burned Volume Fraction (BVF), derived from the ideal gas law by Heywood [22], is used to approximate burned and unburned volume using Equation (III.10).

$$BVF = [1 + \frac{\rho_u}{\rho_b}(\frac{1}{BMF} - 1)]^{-1} \tag{III.10}$$

The density ratio in Equation (III.10) depends on the equivalence ratio, burned gas fraction, along with unburned mixture temperature and pressure. Heywood simplifies the calculation by observing that the density ratio is close to 4 for most spark-ignition engine operating conditions. Another method to calculate the burned volume fraction was reported by Patterson [128], as shown in Equation (III.11).

$$BVF = (1.0754 \times BMF^3) - (2.6659 \times BMF^2) + (2.5923 \times BMF) \tag{III.11}$$

Approximated relationships between burned mass fraction and burned volume fraction from Patterson and Heywood show relatively close results, and therefore, Heywood model is selected because of the simplicity.

III.1.4 TURBULENT INTENSITY MODEL

Turbulence intensity of each operating conditions over a 100 CAD range is extracted from 1-D combustion simulation, which evaluates turbulence using a two equation K-k approach described by Poulos and Heywood [129]. Turbulence intensity is a strong function of mean piston speed for the test engine considered. Similar to previous

researchers Heywood [22] and Prucka [130], a linear relationship between mean piston speed and turbulence intensity was observed. To reduce the computation time, a linear equation of turbulent intensity is fitted based on mean piston speed and validated with the simulation results, and can be expressed in Equation (III.12):

$$u'(i) = c_1 V_{mps} i \tag{III.12}$$

The test engine is not equipped with flow varying actuators, such as charge motion control valves or variable valve timing. For more a more complex engine configuration, a control-oriented turbulence intensity model was developed by Prucka et al. [130]. The model generates a prediction based on engine speed, torque, ignition timing, charge motion control valve position, and variable valve phasing.

III.1.5 LAMINAR FLAME SPEED MODEL

The chemical kinetics and diffusion rates of an air, fuel, and residual gas in a non-moving mixture are commonly lumped into a single parameter called the laminar flame speed. Within turbulent flows there are small length-scales over which convective mixing does not dominate and the flame is assumed to travel at the laminar flame speed. Equation (III.2) captures this concept in the selected quasi-dimensional combustion model as a diffusive burn-up process. Laminar flame speed is a function of residual gas fraction, fuel type, pressure, temperature, and relative fuel-to-air ratio. A semi-empirical model for the prediction of laminar flame speed based on the above criteria was reported by Heywood [22], as shown in the Equation (III.13). The laminar flame speed model will be used as an input to the feed forward combustion duration prediction model in the closed-loop control algorithm for multi-fuel adaptive SI engines. This model is widely

accepted and well-proven for gasoline. Empirical constants for different fuel types are experimental studied, for example, the constants for E85 of this study is taking from Syed et al. [131].

$$S_L = C_1(\frac{T_u}{T_0})^{C_2}(\frac{P}{P_0})^{C_3}(1-C_4 x_d{}^{C_5}) \quad \text{(III.13)}$$

III.1.6 TAYLOR MICROSCALE OF TURBULENCE

Taylor microscale is an assumed length scale over which laminar diffusion occurs; justifying the use of laminar flame speed in the calculation of the mass burn up period Tabaczynski et al. [151]. Taylor microscale of the burn-up eddy is calculated using the below Equation (III.14):

$$\frac{\lambda}{L} = \sqrt{\frac{15}{\xi}}\frac{u'L}{\nu}^{-\frac{1}{2}} \quad \text{(III.14)}$$

III.2 MODEL RESULTS

Combustion model results are obtained from two set of sub models that (i) utilize inputs from 1D combustion simulation results, and (ii) standard engine sensors. It is assumed that the combustion model with inputs from 1D combustion simulation results will provide the best accuracy. A simplified model which only uses standard engine sensors is developed for real-time control purpose and compared to 1D simulation results for validation. Results from simplified real-time model will compare to the high fidelity model.

For high-fidelity combustion model, turbulent intensity results are from 1D combustion simulation; flame front area is calculated using unburned volume fraction from heat release analysis using experimental cylinder pressure data; laminar flame speed and unburned density are calculated through out the combustion with experimental cylinder pressure and unburned gas temperature from two zone heat release analysis. The simplified combustion model uses a linear equation for turbulence intensity from regression fit. Laminar flame speed and unburned density are calculated based on the cylinder pressure and unburned gas temperature determined from intake manifold pressure and temperature assuming polytrophic compression. Flame front area is using a table calibrated with experimental data.

Sub models are also calculated with gasoline and E85 experimental data to investigate the sensitivity of combustion behavior to fuel properties. Comparison of results obtained with high fidelity and simplified sub model with multi fuel sources results are shown in Figure III.3.

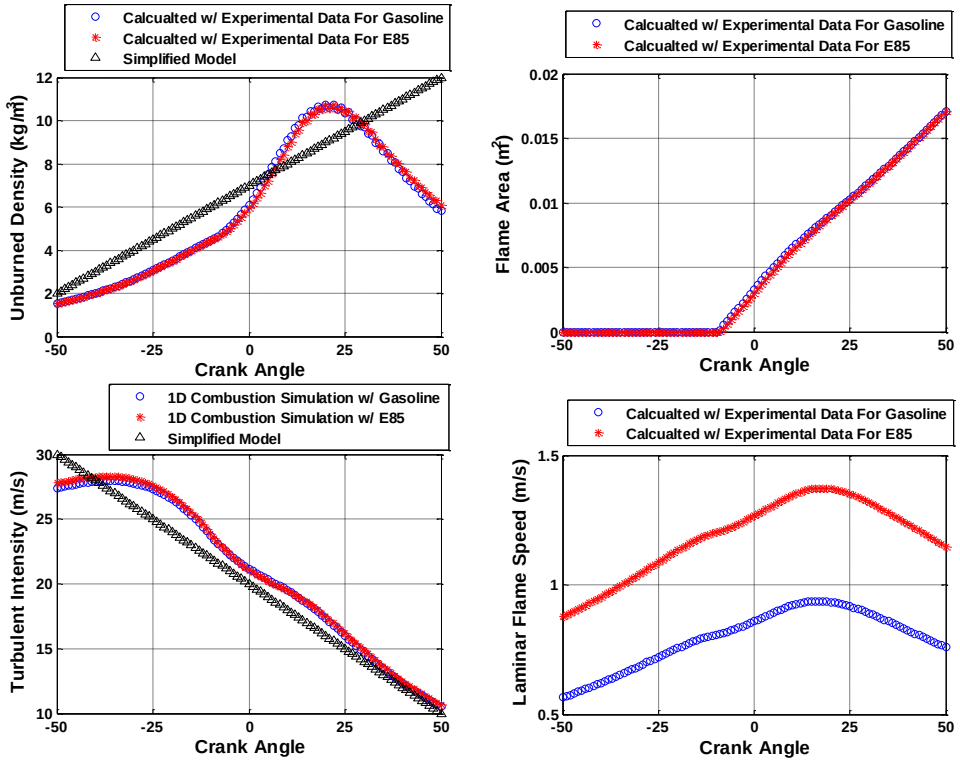

Figure III.3. Results of high-fidelity and simplified sub-models for the turbulent flame entrainment combustion model with gasoline and E85 fuel source, at 2500RPM, 50kpa MAP, 16 CA50, and 11.5% EGR.

The level of in-cylinder turbulence is defined by the root-mean squared velocity fluctuation, called turbulence intensity. Turbulent intensity are mainly related to the gas exchange dynamics of the specific engine, for example, intake runner and port design, combustion chamber design, valve lift and timing strategy etc. Different fuels are likely to have minor effect on the gas exchange dynamics. For example better charge cooling by E85 and results in slightly higher volumetric efficiency. Same results for residual gas fraction can be observed (not shown in the plot) because it is also closely related to gas exchange dynamics.

Unburned density and flame front area are calculated from unburned volume (entrained volume), as shown in Equation (III.4) and (III.9). During mass entrain period described by Equation (III.2), turbulent intensity dominates mass entrain rate because it is an order of magnitude higher than the laminar flame speed. Therefore, unburned density and flame front area have minimal sensitivity todifferent fuel type.

Simplified unburned density model uses Equation (III.8) assuming the rapid distortion theory therefore does not capture the piston motion in the exhaust stroke, nor after the flame front reaches the cylinder wall, piston top or combustion chamber etc.

Flame front area was found to be the most difficult to model, but very important for the combustion model accuracy. It directly reflects the start and the rate of rapid combustion (CA10-CA90), after initial flame preparation (SPK – CA10). In this research, it is calculated inversely from experimental mass fraction burned profile, using physical definition and geometrical assumption of the flame front area to make sure its results as close to the real value as possible. However, this engine specific and operating condition sensitive data table for flame front area prediction scarified the intention of using physics based feed forward model.

Results shown in Figure III.4 demonstrate the prediction of mass entrained and burned profile from simplified turbulent flame entrainment model compared with experimental data. The results are calculated for the combustion events with gasoline and E85 with same combustion phasing (CA50 @ 16). Deviation of the results above CA50 location might be because of the assumptions invalid with simplified unburned density model and spherical flame area.

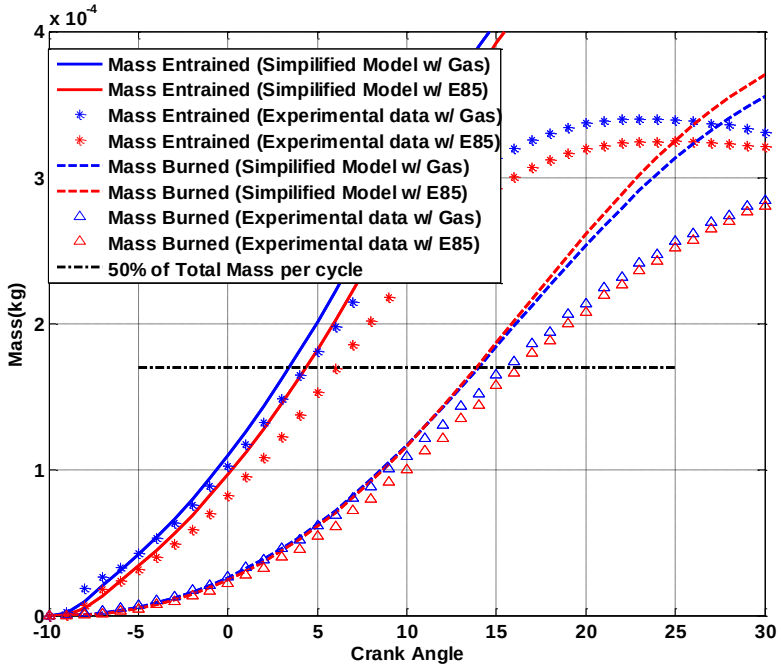

Figure III.4. Mass entrained profiles for same CA50 location from a high-fidelity combustion model, experimental data and simplified real-time model indicate the reasonable accuracy for the simplified model at 2500RPM, 50kpa MAP, 16 CA50, and 11.5% EGR.

As discussed above, the fuel sensitive nature of the turbulent flame entrainment model makes it ideal for multi fuel engine model based spark timing control. Prediction for combustion duration results over a wide range of engine operating points with two fuel inputs are shown in Figure III.5.

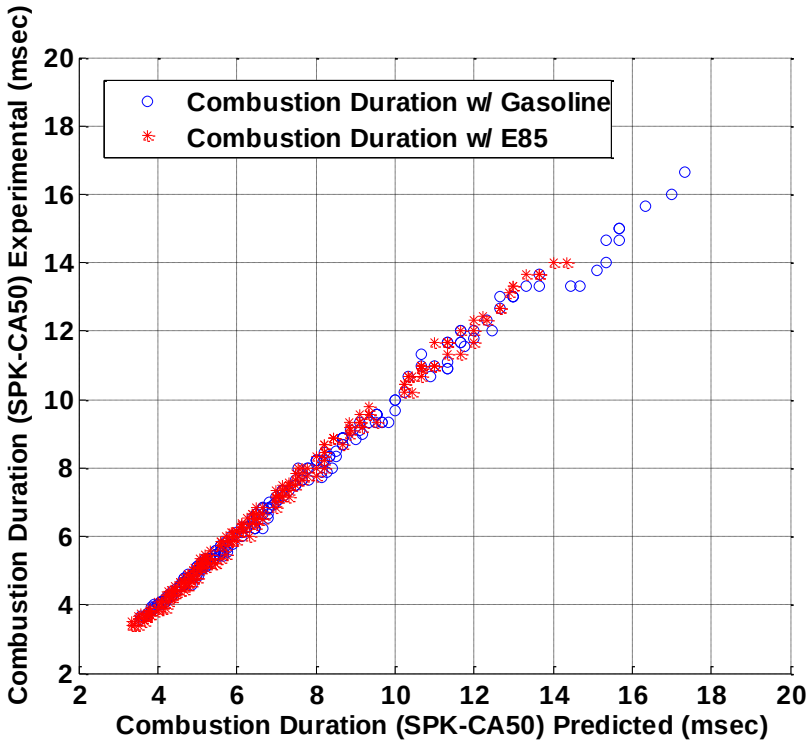

Figure III.5. The combustion duration prediction from simplified real-time model is able to match the experiments results

Root-Mean-Square-Deviation (RMSD) is used to quantify the performance of the turbulent flame entrainment model accuracy, results as shown in Table III.1. A good agreement of the model results with experimental data is observed.

Table III.1. RMSD of the simplified turbulent flame entrainment model results compared with experimental data

RMSD	Time basis (ms)	CAD basis (CA)
Gasoline	0. 274	1.32
E85	0. 199	1.19

III.3 CONCLUSION

Quasi-dimensional turbulent flame entrainment combustion duration models have been studied for real-time feed forward spark timing control of multi-fuel adaptive SI engines. The turbulent flame entrainment model shows an excellent accuracy for reconstructing the mass fraction burned during combustion. RMSD analysis of the model results showing the physics based approach realized around 1.3 CAD deviations in combustion duration prediction from spark to CA50 of both gasoline and E85. However the quasi-dimensional combustion model will be limited by:

- In-cylinder conditions are too computational intensive to predict after the start of combustion.
- Accuracy of sub-models such as flame front area and unburned density will need good understanding of in-cylinder flow pattern, 3D geometry shape of the combustion chamber and crank angle resolution heat release analysis.
- Crank angle resolution of the burn rate will be unnecessary for just the spark timing prediction.

IV VIRTUAL SENSING OF FUEL PROPERTIES

This virtual fuel property sensor aims to assist the development of model-based adaptive combustion phasing control strategies for multi-fuels engines through feedback of fuel property information. The selection of an optimal ignition timing to satisfy a desired combustion phasing can only be determined if an accurate estimate of combustion duration can be calculated prior to ignition. Burn duration for a given set of in-cylinder conditions is a function of many factors (e.g. air-to-fuel ratio, residual gas fraction, charge motion, pressure, temperature, fuel type, coolant temperature, etc.), and accurate predictions or measurements of each are required for robust combustion phasing control. The focus of this research is fuel property sensing because it has been shown to have a significant influence on spark-ignition engine combustion.

The fuel property that primarily influences combustion rate can be described by laminar flame speed. Laminar flame speed is a function of residual gas fraction, fuel type, pressure, temperature, and relative fuel-to-air ratio. A semi-empirical model for the prediction of laminar flame speed based on the above criteria was reported by Heywood (1988, p. 403). This model is widely accepted and well-proven for gasoline, but the empirical constants for most new fuel types are not available. Experimental data of different fuel sources will be used to generate estimates of these empirical constants.

The fuel property sensing routine does not assume that fuel types are known. Rather, it considers the possibility that unknown fuel blends (bio-fuel, or others) could be introduced to the market after initial development and calibration of the engine control system. The multiple fuel sources can be blended together based on the availability,

regulation or market drivers. In this case, it would not be possible for calibrators to test all the available combinations of fuels prior to release of the engine in the marketplace. The proposed virtual sensing method determines laminar flame speed based on the fuel behavior instead of the actual fuel type; therefore simplifying the calibration process of the multi-fuel adaptive engines.

IV.1 ASSUMPTIONS AND MODEL DERIVATION

Several assumptions are required to extract a laminar flame speed estimate from cylinder pressure data using an inverse-combustion model when fuel type is changed. The key consideration is that spark-ignition engine combustion rate is primarily dictated by chamber geometry, turbulent flame entrainment rate, and the laminar flame speed of the mixture during burn-up and the quasi-dimensional turbulent flame entrainment model characterizes each of these phenomena. The influence of a fuel change on combustion must be isolated from other possible changes (e.g. residual gas fraction, charge motion, etc.) to avoid attributing changes in burn-rate caused by non fuel-related factors to the fuel itself. To do this, it is assumed that both residual gas fraction and turbulence intensity remain largely unchanged when fuel type is altered.

Internal residual gas content is mainly affected by intake and exhaust pressure and dynamics, engine speed, compression ratio and valve timing. When the intake valve opens there is some backflow of combustion products into the intake port, this part of the burned mass will be brought back into the cylinder by fresh mixture. This exhaust

residual together with the left over combustion products at the end of the exhaust valve closing, comprise the total residual gas mass.

Generally speaking, residual gas dynamic is related primarily to gas exchange process, which has very weak relationship with fuel type. On the other hand, fuel type might have different charge cooling effect on the volumetric efficiency that will alter the gas exchange dynamics. Mixture density might be different because of different stoichiometric ratio, and this can result in different residual gas mass. However it can be normalized in the residual gas fraction (ratio of residual gas mass to total mass of charge) representation. Residual gas fraction results obtained from GCA, as shown in Figure IV.1, suggested fuel type has minimally influence on the residual gas level.

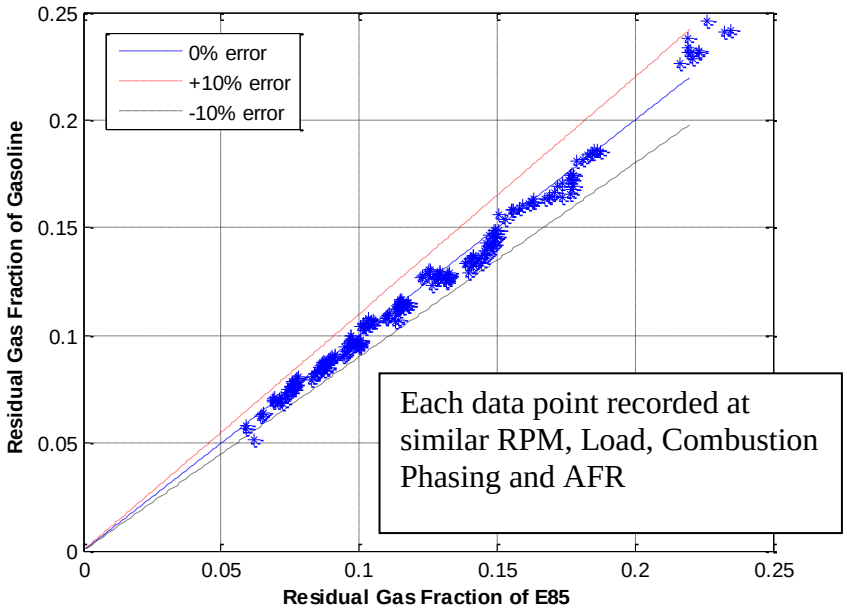

Figure IV.1: Experiments suggest residual gas fraction levels are not significantly influenced by fuel type.

The level of in-cylinder turbulence is defined by the root-mean squared velocity fluctuation, called turbulence intensity. Previous researchers have demonstrated that turbulence intensity scales linearly with mean piston speed (MPS) [130] for fix valve actuation system. Turbulence intensity is the quantification of in-cylinder charge motion. Therefore no correlation with fuel type will be expected. Turbulence intensity results, as shown in Figure IV.2, are calculated using a two equation K-k approach [129] which will be explained in the following chapter.

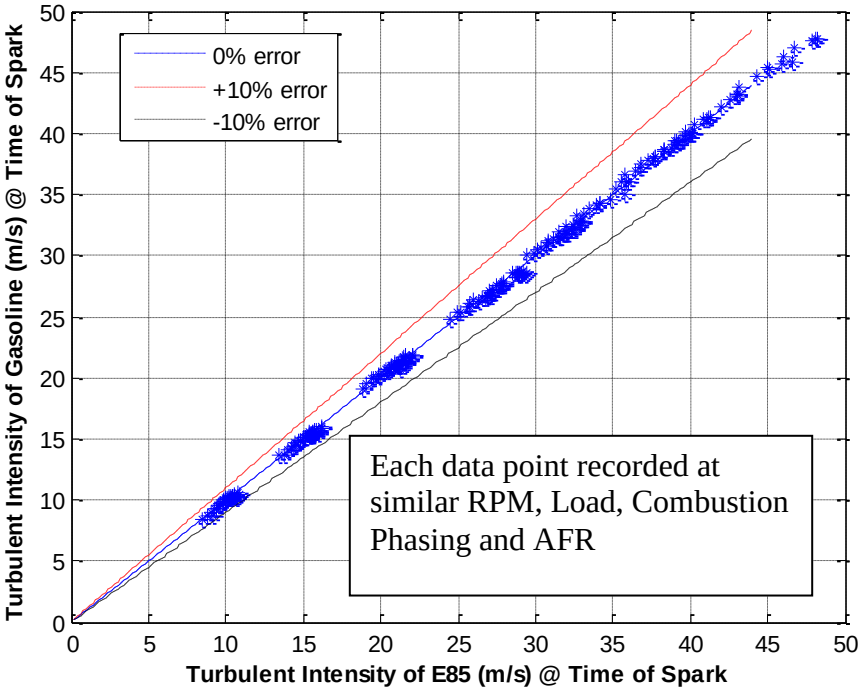

Figure IV.2: Experiments suggest turbulent intensity levels are not significantly influenced by fuel type.

Two further simplifications are made to the prediction model to reduce computational complexity (1) during the flame entrainment period the influence of laminar flame speed can be neglected because it is one order of magnitude smaller than

turbulent intensity, and (2) the flame front thickness is low and can be ignored. The ratio of flame thickness to flame radius is close to 0.1 during early combustion, as documented by several studies of initial flame kernel development [134][135][136][137][138]. Therefore the flame front area can be simplified to burned volume front area. Flame thickness is calculated by knowing the difference between the burned volume radius and entrained volume radius assuming spherical pattern. Model detail will be explained in the following chapter. The inverted and simplified flame entrainment model for virtual laminar flame speed calculation is shown as Equation (IV.1).

$$S_L = lm \frac{dm_{burned}}{dt} \Big/ \int \rho_{unburned} A_{burned} u' - m_{burned} \tag{IV.1}$$

The fuel property sensing method works by comparing the burn rates between two different fuels (a baseline and a test fuel) operating with similar boundary conditions (i.e. engine speed, load, relative air-to-fuel ratio, and ignition timing). When burn-rate is observed to be different from a baseline value (e.g. gasoline), as shown in Figure IV.3. The measured burn rate will be analyzed with the inverse-combustion model, as described in Equation (IV.1), and a new laminar flame speed estimate will be calculated using the methods described in the following sections.

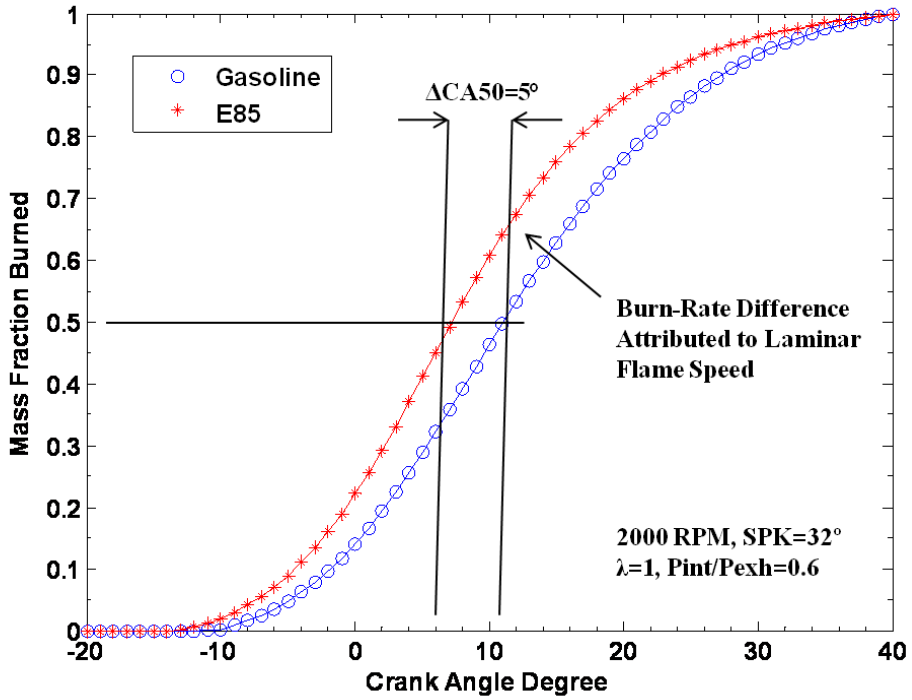

Figure IV.3: With similar boundary conditions two fuels demonstrate different combustion characteristics.

IV.2 VIRTUAL FUEL PROPERTY MODEL INPUTS CALCULATION

Virtual fuel property model structure can be described in Figure IV.4. Model requires four primary inputs; (1) unburned charge density, (2) flame front area, (3) turbulence intensity, and (4) Taylor microscale of turbulence. Each of these inputs has specifically designed sub-models to predict their values throughout the engine operating range in real-time. Description of each model is provided in the quasi-dimensional model basic chapter.

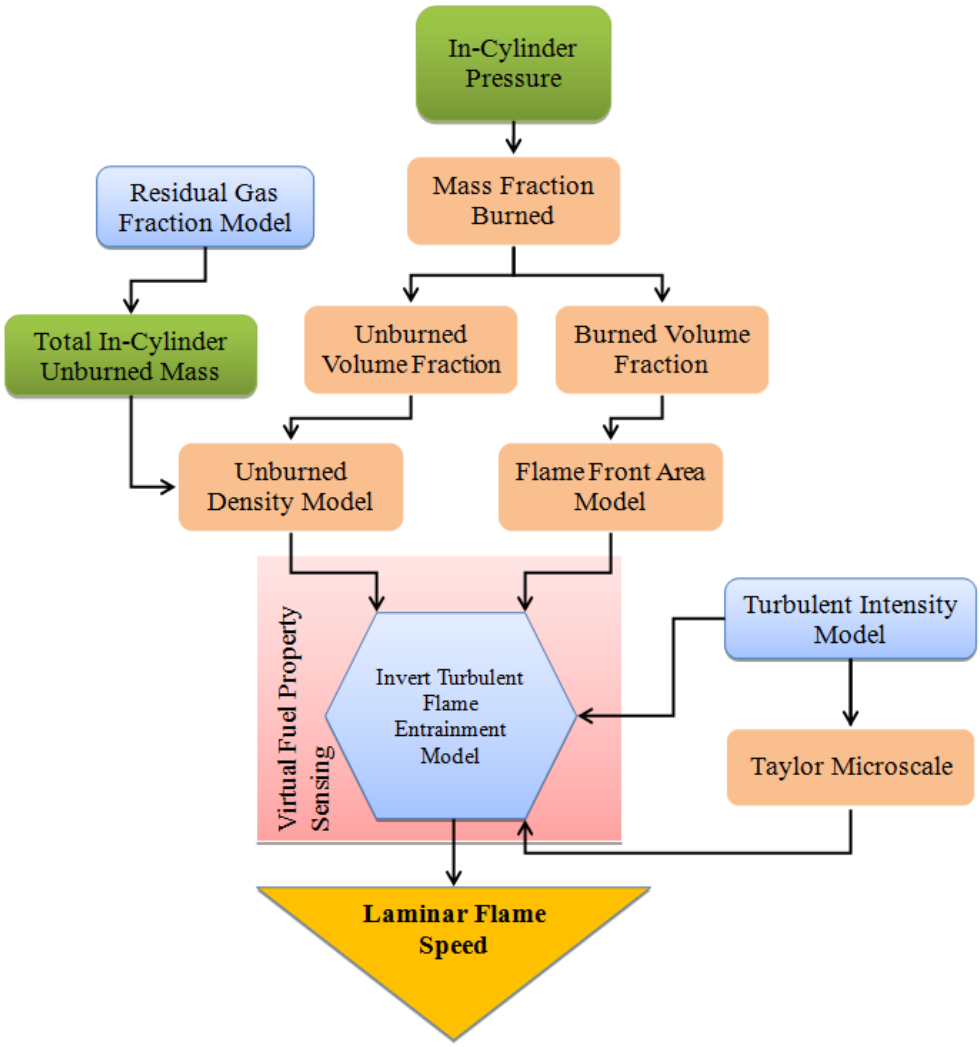

Figure IV.4: Structure of virtual fuel property sensor.

IV.3 LAMINAR FLAME SPEED MODEL

Chemical kinetics and diffusion rates of air, fuel, and residual gas in a non-moving mixture are commonly lumped into a single parameter called the laminar flame speed. Within turbulent flows there are small length-scales over which convective mixing does not dominate and the flame is assumed to travel at the laminar flame speed. Laminar flame speed is a function of residual gas fraction, fuel type, pressure,

temperature, and relative fuel-to-air ratio. A semi-empirical model for the prediction of laminar flame speed based on the above criteria was reported by Heywood [22], as shown in the Equation (IV.2). The laminar flame speed model will be used as an input to the feed forward combustion duration prediction model in the closed-loop control algorithm for multi-fuel adaptive SI engines. This model is widely accepted and well-proven for gasoline. Empirical constants for other fuel types are experimentally determined, and the constants for E85 in this study were reported by [131].

$$S_L = C_1(\frac{T_u}{T_0})^{C_2}(\frac{P}{P_0})^{C_3}(1-C_4 x_d{}^{C_5}) \quad \text{(IV.2)}$$

IV.4 LAMINAR FLAME SPEED OBSERVER VALIDATION

Observer results are validated using Equation (IV.1) with two sets of empirical constants for gasoline (Heywood [22]) and E85 (Syed et al.[131]). Inputs to the prediction model (e.g. pressure, unburned gas temperature and residual gas fraction) are calculated from experimental data to ensure the results are able to accurately represent the laminar flame speeds of the fuel source. The observer model calculates the laminar flame speed based on the proposed method and cylinder pressure data from engine experiments. Estimates are made assuming a known fuel (gasoline or E85) as baseline and laminar flame speed is calculated for the other fuel. Therefore, validation of the observer can be carried out for feedback of laminar flame speed for both gasoline and E85, as shown in Figure IV.5. Overall 440 data points (see engine test point description) are selected for observer validation. Each of the data points represents an average of 500 consecutive cycles, which minimizes the influence of combustion variability. The process

demonstrates accuracy, based on Root-Mean-Square-Deviation (RMSD), for all gasoline data points of 1.27 (cm/s) and 2.17 (cm/s) for E85. Validation results also show that observer accuracy is not influenced by operating conditions.

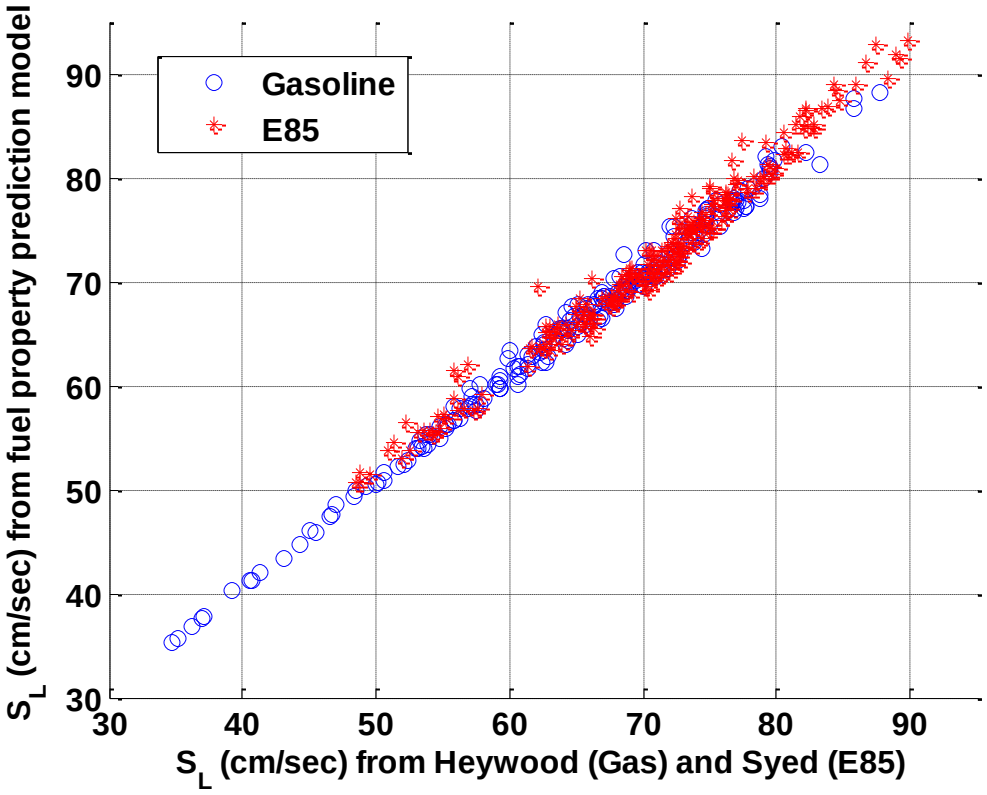

Figure IV.5: The laminar flame speed model predicts the experiment calculation with an RMSE of less than 2.2 (cm/s)

IV.5 Real-Time Laminar Flame Speed Model Re-calibration

The observer feedback algorithm consumes a relatively large amount of computing power which may limit it to off-line (non real-time) use. The observer algorithm may only need to run when fuel properties are expected to change (e.g. after a

refuelling event). Additionally, the best time for sensing laminar flame speed is when engine is at idle or low engine speed conditions. Recall in Equation (III.1) that turbulent intensity normally is one order of magnitude greater than laminar flame speed especially at high engine speed range. The dominate influence of turbulence intensity on combustion may reduce observer sensitivity to laminar flame speed as engine speeds increase.

The power law model for laminar flame speed (Equation (IV.2)) contains five empirical constants for each fuel type. Current research [131] suggests that variation of certain constants between gasoline and ethanol is insignificant, especially for the residual gas dilution terms (C4, C5). However, the proposed research aims to develop a method that is valid for other fuel types (beyond gasoline and E85) as well as any blend ratio of these available fuel sources. Further simplification was avoided in this research because the coefficients of new fuel types may vary significantly from those of gasoline or E85.

Re-calibration of laminar flame speed model empirical constants (Equation (IV.2)) is important for physics-based feed-forward control purposes. This process is performed by using several distinct operating points (i.e. several different load and speed points) and inverse-fitting the unknown constants based on the laminar flame speed observer feedback. The re-calibration method is based on an unconstrained nonlinear minimum small scale search of a multivariable function using a derivative-free method. The number of optimization iterations is set to 1000 (200*number of variables), which roughly takes one second to process on a desktop with a Quad core 2.66 GHz CPU.

A study of the number of distinct feedback data points versus accuracy of the re-calibration method is discussed below. Each of the distinctive data points is randomly picked within the entire test point map. A comparison of the re-calibrated constants and number of available feedback data points is provided in Table IV.1, assuming fuel type switching from gasoline to E85. Initial guesses are constants for gasoline and the recalibrated results are compared with the original constants for E85. Re-calibration accuracy also depends on the data point selection, so laminar flame speeds are first generated using the re-calibrated constants for all engine test points. Then, new results are compared to the original model. An error bar map of RMSD is shown in Figure IV.6 with different selections of data points. It is shown that accumulation of approximately 40 data points is sufficient. Results from the re-calibrated model have an average deviation of 2.73 cm/s (less than 5% error) compared to its original model. Finally the re-calibrated laminar flame speed model results are plotted against the original model, as shown in Figure IV.7.

Table IV.1: Five empirical constants comparison between the available numbers of cycle feedback

Coefficient	C1	C2	C3	C4	C5
Initial guess	30.5	2.129	0.217	2.06	0.77
Original model	48.2	1.9	-0.38	1.5	0.66
5 data points	49.8	1.6	-0.36	5.3	1.38
20 data points	48.2	1.9	-0.32	1.5	0.58
40 data points	52.6	1.6	-0.32	1.8	0.80

80 data points	50.0	1.58	-0.32	2.79	1.066
220 data points	50.2	1.74	-0.35	2.08	0.846

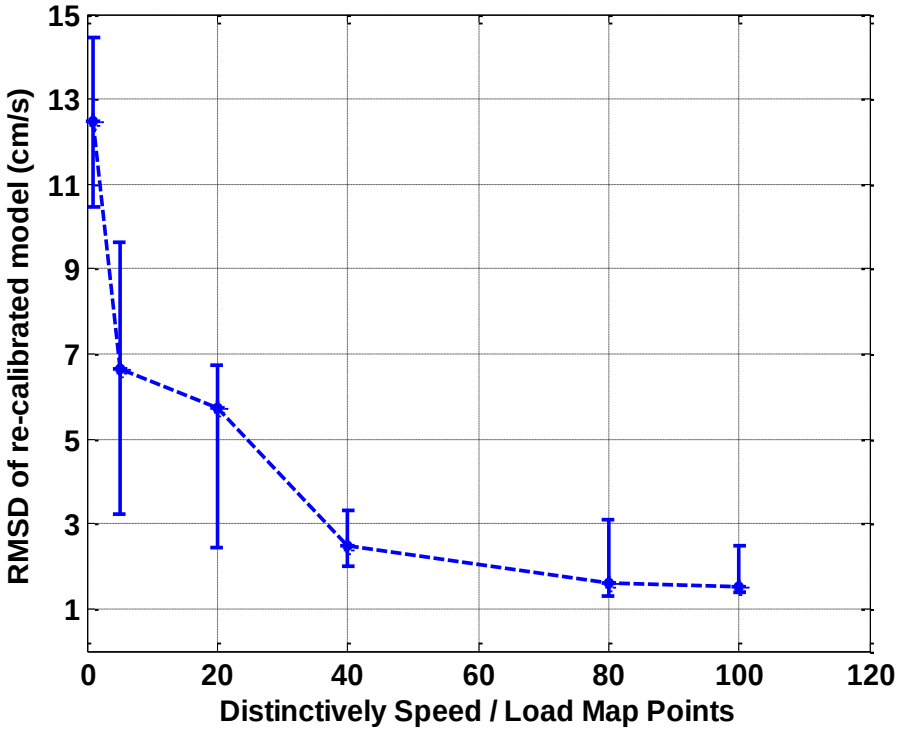

Figure IV.6: Root-Mean-Square-Deviation of the re-calibrated model comparison between the available numbers of data point feedback

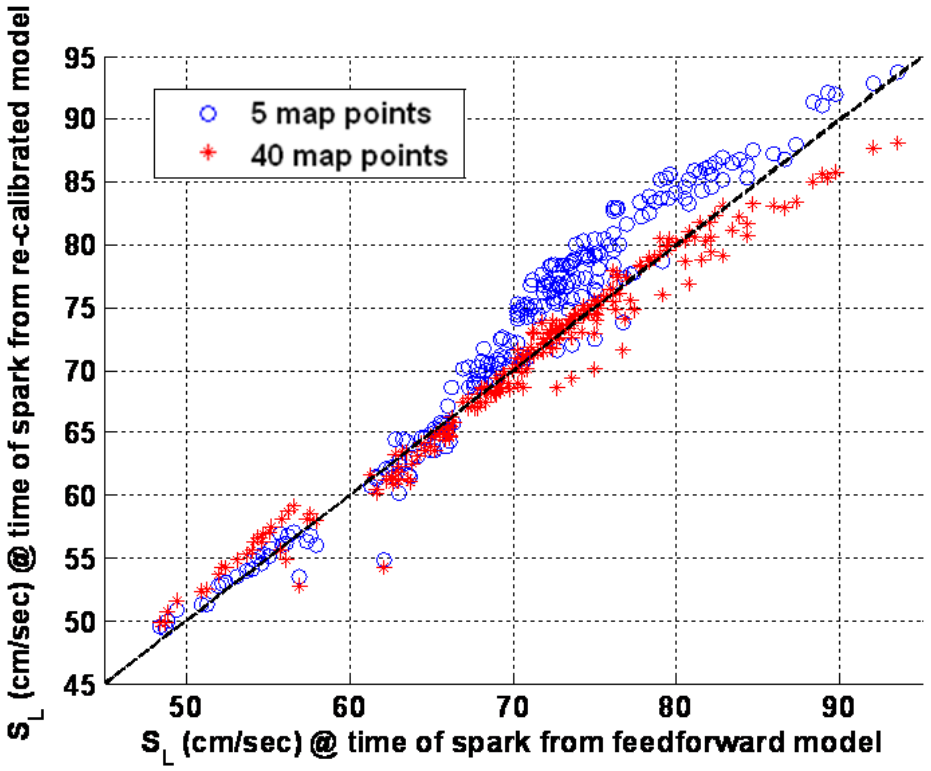

Figure IV.7: Validated results of laminar flame speed re-calibrated model compared to the original prediction model

IV.6 SUMMARY AND CONCLUSIONS

In this chapter, a simplified modeling approach is carried out to investigate a new concept of fuel property sensing for multi-fuel adaptive SI engines. The sensorless virtual fuel property sensing routine utilizes a simplified quasi-dimensional flame entrainment combustion model, and calculates laminar flame speed based on the derivation of the burn rates from baseline. A method for re-calibrating a feed-forward laminar flame speed prediction model is also investigated. Results and findings are summarized as follows:

The virtual fuel property sensor (observer) is able to calculate laminar flame speed for a wide range of operating conditions with RMSD of 1.27 (cm/s) for gasoline and 2.17 (cm/s) for E85.

Re-calibration of the feed forward laminar flame speed prediction model with 5 constants has been investigated for accuracy and response time. Using 40 distinct engine operating points as feedback for re-calibrating the 5 unknown constants is able to reproduce laminar flame speed for wide range of operating conditions with RMSD of 2.73 (m/s). This represents less than 5% error to well-known values.

V COMBUSTION PHASING TARGET ADJUSTMENT MODEL

Feed-forward model-based ignition timing control requires a target combustion phasing for proper calibration, generally based on CA50. The optimal CA50 location (MBT timing) is a balance between early combustion (high heat losses) and late combustion (high expansion losses). For combustion with low octane number fuel sources, the best CA50 location may also be limited by abnormal combustion (spark knock). Based on compression ratio or boost level, the desired combustion phasing will be determined by the calibrator for a particular engine with a known fuel source. When fuel type is altered (e.g. gasoline to E85) the engine can be subjected to a different octane number, requiring an updated CA50 target in the 'knock region' to avoid mechanical damage and still maintain high thermal efficiency.

To speed up this process a feed-forward knock prediction algorithm is desired in the multi-fuel adaptive engines because of the possible wide range of fuel property variations. Spark knock is the consequence of auto-ignition in the unburned end-gas ahead of the propagating spark ignited flame front. The auto-ignition characteristic therefore is greatly related to the octane rating of the fuel source and governed by composite chemical reactions under the time history of temperature and pressure of the unburned end gas. Auto-ignition models [108]-[111] are available with a wide variety of fidelity options. Two other fuel properties of particular interest for knock control are; 1) laminar flame speed that describes the potential mass burn rate which can reduce the time scale of the end-gas exposure prior to combustion, and 2) fuel heat of vaporization which alters charge cooling effects and unburned mixture temperatures.

This chapter aims to eliminate the drawbacks of knock feedback control by developing a feed-forward prediction model for multi-fuel adaptive SI engines, and to generate a combustion phasing adjustment map in the knock region for model based ignition control. A semi-physical virtual octane sensor and laminar flame speed observer are used for fuel property feedback. A knock prediction model, based on an Arrhenius function combined with a quasi-dimensional turbulent flame entrainment combustion model, is described that identifies the limits of the knock region for a given fuel. The combustion duration model is used to calculate in-cylinder thermal conditions for a range of operating points in the knock region. Calculated in-cylinder thermal conditions are analyzed with a knock correlation that accounts for the negative temperature coefficient and air/fuel ratio. The model then calculates the "best achievable" combustion phasing at discrete points in the knock limited region and updates the target CA50 map accordingly. The routine operates off-line once the fuel octane number/fuel properties are observed to have changed and re-calculates desired combustion phasing targets. The method is shown to be capable of predicting desired combustion phasing for the entire knock region based on feedback from a single operating point. Experimental measurements are used to correlate and validate the routine using both gasoline and E85.

In order to calculate the "best achievable" combustion phasing target, knock limits must be determined for a particular engine with current fuel source. A wide range of bio-fuel sources might be blended together in future multi-fuel adaptive engines. Therefore, two virtual fuel behavior sensors are placed in the control algorithm to feedback octane number and laminar flame speed of the mixed fuel source. Octane number describes the ability of the fuel source to withstand compression before

detonating. Laminar flame speed represents the fuel property that affects combustion burn rates. The quasi-dimensional turbulent flame entrainment model generates mass burned rates off-line for different combustion phasings at each engine operating condition (e.g. RPM, MAP). The first Law of Thermodynamics and heat release analysis is used to reconstruct cylinder pressure and unburned gas temperature profiles for each predicted combustion phasing. Then, the predicted in-cylinder thermodynamic conditions are used in the Livengood & Wu integral [109] to analyze if knock will occur at each particular combustion phasing. Finally the algorithm identifies the achievable combustion phasing closest to MBT timing and generates the updated CA50 target for model based spark timing control. The off-line "what if" algorithm for determining the "best achievable" combustion phasing is shown in Figure V.1. Each component of the described algorithm will be explained in the following sections.

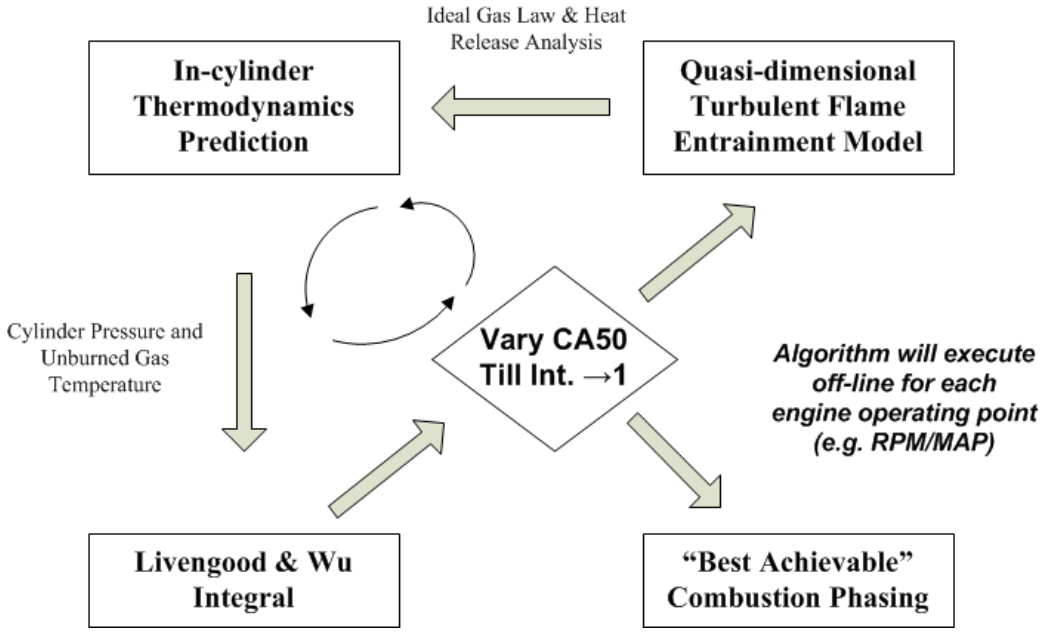

Figure V.1. Off-line "what if" algorithm for determine the "Best achievable" combustion phasing in the knock region when the fuel source is altered.

V.1 AUTO-IGNITION MODELING AND PREDICTION

Various levels of sophistication for auto-ignition characteristic modeling are available, from comprehensive chemical kinetic simulations [108], to a global single step Arrhenius function that describes all hydrocarbon oxidation reactions [109]. Reduced chemical kinetics descriptions are also available [110]. In the above methods, the single step Arrhenius function is recognized as the most practical way of predicting the ignition delay for control purposes because of its simplicity and relatively good physical representation [111]. It is widely studied based on experimental data for auto-ignition prediction in constant volume bombs, steady flow reactors, rapid compression machines and IC engines [139]-[140].

Phenomena for ignition delay are observed both experimentally, in rapid compression machines (RCM) [141] and in detailed chemical kinetics simulations [142]. Typical results for gasoline are shown in Figure V.2. This figure demonstrates monotonic behaviors in the cool flame ignition delay region on the upper right, the intermediate region of negative temperature coefficient (NTC) behavior and the high temperature ignition region in the lower left hand corner [143]. Auto-ignition generally occurs when the unburned gas reaches around 900K to 1000K, where the NTC behavior is observed. Therefore, it is important for the knock prediction/auto-ignition delay model to capture this phenomenon.

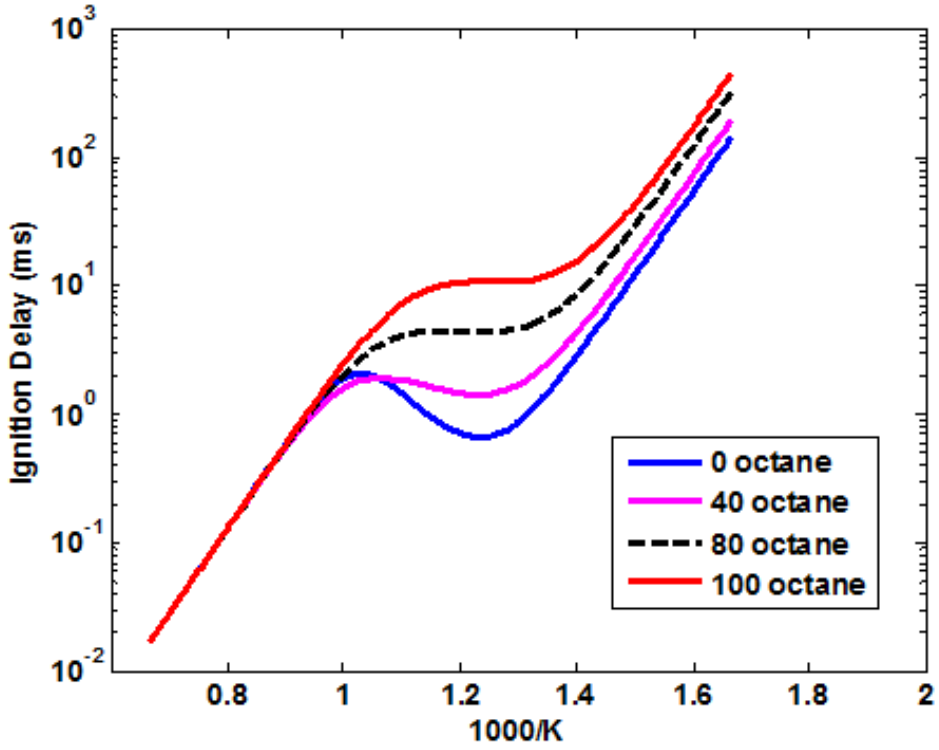

Figure V.2. Yates et al. 2008 developed coefficients for ignition delay correlation which take into consideration different octane numbers of current gasoline fuel.

A typical commercial automotive gasoline contains approximately seven hundred types of molecules [143]. For highly detailed chemical kinetic modeling ignition characteristics of each individual molecule in the temperature and pressure domain is required. This information is rarely available and time consuming to calculate, so a global reaction that describes all the hydrocarbon oxidation processes in a single-step Arrhenius function is favored in this research. The equation relates the rate of reaction of an auto-ignition product as a function of pressure and temperature, assuming single-step chemical kinetics:

$$\frac{d(x)}{dt} = A_G^{'}(X)p^n \exp(-\frac{B_G}{T}) \quad \text{(V.1)}$$

The ignition delay, in milliseconds, can be expressed as the inverse of the reaction rate of the global single-step mechanism:

$$\tau_G = A_G p^{-n_G} e^{(\frac{B_G}{T})} \quad \text{(V.2)}$$

Equation (V.2) is developed to represent the ignition delay in a RCM with coefficients extracted from experimental data. In a RCM, the pressure is assumed approximately constant until combustion occurs. However, for a spark-ignited engine, the end gas is compressed by the propagating flame and the temperature rises following a polytropic process. Livengood and Wu [109] proposed that the end gas auto-ignition chemistry is cumulative and can be predicted by integrating the reaction rate of the end gas at discretized pressure and temperature time steps until the critical time when the integral value is equal to one, as shown in Figure V.3.

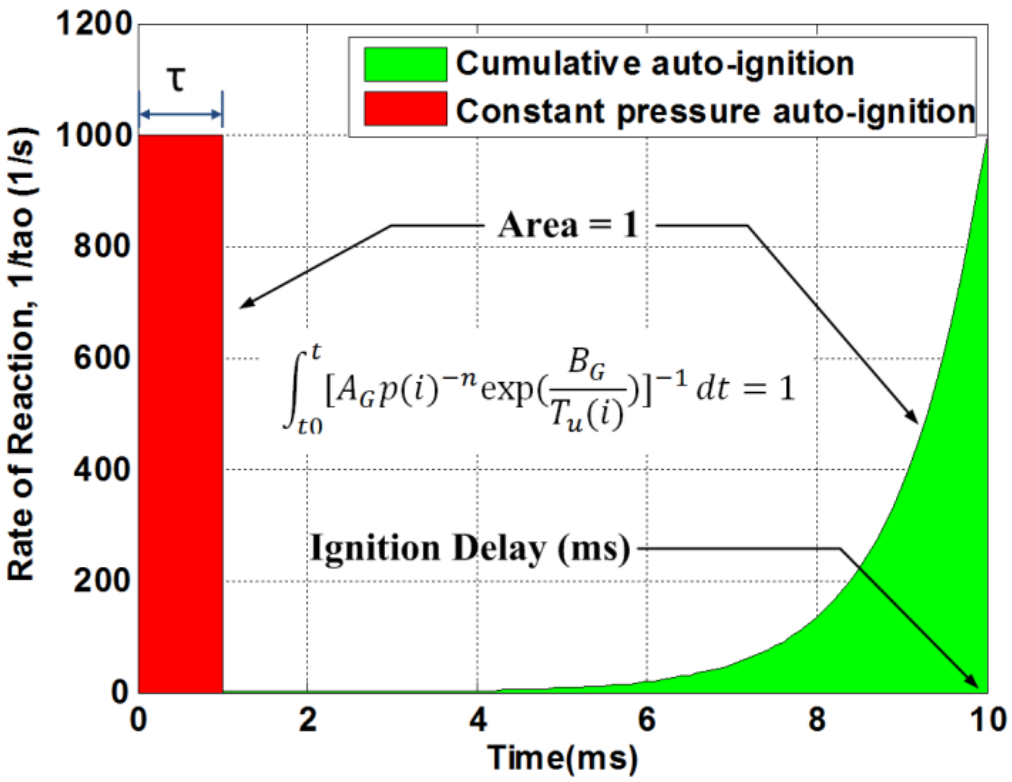

Figure V.3. Illustration of the Livengood-Wu Integral for predicting auto-ignition in a changing pressure and temperature environment

Several researchers have fit coefficients of the L-W integral by polynomial regression to a chemical kinetic model for ignition delay prediction [144][143][145]. These techniques are empirical, but have proven capable of adapting to changing octane number. Their model results, shown in Figure V.2, provide a good correlation to the experimental/physical system and are chosen for this research.

V.2 Reconstruction of In-Cylinder Thermodynamic Conditions

Off-line knock event prediction is done by a "what if" analysis using the predictive turbulent flame entrainment combustion model which can generate mass burned profiles for each combustion phasing at each operating condition.

Thermodynamic conditions such as cylinder pressure and unburned gas temperature are calculated based on the ideal gas law and heat release approach. Then, the re-constructed pressure and temperature are analyzed through the Arrhenius function to predict if the engine will knock at the assumed operating conditions.

In-cylinder pressure is first calculated assuming polytropic compression from the intake manifold pressure at IVC to the time of spark, using Equation (V.3). Polytropic coefficients are determined based on the experiment value and stored in a Look-Up table.

$$P_{cyl,\theta} = P_{MAP}(\frac{V_{IVC}}{V_\theta})^n \tag{V.3}$$

Then the heat release differential Equation (V.4) is solved with the cylinder pressure initial conditions from Equation (V.3).

$$\frac{dp_{cyl}}{d\theta} + \frac{r}{V_{cyl,\theta}}\frac{dV_{cyl}}{d\theta}P_{cyl,\theta} = \frac{r-1}{V_{cyl,\theta}}(\frac{dQ_g}{d\theta} - \frac{dQ_{ht}}{d\theta}) \tag{V.4}$$

Knowing the mass burned fraction xb from the prediction combustion model, gross heat released at each crank angle is calculated using Equation (V.5), assuming perfect mixing (indicated fuel conversion coefficient = 1).

$$Q_{gross,\theta} = \eta_{f,i} m_f x_{b,\theta} Q_{LHV} \tag{V.5}$$

Convection heat transfer, shown in Equation (V.6), is considered the main loss during combustion.

$$Q_{ht} = hA(T_{burned} - T_{wall}) \tag{V.6}$$

Heat transfer coefficient h obtained from Woschni [156] correlation:

$$h = \frac{C_0 P_{cyl}^{0.8}}{V^{0.06} T_{burned}^{\ 0.4}} (v_{piston} + 1.4)^{0.8} \tag{V.7}$$

Dual-zone cylinder mixture unburned and burned temperatures are calculated assuming isentropic compression, and known values of p, V, mf and heat release rates:

$$T_{(unburned,\theta)} = T_{IVC} \left(\frac{P_\theta}{P_{IVC}}\right)^{\frac{n-1}{n}} \tag{V.8}$$

$$T_{burned,\theta} = \frac{R_{unburned}}{R_{burned}} T_{unburned,\theta} + \frac{P_\theta V_\theta - mR_{unburned} T_{unbrned,\theta}}{mR_{burned} x_{burned}} \tag{V.9}$$

V.3 VIRTUAL OCTANE SENSING

Octane number of the currently used fuel source is needed for off-line knock event prediction. Depending on the available sensor setup, different approaches can be selected to sense the octane number virtually. Important information for the octane sensing routine is the "time" from start of combustion (spark) until the unburned end gas auto-ignites. The end gas "ignition delay" can be obtained from an in-cylinder pressure sensor, if equipped, or an advanced knock sensor that can sense the first start of knock and calculate the ignition delay from the known value of spark timing.

An inverse Livengood-Wu [109] integral is formulated using Douaud & Eyzat [140] coefficients, assuming the integral of in-cylinder pressure and unburned temperature over the "ignition delay" period is equal to one when knock occurs. The pressure trace can be obtained from the combustion model (or a real-time in-cylinder pressure sensor based on availability) and unburned temperature is calculated using Equation (V.10).

$$ON = 100\left\{\frac{1}{17.68}\int_{t_{SPK}}^{t_{Knock}}\left[P_{cyl}(t)^{-1.7}\exp\left(\frac{3800}{T_{unburned}(t)}\right)\right]dt\right\}^{-\frac{1}{3.402}} \quad \text{(V.10)}$$

The Douaud & Eyzat coefficients do not capture the NTC behavior, therefore the results from Equation (V.10) are aimed to represent the "anti-knock" behavior of the currently used fuel instead of the actual octane number of the fuel source.

V.4 KNOCK PREDICTION VALIDATION

Mild and heavily knocking cases, as shown in Table V.1, from experimental engine data are selected to validate the in-cylinder thermodynamic reconstruction algorithm and knock event prediction.

Table V.1. Mild and heavily knocking cases for validation of off-line knock prediction at 900 RPM, WOT, stoichiometric air/fuel ratio and 87 octane gasoline.

	Cas	Case
CA50	17	30
Knock	4	20

Reconstructed cylinder pressure and unburned gas temperature for case 1 and case 2 are shown in Figure V.4. Results indicated reasonable accuracy for both combustion phasing.

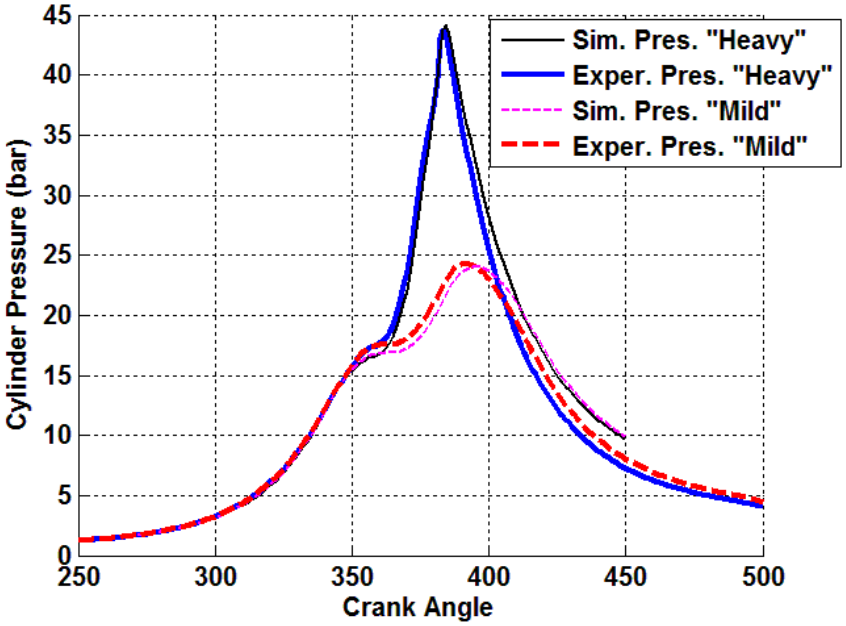

(a)

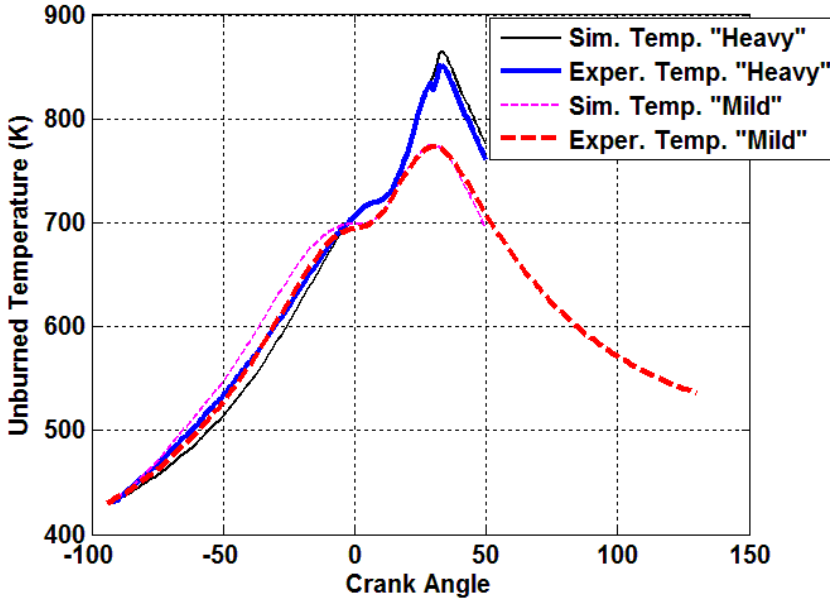

(b)

Figure V.4. Comparison of measured and reconstructed in-cylinder conditions for (a) cylinder pressure and (b) unburned temperature show reasonable accuracy.

Pressure and temperature data from case 1 is analyzed with Livengood-Wu integral using both Yates and Viljoen [144] and Douaud & Eyzat [140] coefficients, as shown in Figure V.5. Half crank angle resolution cylinder pressure data is processed with an 11kHz cutoff frequency high pass filter to indicate the start of knock. L-W integral results using Yates and Douaud & Eyzat coefficients are observed to have 10 CAD difference in predicting the start of auto-ignition. Douaud & Eyzat coefficients predict shorter ignition delays in the low temperature region compared to the Yates and Viljoen coefficients. Douaud & Eyzat coefficients correlate the start of knock event to the first moderate peak of the high passed cylinder pressure data and Yates coefficients capture the second severe rise. For the purpose of this research, the accuracy of both approaches is acceptable, and Douad & Eyzat method is selected for its simplicity. L-W integral results for case 2 show a tendency of the final value to approach one. A "confidence level" of the integral results can be implemented into the algorithm that lowers the criteria for the knock event correlation. For example, instead of the integral being equal to one indicating auto-ignition; the criteria can be adjusted to 0.9 or lower for conservative purposes.

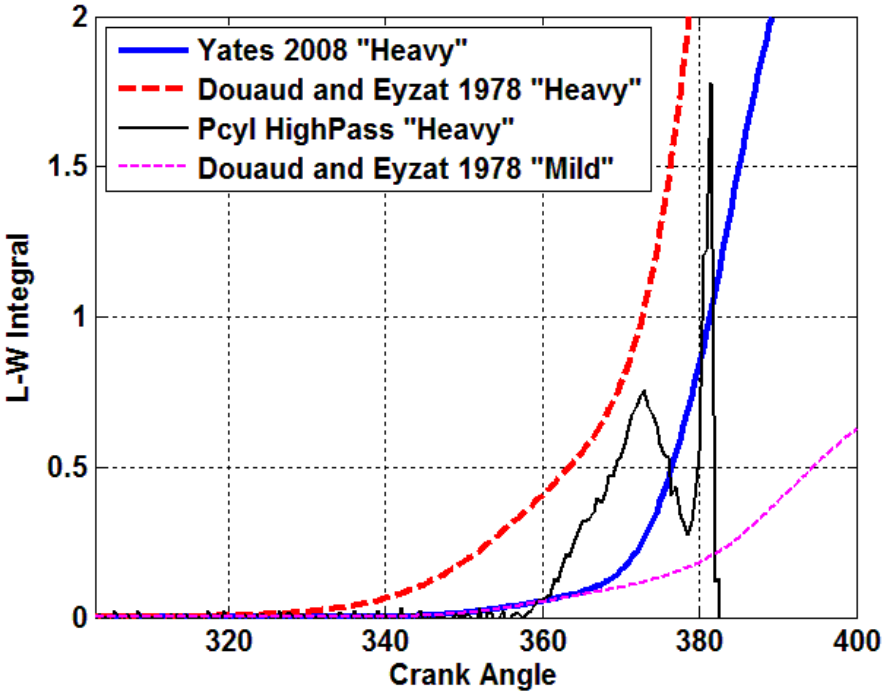

Figure V.5. Comparison of Livengood-Wu integral using multiple coefficient models for engine combustion with knock intensity at 20 (bar) and 4(bar).

V.5 ACHIEVABLE COMBUSTION PHASING MAP

In this research, the desired combustion phasing in the knock limited region is of particular interest because it will be significantly different if the fuel source input is altered. The proposed algorithm was used to perform a CA50 sweep at each engine operating point using an assigned MBT timing. Combustion phasing will be retarded on a 2CA interval if a knock event is predicted. The achievable CA50 map generated with 87 octane gasoline fuels for the test engine is shown in Figure V.6. Calculation routines were also carried out for E85 and results show the test engine is not knock-limited for the experiment points chosen; this is in agreement with experimental observations.

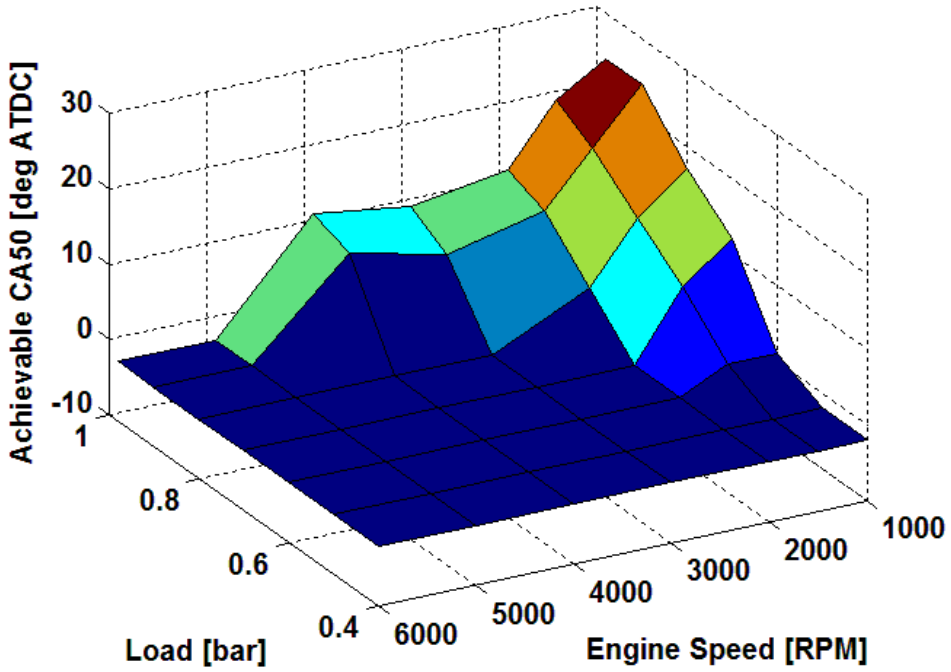

Figure V.6. Achievable CA50 calculated from the proposed method for test engine with 87 octane gasoline

V.6 CONCLUSIONS

In this study, an off-line combustion phasing adjustment algorithm for the SI engine knock limited region was developed for multi-fuel spark timing control and calibration. The algorithm utilizes a global reaction rate theory (Arrhenius function) and chemistry accumulative integral for knock event prediction. Comparisons between multiple fuel model coefficients for the integral were made to investigate effect of negative temperature coefficient (NTC) on SI engine knock prediction. It is concluded that both the methods are able to observe mild and heavy knock situations and only have slight differences in sensing the start of auto-ignition.

In the knock prediction routine, cylinder pressure and unburned gas temperature are reconstructed from a quasi-dimensional turbulent flame entrainment combustion model together with ideal gas law and heat release analysis. Two virtual fuel properties observers are derived, aimed at capturing two fundamental factors related to the fuel source that cause different SI engine knock characteristics.

Achievable combustion phasing maps are generated for 87 octane gasoline and E85 fuel sources with the proposed "what if" analysis. Significant differences in the knock limited region for the two different fuel sources are observed. The proposed feed forward map generation compared to the traditional knock feedback control has the benefit of faster and safer adjustment map generation, especially for multi-fuel adaptive engines where fuel properties might change over a large range.

The proposed combustion phasing adjustment map generation algorithm relies on the accuracy of the predicted cylinder pressure and unburned gas temperature. Therefore, a combustion model that is able to represent the actual physical phenomenon is critical, especially for advanced high degree of freedom engine applications.

VI SEMI-PHYSICAL ARTIFICIAL NEURAL NETWORK COMBUSTION MODELING

As discussed in the previous chapter, the turbulent flame entrainment combustion model offers a great insight to predict the combustion duration. However, using pure physics based model for real time control purpose may not be possible. For example the unburned density and flame front area which are highly coupled with 3D combustion chamber geometry with piston motion; In-cylinder turbulent during combustion is a typical example for chaos theory which its model involves three differential equations. Because of the current computation power limits, one of the solutions for model based control is utilizing empirical mapping techniques coupled with physics models. Empirical mapping tools such as Artificial Neural Network (ANN) is well-known for non-linear dynamic modeling. However, its accuracy is guaranteed only exist within the training data range and NN cannot extrapolate outside of that range. Therefore, large amounts of training data are required to cover every possible operating condition. Moreover, the mathematical network can be very computational intensive and have the risk of overfitting the training data.

To reduce computation load, combined physical models and ANN technique is introduced. Physical models will be used to preprocess the engine sensor output such as RPM, MAP, A/F ratio etc. and calculate in-cylinder pressure and temperature until combustion starts using polytrophic compression assumption. Simplified models will evaluate residual gas fraction, total in-cylinder mass, turbulent intensity and laminar flame speed which can represent gas preparation dynamics and mass burn rate. ANN will

subsequently replace the crank angle resolution discrete event mass burn rate model, and turns the system into a mean value model that outputs combustion duration. The semi-physical neural networks will be placed in a closed loop spark timing control algorithm as shown in Figure VI.1. Feed forward path will take fuel properties into consideration for multi-fuel adaption.

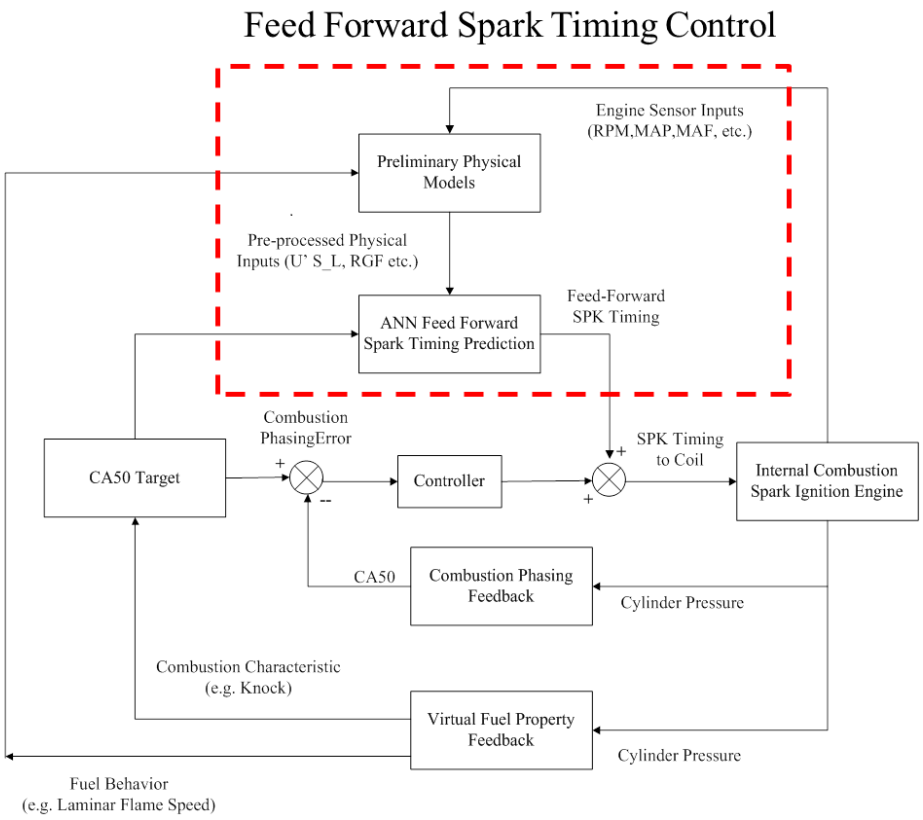

Figure VI.1. Semi-physical artificial neural networks modeling for feed forward spark timing control will be placed in a closed loop multi-fuel engine spark timing control algorithm for transient performance.

VI.1 ANN STRUCTURE ANALYSIS

Artificial neural network shared some unique advantages, such as the non-parametric structure, arbitrary decision boundary selection, and easy adaptation of different types of data. In order to produce satisfactory performance, external inputs, outputs and internal structure need to be carefully selected and optimized. Internal structure of the neural network including the number of hidden layers and number of neurons within each layer could be different for a single set of data. There is no clear answer on the size of the network besides trial and error for each particular problem. However, the performance of the network is strongly influenced by the size of the network through mathematical complexity, and training time, but most importantly, it affects the generalization capabilities of the network (Taskin 1999 [157]). Generalisation is the ability of the neural network to represent unseen data (Atkinson and Tatnall 1997 [158]). Evaluation of a neural network not only depends on how well it can interpolate between the training data, but also whether the network can still perform outside the boundary. Neural network learning process is very similar to polynomial curve fitting. When the network size (like the order of the polynomial function) is smaller than necessary, the results cannot even recognize the pattern within the training data set. On the contrast, if the network structure is more complicated than necessary, 'over fitting' problem occurres. That is the model will trying to capture all the detailed pattern of the training data set but performs very poorly outside the training region (Bebis and Georgiopoulos 1994 [159]).

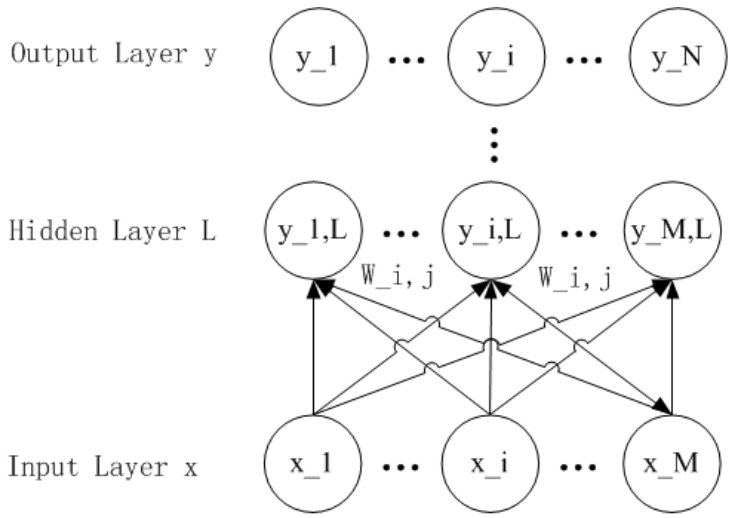

Figure VI.2. General structure of linear associative feed forward neural network

In this research, a feed forward neural network will be discussed. The network is constructed by several layers of processing unit (neurons), each layer feeding input to the next layer by multiplying of individual weight in a feed forward manner. Typical multi-layer feed forward neural network is shown in Figure VI.2, and can be represented by Equation (VI.1).

$$y_i = \sum_{i=1}^{M} w_{j,i} x_{l,i}, \quad j = 1,2,...,N, i = 1,2,...,M \tag{VI.1}$$

While N is the number of outputs, M is the number of inputs, l is the number of hidden layers, and w is the weighting matrixes. The final out y is the summation of the product at each neuron. Error function for training the neural network is defined by Equation (VI.2) which is the total mean square error between the actual output values and desired output values. Individual weight can be calculated based on several learning laws as introduced in the previous chapter.

$$E(W) = \frac{1}{L}\sum_{l=1}^{L}\sum_{j=1}^{N}(y_{l,j} - y_{l,j}^{'})^2 \tag{VI.2}$$

A typical learning law for training a multilayer feed forward neural network, called back propagation is derived based on Equation (VI.3) which describes a gradient decent along the error surface to arrive at the optimum set of weights. The optimum set of weights then is obtained when the gradient descent is made along the total error surface.

$$\Delta w_{i,j}(m) = -\eta \frac{\partial E(m)}{\partial w_{i,j}} \tag{VI.3}$$

Equation (VI.4) is derived from substitute the error function Equation (VI.2), into Equation (VI.3), where the 'f' function represents the error propagated back to the output of the hidden units from the next layer, therefore the algorithm named back propagation.

$$\frac{\partial E(m)}{\partial w_{i,j}} = \frac{1}{2}\frac{\partial}{\partial w_{i,j}}\left[y_i - f_i^{N}\left(\sum_{j=1}^{J} w_{i,j} s_j^{l} \right) \right]^2 \tag{VI.4}$$

Based on the Equation (VI.3) & (VI.4) from back propagation learning laws, a large network (e.g. large number of neurons) will separate the gradient decent into many finer grids therefore takes a long time to learn the characteristic of the input data, while a small network may be trapped into a local error minimum surface and not able to learn from the training data.

From the neural network structure, see Equation (VI.1), it is observed that the size of hidden layer (neurons) is directly related to the number of inputs. Increasing number of inputs will generally require more neurons and hidden layers. There is also a strong correlation between the number of neuron, hidden layer and the number of training sample required. Large network demand more training samples to ensure good

generalization performance. In other word, the network will produce unsatisfactory results if limited numbers of training sample are available. Although adding inputs can provide more information to the network for calculating outputs, this will increase the computation time to train the network by the order of 2, as can be seen from the Equation (VI.2). Adding outputs will also increase the network complexity because more boundaries are set. Therefore, it is very important to select optimum number of inputs and outputs. The input will be only added if it contributes to classify the output relationships.

VI.2 TRAINING DATA SELECTION

Neural network will be trained with different type of inputs for multi-fuel engine spark timing control application. Input candidates for the neural network are choosing from: 1) standard engine sensor signals such as RPM, MAP, Lambda, fuel flow, and 2) physical model calculations such as turbulent intensity, laminar flame speed, Taylor microscale, and residual gas fraction. Two types of input data are available including: 1) steady-state operation data with 500 cycle average which aims to minimize the natual combustion variation. Data set cover partial engine operating range; spark sweeps (7-24 ° ATDC CA50), load sweeps (0.3-0.98 bar of MAP) and RPM sweeps (1000-3500 RPM) which contains total 440 data points for both gasoline and E85. 2) Transient operation data with unfiltered cycle to cycle variation which aims to capture combustion transient responses and variance patterns. Data set cover almost entire engine operating range, as shown in Figure VI.3, which contents around 22,000 data points from transient operations.

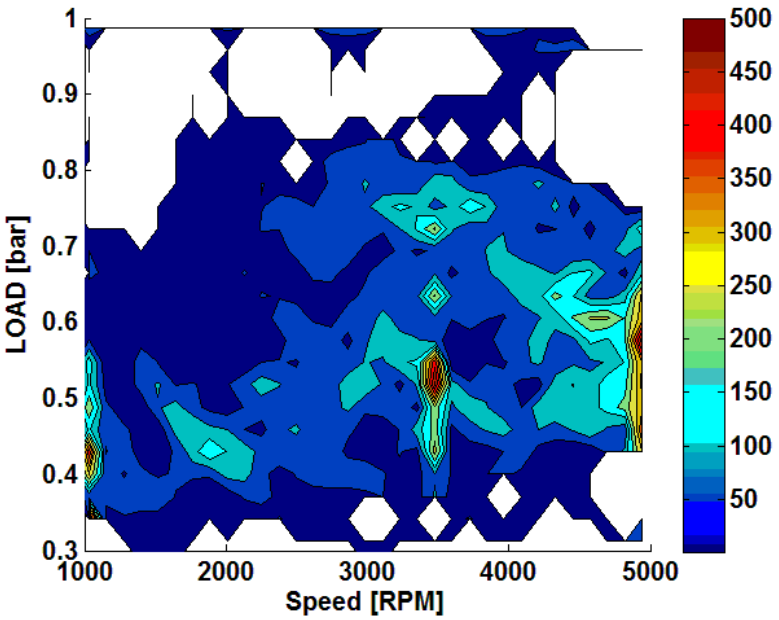

Figure VI.3. Data density plot of transient operation training samples shows most of the engine operating range has been covered.

Once the input of the neural network is decided, there are two approaches to determine the number of neurons within the hidden layer. The first method is called constructive technique (Hirose et al. 1991 [160]) which iteratively increase the neurons from a small number until satisfactory output results are obtained. However, the small network is very sensitive to initial conditions and learning process which might results in network output trapped in a local minimum as the error surface of a smaller network is more complicated and includes more local minima compared to the error surface of a larger network (Bebis and Georgiopoulos 1994 [159]). As a consequence, large number of networks with different number of neurons must be trained to avoid the local minimum trap and find the optimum network structure (Taskin Kavzoglu 1999 [157]]. The second approach utilizes an opposite method that is to begin with a large network and iteratively

eliminate neurons in the hidden layer or interconnections between neurons. After a network is trained to produce a desired solution, neurons or interconnections are analyzed to find out which ones are not participating in the solution, and then they can be eliminated (Kavzoglu and Mather 1998 [161]).

VI.3 ANN MODEL CONSTRUCTION

A sensitivity analysis is used to indicate which parameters are considered most important for the particular neural network. Sensitivity analysis gives important insights into the usefulness of individual variables, helps identify variables that can be safely ignored in subsequent analyses, and key variables that must always be retained which will reduce the overall complexity of the networks. The output used to evaluate accuracy is the combustion duration from spark to CA50 on time basis as compared to experimental results. The sensitivity analysis is done by first training a network with all the available inputs, which gives the best correlation with the experimental data. Each input is then removed, the network is re-trained, and correlation to experimental results is evaluated [132]. Since some information has been removed, some deterioration in accuracy is expected to occur; the correlation coefficient of the output is used to quantify this error.

The result of sensitivity analysis is shown in Figure VI.4. The Taylor microscale was found to be the least important to this particular network; likely because the Taylor microscale is coupled with turbulence intensity in the closed combustion environment. Residual gas fraction does not have a major impact on accuracy for two possible reasons: (1) the test engine is not equipped with an external EGR or VVT system that can vary the

in-cylinder residual gas over a large range, and (2) RGF is also taken into account in the laminar flame speed model. Factors that had a major influence on accuracy were turbulence intensity, laminar flame speed and total in-cylinder mass. These inputs were selected for the semi-physical neural network derived in this research.

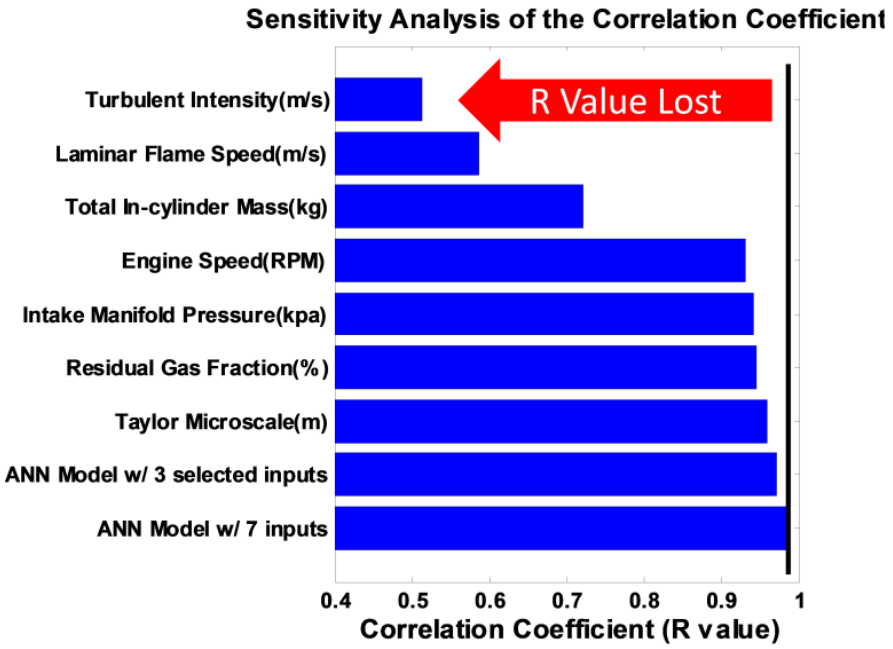

Figure VI.4. Sensitivity analysis for neural networks with different physical inputs suggests turbulent intensity, laminar flame speed and total in-cylinder mass are the most significant factors for accurate spark timing prediction.

One of the most important characteristics of an ANN is the number of neurons in the hidden layer. If an inadequate number of neurons are used, the network will be unable to model complex data and the resulting fit will be poor. If too many neurons are used, the network may over fit the data. When over fitting occurs, the network will begin to model random noise in the data. The result is that the model fits the training data

extremely well, but it generalizes poorly to new unseen data. An optimization of the number of neurons in the hidden layer has been performed as shown in the Figure VI.5.

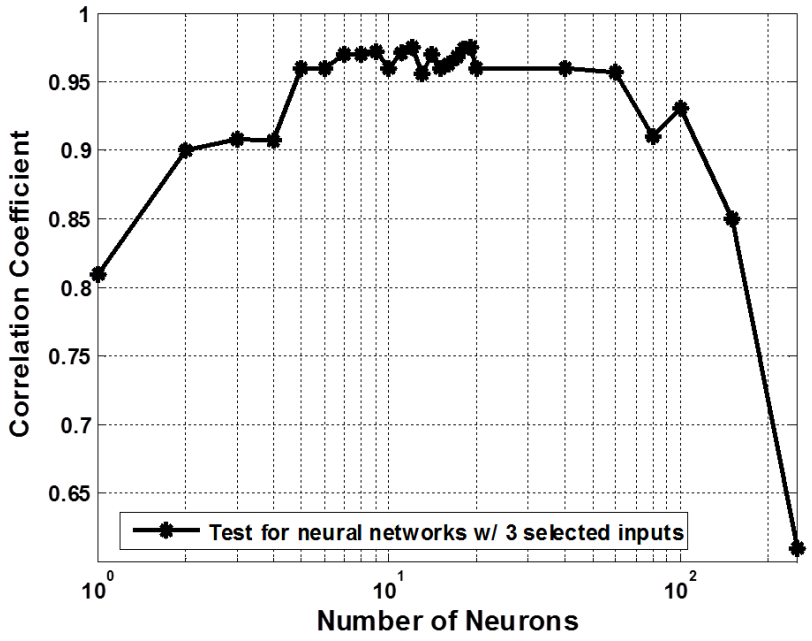

Figure VI.5. Optimization of number of neurons for the neural network with turbulent intensity, laminar flame speed and total in-cylinder mass as inputs suggest the minimum of 5 neurons can be used and still maintain a 0.96 correlation coefficient.

A two-layer, feed-forward network with sigmoid hidden neurons and linear output neurons with Levenberg-Marquardt back propagation algorithm training is used to construct the ANN model. Consistent training data and sufficient neurons in its hidden layer contribute to the final model accuracy. Based on the optimization results, 5 neurons in 1 hidden layer were used in the ANN model. Finally, an optimized semi-physical ANN model is constructed, as shown in Figure VI.6.

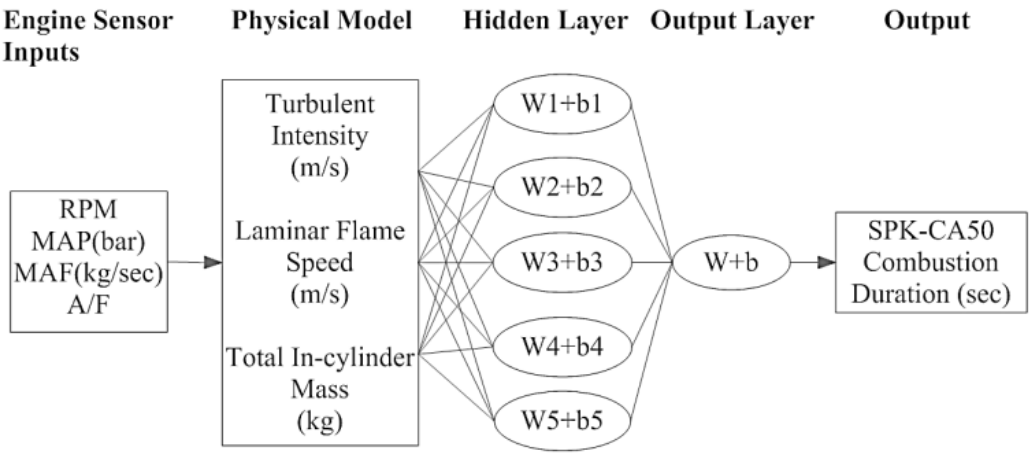

Figure VI.6. Semi-physical neural network structure for combustion duration prediction with 3 selected physical sub-models and 5 neurons in one hidden layer.

VI.4 SEMI-PHYSICAL ANN MODEL RESULTS

The semi-physical ANN spark timing prediction model is evaluated based on the performance of combustion phasing control under both steady-state conditions and transient conditions with gasoline and E85 as fuel source inputs. Validation for steady-state condition predicted performance is based on the experimental data from engine dynamometer tests. Preliminary transient combustion phasing control validation is carried out by vehicle driving cycle simulation with virtual engine in the loop. Then, the control algorithm is implemented into the engine controller for real-time engine dynamometer testing

VI.4.1 STEADY-STATE SPARK TIMING PREDICTION EVALUATION

Combustion duration calculated from the semi-physical ANN model for each data point under steady-state operating conditions is compared with the experimental data as shown in Figure VI.7. Each of the data points represents an average of 500 consecutive

cycles, which minimizes the influence of combustion variability. Data points are randomly selected engine operating points which are used for network training. However, the overall validation data are still within the training region of the neural network which is between 1000 to 3500 RPM, 0.3 to 0.98 bar MAP and 7 to 24 °ATDC CA50.

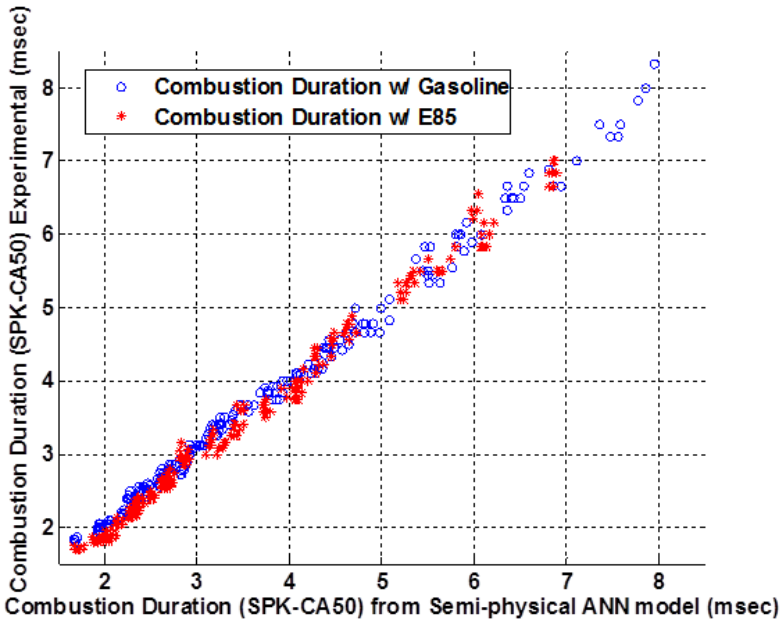

Figure VI.7. Combustion duration prediction from the semi-physical ANN model is able to closely match experiments results. Data points on this plot are different from those used for model training.

Results are calculated and compared with gasoline and E85 fuel source inputs which both show agreement with experimental data. This is probably due to the input of laminar flame speed to the ANN model which captures the effect of fuel properties on combustion reaction rates. It has been proven that laminar flame speed is the only major fuel property in fuel sources that will have impact on combustion duration [133]. Therefore, if a wide range of laminar flame speed data is available as training data, the

trained network will most likely be fuel type sensitive and still perform well when a different fuel source is used or blended (with laminar flame speed observer feedback).

Root mean square deviation (RMSD) results are shown in Table VI.1. A good agreement of the semi-physical ANN model with experimental data is observed. The RMSD results will also be used in the next section to compare with spark timing predictions from transient conditions and quantify the difference in feed forward control performance.

Table VI.1. Steady-state combustion phasing RMSD from the semi-physical ANN model, compared to experimental data

RMSD	**Time basis (ms)**	**CAD basis (CA)**
Gasoline	0. 128	1.64
E85	0. 133	1.77

To ensure the spark timing predictions are accurate across different load and RPM closer observations of prediction results are provided in Figure VI.8. Individual spark timing prediction from RPM and load sweeps are able to match experimental data, and the agreement remains strong over a range of engine speed or load. Therefore, it is concluded the trained network should be able to perform relatively well for all engine speeds and loads within the training zone.

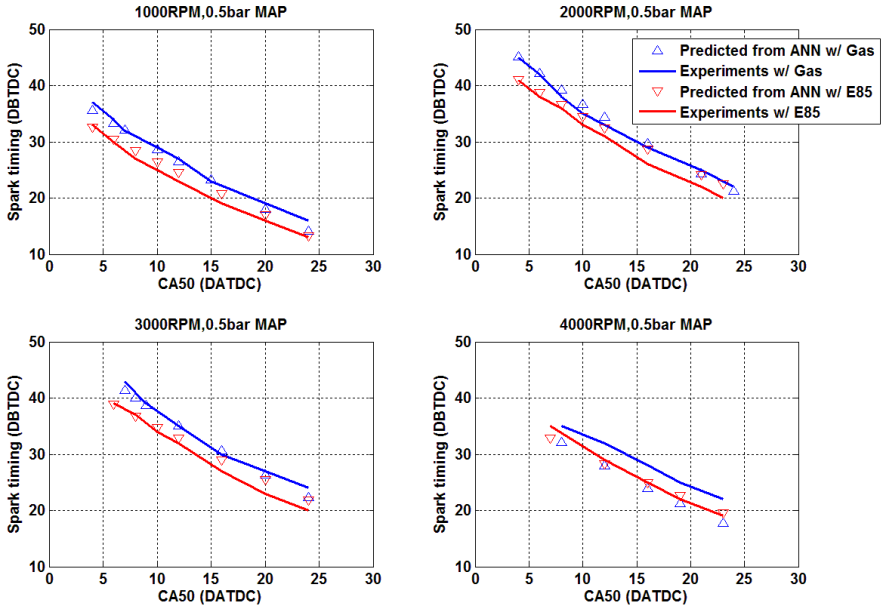

(a)

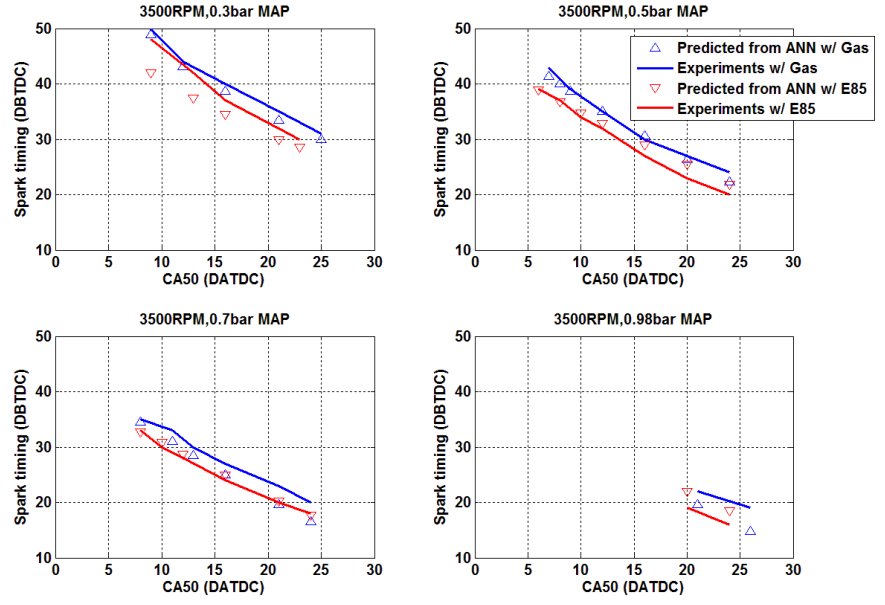

(b)

Figure VI.8. The semi-physical ANN combustion model is able to predict the spark timing based on desired CA50 across different engine speeds (a) and loads (b) under steady-state conditions.

VI.4.2 TRANSIENT SPARK TIMING PREDICTION EVALUATION

Transient engine operation is a major control challenge which motivates this proposed research of feed forward spark timing control algorithm. A GT-POWER virtual engine is used to demonstrate transient spark timing prediction performance results. The virtual engine is placed in Simulink for driving cycle simulation. A full vehicle dynamics, powertrain and driver models are utilized to best simulate realistic operating conditions. The semi-physical neural network combustion duration model is implemented to control the spark timing. Gasoline and E85 are used as two different fuel source inputs.

Development of The Virtual Engine

The 1-D engine model was developed based on test engine geometry and a predictive combustion model that utilizes a quasi-dimensional flame propagation process. A 3-D combustion chamber shape model is used to calculate flame propagation area. Predicted cylinder pressures from the GT-POWER simulation were compared with experimental results under the similar operating conditions for validation. Areas of particular focus for model validation were cylinder pressure during gas exchange and combustion to evaluate both the performance of the intake and exhaust system as well as the predictive combustion model. Proper knowledge and technique was used to analyze the system error and reasonable corrections were made to tune the simulation model in order to represent the real engine operation. Validation of the cylinder pressure was carried out for gasoline and E85 fuels.

Transient Algorithm Validation

The virtual engine was controlled by spark timing predicted from the semi-physical neural network combustion duration model to assess predictive ability under transient conditions. The combustion phasing results from the GT-POWER virtual engine were evaluated based on the deviation from the desired combustion phasing which was assumed to be 8 CA ATDC for simplicity. The Urban Dynamometer Driving Schedule (UDDS) is used to evaluate the transient performance of control algorithm. Results with gasoline fuel source are shown in Figure VI.9, with two zoom-in periods of entire cycle representing city (a) and highway (b) driving. Both scenarios observed overall acceptable results compared to the constant target of 8CA. Engine load control and the clutch model of manual transmission are not fully developed which causes the oscillations of MAP and engine speeds (170 seconds). In the first few seconds of plot (a), when the engine accelerates with 100% throttle from idle speed, the spark timing is over predicted because the engine operates out of the training region of the neural network that results in early combustion phasing. This condition could be solved with retraining the neural network with a wider operating range of data. Over prediction also exists when engine speeds are between 2000-2500 RPM and 0.3-0.4 bar MAP, which is caused by low fidelity of the control model. This can be solved by artificially retarding the desired combustion phasing target or retraining the neural network with more data samples to improve fidelity.

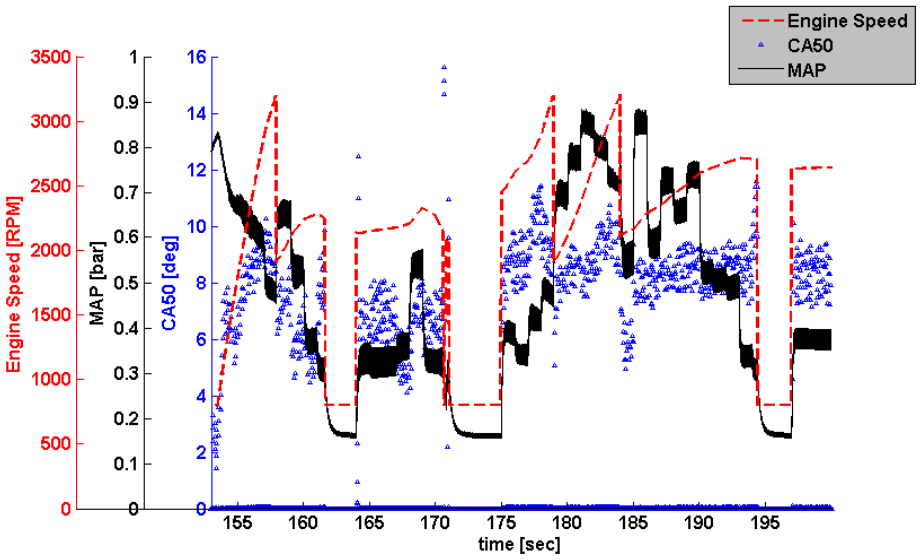

(a)

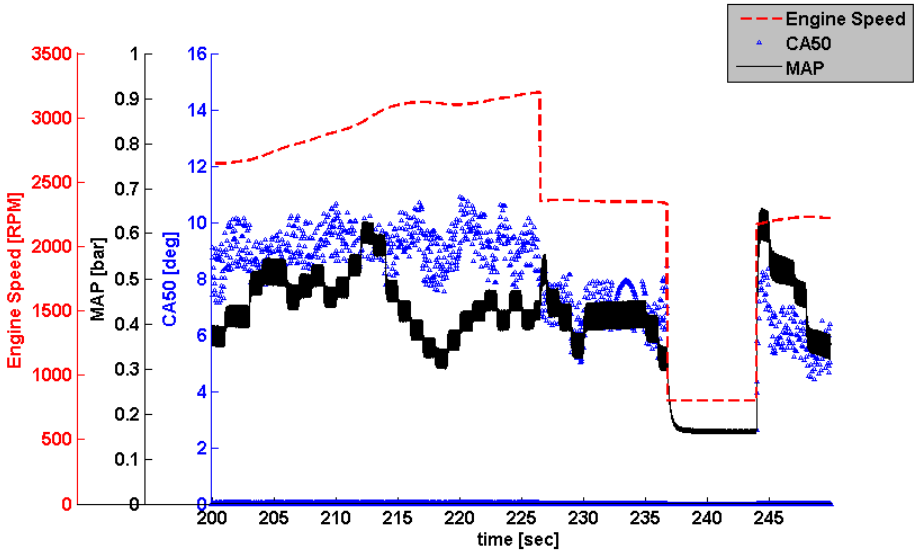

(b)

Figure VI.9. Combustion phasing (CA50) results from the virtual engine simulation with gasoline in a transient driving cycle (UDDS) (a) 150-200 sec, and (b) 200-250 sec.

Combustion phasing results shown in Figure VI.10 are obtained from the same driving cycle simulation routine and neural network, but with an altered laminar flame speed sub model to reflect E85. The predictive combustion model in GT-POWER virtual engine is also calibrated to E85 accordingly. Results observed to have similar accuracy compared to simulation with gasoline fuel. A similar error region can be also recognized when engine speeds are between 2000-2500 RPM and load is between 0.3-0.4 bar MAP.

The UDDS simulation is driven for a total of 500 seconds, although only 100 seconds are shown in the previous figures for simplicity. The full drive-cycle RMSD of the difference between target and actual CA50 for each fuel is shown in Table VI.2. An average of 2 CA deviation from the constant desired combustion phasing target is observed. The transient results have slightly larger deviation, about 0.4 CA more, than the steady state conditions. The model was calibrated with steady-state data, so these results are promising and suggest that this approach is able to control the combustion phasing for multi fuel adaptive SI engines under both steady state and transient conditions.

Table VI.2. RMSD for the combustion phasing control results in a transient driving cycle with a constant desired combustion phasing (CA50 @ 8)

RMSD	CAD basis (CA)
Gasoline	1.96
E85	2.1

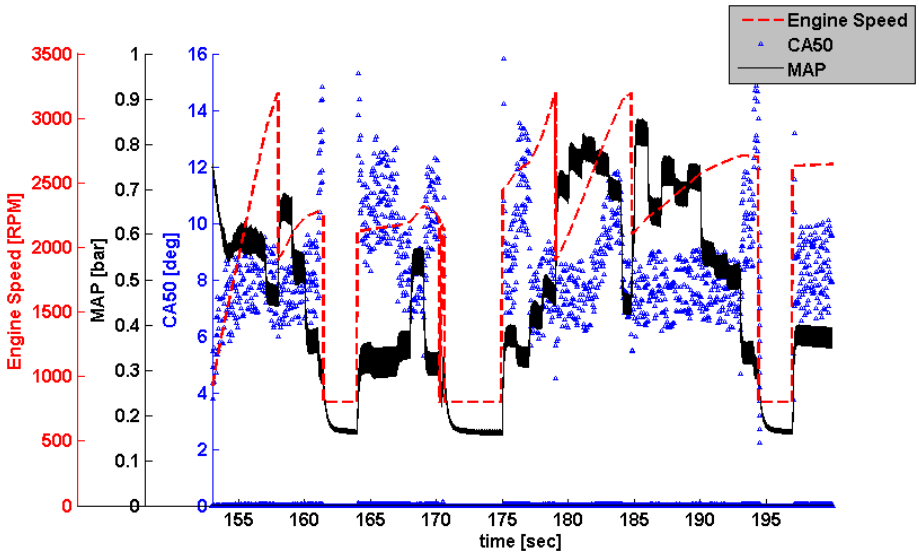

(a)

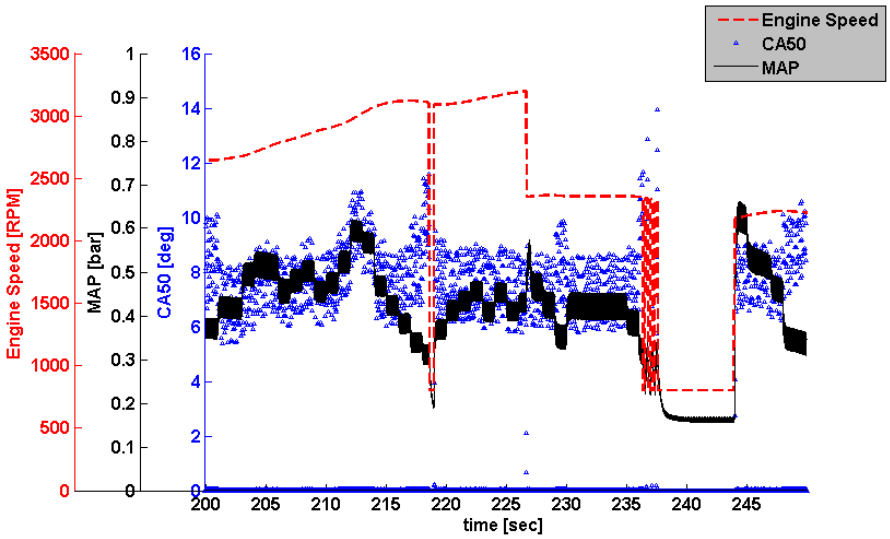

(b)

Figure VI.10. Combustion phasing (CA50) results from the virtual engine simulation using E85 in a transient driving cycle (UDDS) (a) 150-200 sec, and (b) 200-250 sec.

VI.5 REAL TIME ENGINE DYNAMOMETER TESTING RESULTS

After satisfied results observed from the virtual engine co-simulation, the semi-physical neural network model is implemented into the A&D prototype engine control unit. Standard production sensors are used as inputs, such as crankshaft position sensor, intake manifold sensor and lambda sensor etc. Spark timing is then calculated from the model and directly send to the coil for ignition signal. The test engine is highly instrumented as described in the experimental setup chapter. Test cell and test engine are both environmental controlled to ensure the experimental data consistency and repeatability, such as intake air temperature, humidity, oil temperature, coolant temperature, and exhaust back pressure etc. Experimental data presented below are all thoroughly examined to be highest quality for further discussion.

Transient tests are done by manually vary the engine speed from 1000RPM to 5000RPM and load between 0.3 bar to WOT. Combustion is controlled by the ignition signal calculated based on the combustion duration (SPK-CA50) from semi-physical neural network model with user given combustion phasing target (CA50). Steady state and transient CA50 target are tested to investigate system response on both scenarios. Gasoline and E85 will be used as fuel source input to demonstrate the fuel adaptation ability. Error allowance is targeted to be +/- 0.7*standard deviation.

To investigate if the semi-physical neural network model is only locally valid, multiple constant CA50 target is set in the transient engine tests, range from CA50 at 4 CA ATDC to 28 CA ATDC with a increment of 3 CA. Three cases are selected to illustrate the results of ignition control with gasoline fuel as shown in Figure VI.11. The CA50 results are acquired from real-time cylinder pressure signal with a 3 samples

floating average (+/- 1 data sample). Because limited capability of the dynamometer control system, the engine speed and load profile is not 100% repeatable. Therefore, standard deviation for each operating conditions (RPM and Load point) is generated with the empirical model and plotted on the figure to evaluate the performance of the ignition control. As can be seen, the CA50 is almost regulated within +/- 0.7* standard deviation through the entire 2600 cycles engine test for each CA50 target.

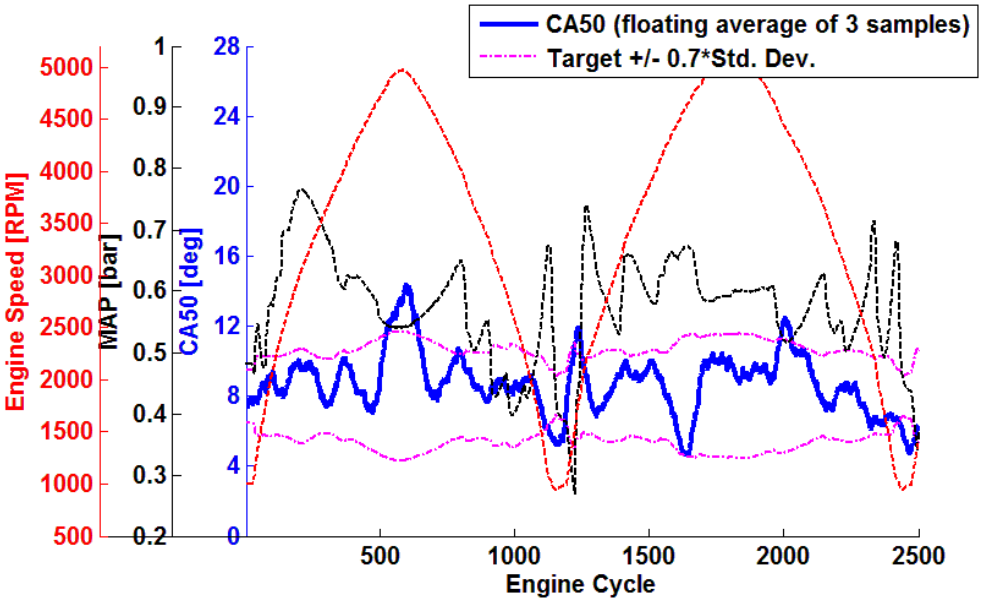

(a)

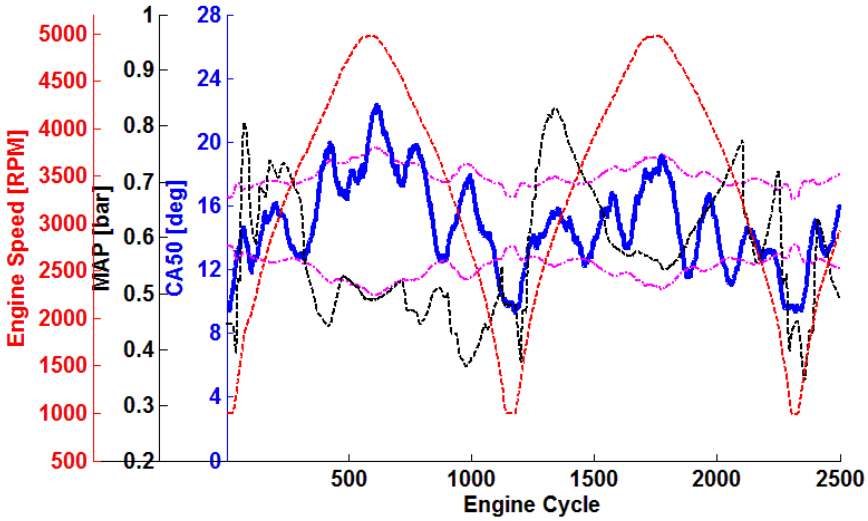

(b)

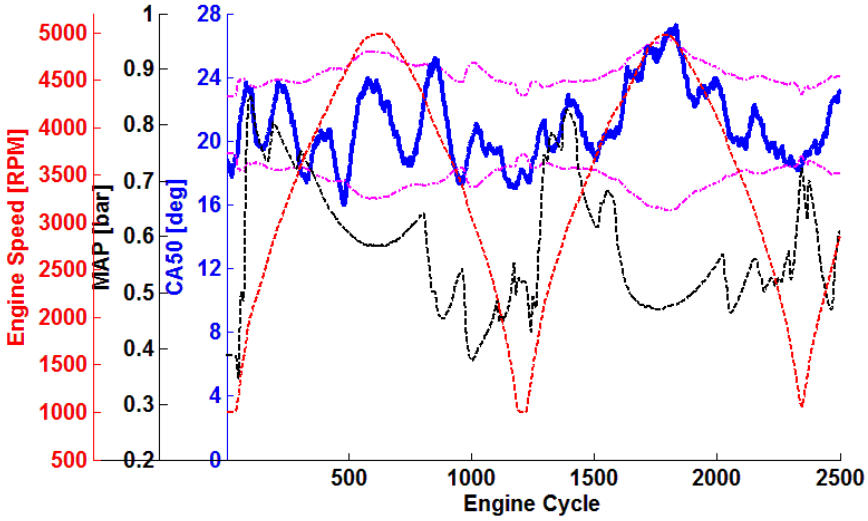

(c)

Figure VI.11. Real-time combustion phasing (CA50 after floating average) control experimental results in transient operating conditions with Gasoline fuel input. CA50 target is set at constant (a) 8 CA ATDC, (b) 15 CA ATDC and (c) 21CA ATDC.

Same method discussed above is carried out to investigate if the semi-physical neural network model can adapt to another fuel sources (E85), as shown in Figure VI.12. Satisfied accuracy is observed for most of the CA50 targets. However, the system seems to over-predict the spark timing using E85 fuel at higher RPM with the combustion target around 15 AC ATDC. Theoretically, this section is outside of the training data region that the system dynamic is extrapolate by the neural network which might results in the extra error margin. Detailed discussion about the robustness of the neural network will be placed at the conclusion chapter.

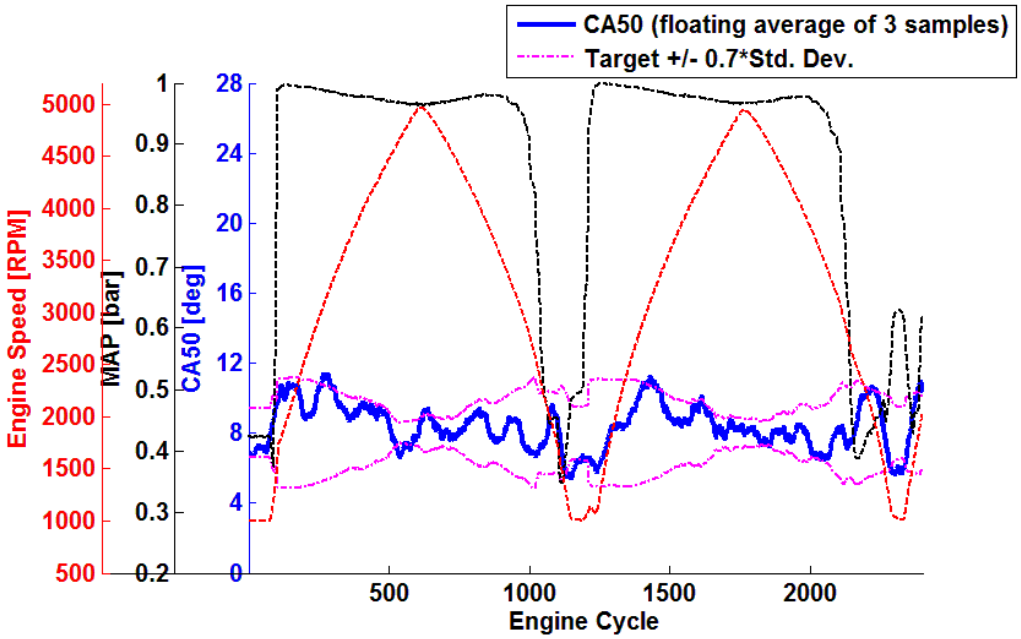

(a)

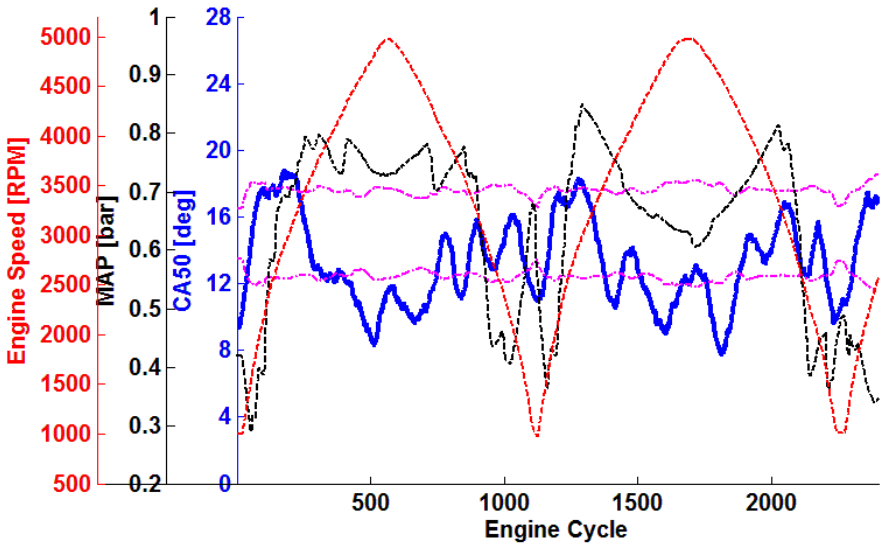

(b)

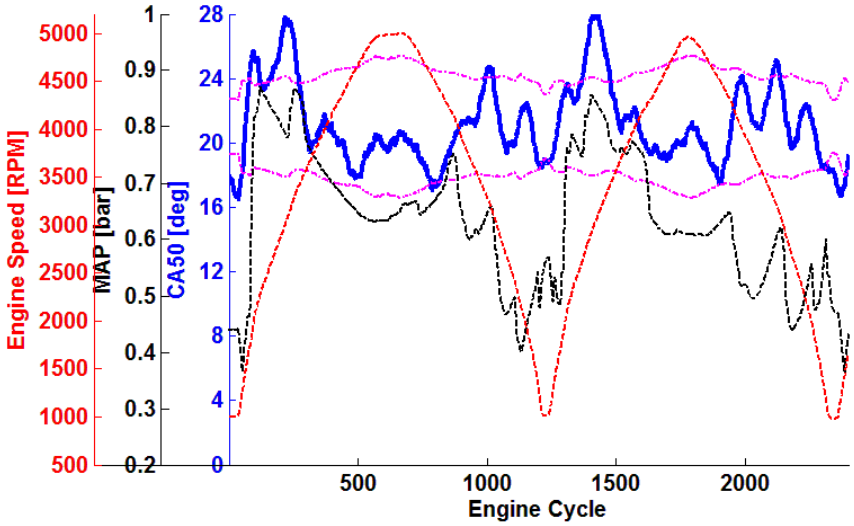

(c)

Figure VI.12. Real-time combustion phasing (CA50 after floating average) control experimental results in transient operating conditions with E85 fuel input. CA50 target is set at constant (a) 8 CA ATDC, (b) 15 CA ATDC and (c) 21CA ATDC.

RMSD, shown in Table VI.3, is used to quantify the error margin of each test above. Compared to Table VI.1 of steady state operation, transient operation is generated roughly 1 CA more RMSD in combustion duration (SPK-CA50).

Table VI.3. Transient combustion phasing RMSD from the semi-physical ANN model, compared to the set control target

RMSD	CA50 @ 8	CA50 @ 15	CA50 @ 21
Gasoline	1.98	2.74	2.31
E85	2.09	2.74	2.42

Engine calibration often requires different combustion phasing targets at each operating "map" point for the purpose of reducing spark knock or NOx emissions etc. Therefore, stable performance of the semi-physical neural network model of tracing the moving CA50 target is also needed. To be able to repeat the operating conditions, engine is fixed at full load with a constant RPM ramp rate (200RPM/sec) from 1000RPM to 5000RPM. Control target is based on the experimental results of CA50 using original manufacturer calibrated spark Look Up Table (LUT) obtained with the same testing schedule. Figure VI.13 indicate the CA50 experimental results from semi-physical neural network is able to trace the given moving targets with either gasoline (a) or E85 (b) fuel source as input. Since the engine is fixed at constant load that greatly increase the ignition control performance compared to the previous changing engine speed and load cases. The control algorithm is able to predict roughly the same spark timing and regulates the combustion phasing close to the required targets.

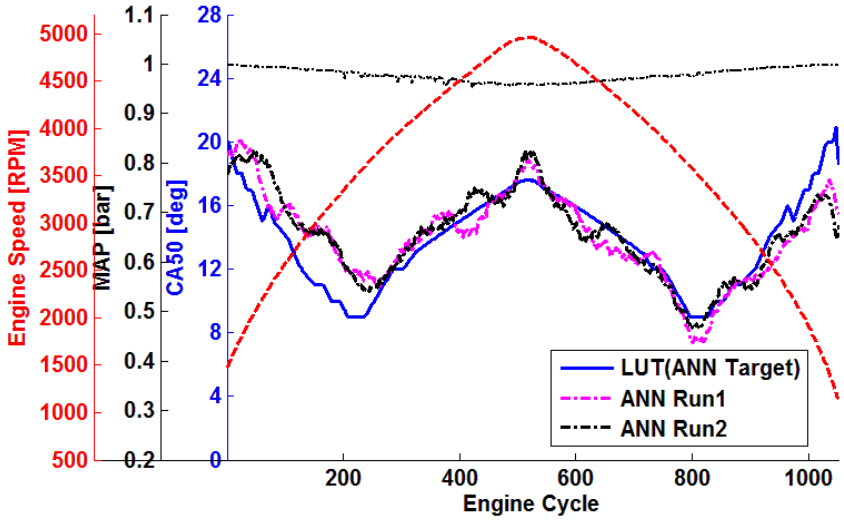

(a)

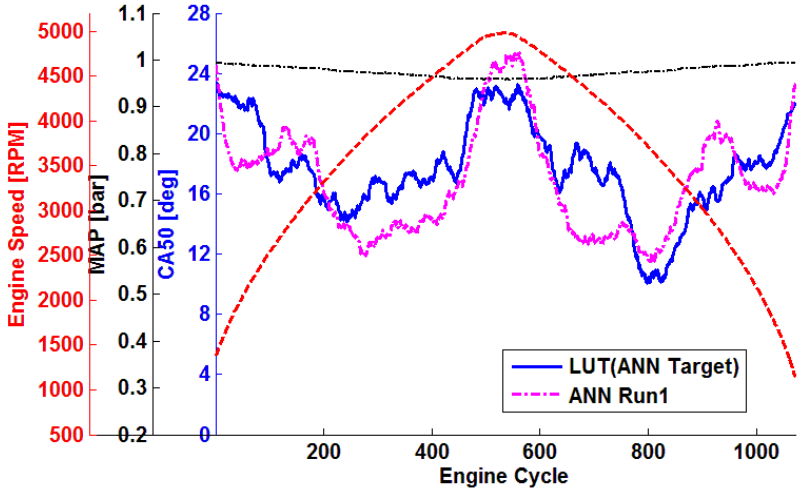

(b)

Figure VI.13. Real-time combustion phasing (CA50 after floating average) control experimental results in transient operating conditions with (a) Gasoline and (b) E85 fuel inputs. CA50 target is set to trace engine experimental CA50 when using original look up table from calibrated ECU.

VI.6 EXPERIMENTAL RESULTS DISCUSSION

VI.6.1 INPUT SELECTION

In many applications, there is always limited number of training samples that are available to populate the entire network. In order to still train a neural network with high fidelity and robustness, one of the techniques is to utilize physical models to process the available training samples that can linearly extrapolates both for inputs and outputs, hence represent wide range of operating conditions (generalization capability). The statement holds when the neural network is linear associative network with all the inputs linearly independent. Recall equation (1) which shows the output of the network is a simply weighted summation of the component values of the input vectors.

For model based engine spark timing control, combustion duration is strong functions of the unburned mixture preparation which can be alter by several engine actuators such as charge motion control valve (CMCV), variable valve timing (VVT) system, and residual gas recirculation (EGR) system etc. In a flex-fuel engine, the combustion burn rates are also directly related to the fuel property which is described as laminar flame speed. Great calibration efforts will be needed to populate entire training samples for all the different combination of available 'freedom' of the engine settings which scarify the meaning of using model based control algorithm. However, physical models are available to capture the above parameters and their relationships with combustion duration, which is turbulent intensity, residual gas fraction and laminar flame speed models and described by the turbulent flame entrainment combustion model. Linearization of each physical model can be made at the time of ignition. The linearized

models are still able to represent mixture properties and dynamics before combustion for a wide range of operating conditions, actuator settings and fuel source input. The neural network is trained based on the physical models at the linear equilibrium origin. Therefore, the semi-physical approach is able to ensure the generalization feature of the neural network without large diversity of training samples.

Benefit of the semi-physical approach can be demonstrated by the multi-fuel adaptive engine spark timing control. The previously described models utilize a combination of turbulence intensity, laminar flame speed and total in-cylinder mass as inputs for the neural network and successfully proved the fuel adaptation ability as shown in Figure VI.14 (a). Noticed laminar flame speed is emphasized because it is a primary physical parameter related to ignition timing prediction, and it will change if a different fuel source is used [133]. By accurately predicting the laminar flame speed, the trained network theoretically can represent the combustion duration with wide range of fuel sources input. Alternative neural network is trained for comparison with only standard engine sensor inputs which are engine speed, intake manifold pressure and fuel flow rates. It can be observed from Figure VI.14 (b) that the neural network can predict accurate combustion duration for using gasoline fuel, however, over predict the burn rates for short combustion duration cases. It is not fully clear that why the network will behave like this because of the multi-layer structure with non-linear processing units. One possible reason might be the linear separation of the inputs introducing limitation of the generalization capability which means the pattern of mass fuel flow cannot be fully decoupled from other inputs such as intake manifold pressure.

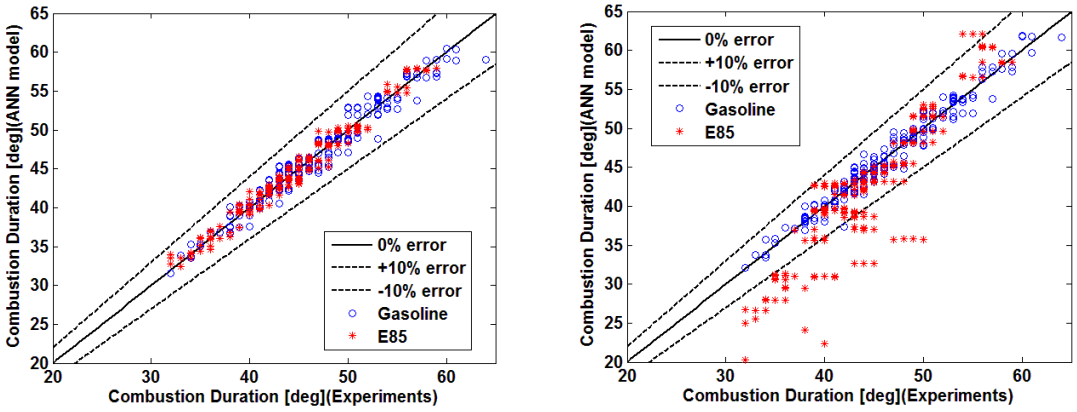

(a) (b)

Figure VI.14. Combustion duration from experiments plotted versus the results from neural network trained with (a) turbulent intensity, laminar flame speed, and total in-cylinder mass. Correlation coefficient is 0.977 for E85 and 0.973 for gasoline. (b) RPM, MAP, and Mass fuel flow. Correlation coefficient is 0.923 for E85 and 0.971 for gasoline.

VI.7 TRAINING DATA SELECTION

Another objective of model based feed forward control is improving transient response time and control performance. It is a difficult problem because each dynamic system or actuator has its own response delay. The model should not only capture the steady state system dynamics but also the transient response behavior. However, the transient behavior of the semi-physical neural network model was not clear even with the satisfied observation of real-time engine testing results under transient conditions. The neural network was trained based on the cycle average steady state data and all the physical sub-models are derived based on steady state dynamics. One possible reason for the satisfied performance of the transient condition may contribute by the 1 ms model

actuation rate. Therefore, question is asked if there is anything can be done internally of the model that can improve the transient performance. Before going to complicated detail physical sub-models, one suggestion is to utilize transient operation data as neural network training samples and hopefully the network is able to capture the transient patterns between inputs and output.

Case study is carried out on the previous developed neural network (N1), as shown in Figure VI.14 (a). Instead of using the steady state 500 cycle average data to train the network, the new network (N2) will be trained with transient operation cycle to cycle data samples. Comparison of the two type data samples is described in experimental setup chapter. Inputs to the network have been kept the same (turbulent intensity, laminar flame speed, total in-cylinder mass). Number of neurons inside the hidden layer has been re-optimized based on Hirose constructive technique. Compared to N1 which only need 5 neurons to generate satisfactory performance, N2 required 70 neurons. Possible reasons for large network needed are: 1) added transient response pattern; 2) cycle to cycle natural combustion variance. Validation on N2 is presented in Figure VI.15 which is done by taking another 2 sets of non-seen transient engine testing data (Gasoline and E85) and process through N2. As can be seen, N2 generally introduce more error band for combustion duration (SPK-CA50) than N1. Also noticed that the network generate larger error for gasoline fuel especially for certain operating conditions.

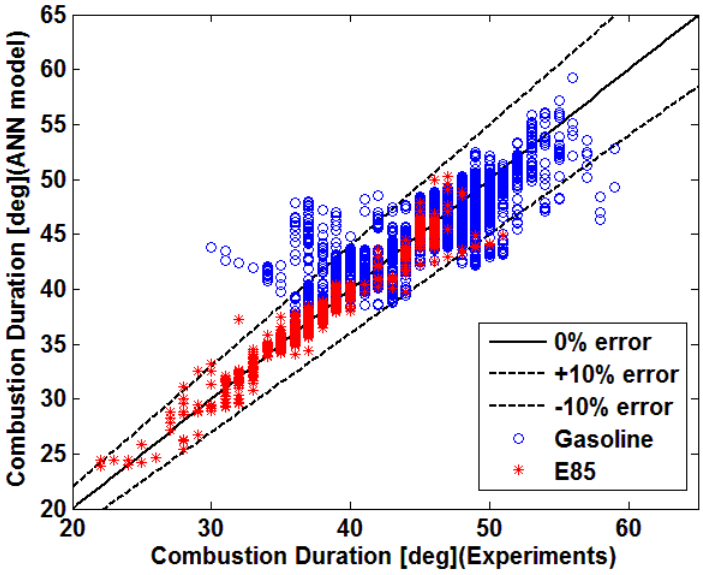

Figure VI.15. Combustion duration from experiments plotted versus the results from neural network trained with transient cycle to cycle calculated turbulent intensity, laminar flame speed, and total in-cylinder mass. Correlation coefficient is 0.967 for E85 and 0.943 for gasoline.

Further investigation on the performance differences between N1 & N2 is carried out on real time engine dynamometer testing. N1 is constructed with one hidden layer and minimum number of 5 neurons which aims to increase the generalization capability (robustness) of the network and reduce the computational burden. Laminar flame speed also plays an important role to network robustness in terms of the fuel adaptation ability. It is the only changing parameter that will affect combustion duration if fuel type is altered. Conclusions can be made based on Figure VI.11, Figure VI.12 and Figure VI.13, the semi-physical approach is able to keep the fuel type sensitive property by taking laminar flame speed as input. Robustness of the neural network is also tested when engine speed is over 3500 RPM which is outside the training region. The overall

performance of N1 is quantified by root-square mean deviation compared to the desired target (CA50 @ 8) is 1.98 CA for gasoline and 2.09 CA for E85. Extensive real-time validations are carried out for several constant combustion targets to ensure the model is not only locally stable, and also "moving" desired combustion target is tested which proved the network is able to perform with continuously changing control target.

Similar method is used for testing N2, and results are shown in Figure VI.16. N2 has same inputs as N1, but trained with 22000 transient data samples which cover almost entire engine operating range. Originally, network with transient training data is studied which aims to capture engine transient behavior and natural combustion variance. However, overall increasing error margin deviated from the desired target is observed for both gasoline and E85. Also notice for gasoline input, Combustion of N2 is very unstable especially when engine is operated at around 2000RPM. Root-square mean deviation compared to the desired target (CA50 @ 8) is 3.58 CA for gasoline and 13.35 CA for E85.

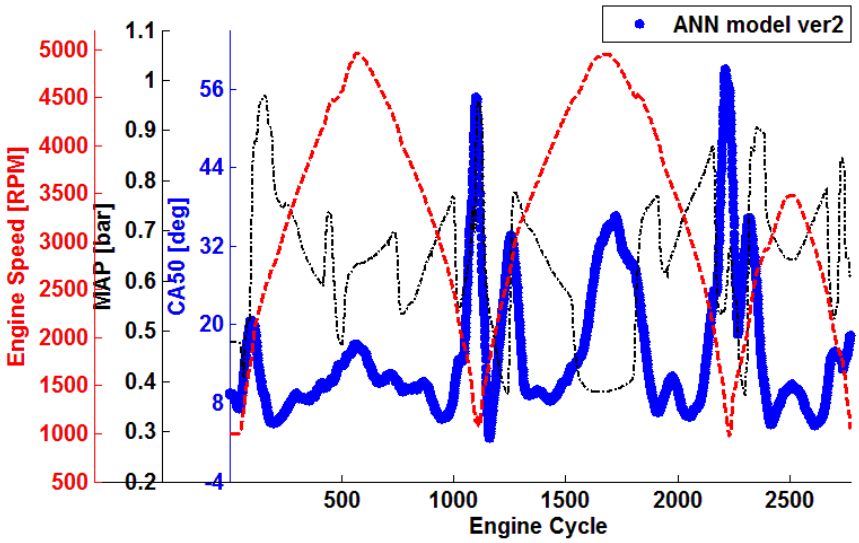

(a)

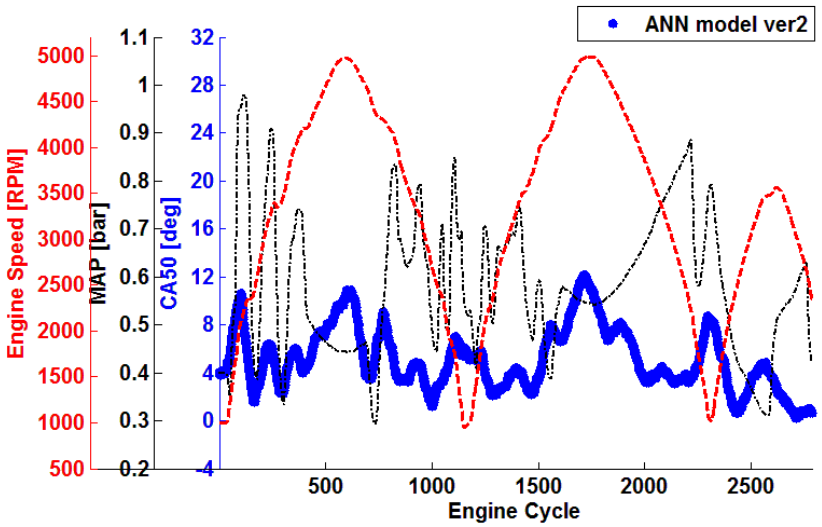

(b)

Figure VI.16. Real-time combustion phasing experimental results in transient operating conditions with (a) gasoline fuel input and (b) E85, tested for N2. Constant combustion target set at 8 CA ATDC.

Investigation on actual ignition signal from N2 reveals the reason for the unstable combustion which is not because of any malfunction on other engine actuators but the spark timing prediction itself. This is probably because of the large network structure required by the N2. Transient training sample contains three patterns: 1) combustion duration dynamics; 2) natural stochastic combustion variation; 3) transient response of combustion to a changing operating condition. N2 requires minimum 70 neurons to be able to produce satisfactory performance compared to only 5 neurons needed in N1. The larger size of the network scarifies the generalization capability as explained in the previous chapter. Although the observed correlation coefficients are above 0.94 on the validation of N2, and experimental results also showing the network can operate at certain conditions, however N2 cannot generate stable predictions when large disturbances or un-seen operating conditions occurred. On the contrast, N1 which is an optimized minimum size network with steady state average training data can perform much stable across a wide range of different operating conditions.

VI.8 CONCLUSIONS

In this chapter, a model based ignition control algorithm for multi-fuel adaptive engines is studied with an aim to provide an alternative method to reduce advanced engine calibration time. A semi-physical approach has been investigated which utilizes an artificial neural network to convert a well-proven discrete time domain quasi-dimensional turbulent flame propagation model into a mean value combustion duration model.

Generalization capability is the main focus of the network formulation because it will greatly affects the stability of the feed forward control algorithm. Generalization is strongly influences by the network structure including the number of hidden layers, number of neurons in each hidden layer, inputs and outputs patterns. Conclusion from the theoretical study on the network structure indicates: 1) increasing number of inputs will generally require larger size network; 2) large networks need more training samples to produce satisfactory output results; 3) adding one extra input will increase the training time by the order of 2. Therefore, a proper optimized network structure contributes to the overall model performance.

Inputs and sub-models were selected based on the physical model to represent mixture preparation, and combustion reaction rates were modeled with a neural network. The structure of the neural network has been optimized by selecting the most sensitive physical inputs and then minimizing the number of neurons in the hidden layer. The optimized neural network is proved to be able to represent the combustion duration with two types of fuels. The algorithm also successfully operated in a transient driving cycle in a computational vehicle simulation.

Validation of the ignition control algorithm was carried out under both steady state conditions with experimental data; transient driving cycle simulation with a virtual engine in the loop, and also the real time engine dynamometer testing. A comparison of the combustion phasing control performance between the transient and steady-state conditions is made which shows an average of 2 CA deviations from the control target for both transient and steady-state conditions with gasoline and E85. It is shown that the ignition control algorithm is able to regulate the combustion phasing with steady state and "moving" CA50 target for both gasoline and E85. Laminar flame speed plays an important role to the fuel adaptation ability. It is the only changing parameter that will affect combustion duration if fuel type is altered. The semi-physical approach is able to keep the fuel type sensitive property by taking laminar flame speed as input. Robustness of the neural network is also tested when engine speed is over 3500 RPM. The neural network is constructed with the minimum number of 3 inputs and 5 neurons which aims to decrease the chance of data over fitting and better control stability. It is concluded that the new semi-physical neural network combustion duration model is able to control the combustion phasing for two fuel sources under both steady-state and transient conditions.

VII SUMMARY AND CONCLUSIONS

VII.1 THESIS SUMMARY

The objective of this thesis is to develop a semi-physical artificial neural network combustion model for feed forward spark timing control of multi-fuel adaptive SI engines. The control algorithm closed loop by feeding back two fuel properties which are octane number and laminar flame speed. An adaptive desired combustion phasing target helps to self calibrate for the current fuel source. Laminar flame speed is emphasized because it is a primary physical parameter related to ignition timing prediction, and it will change if a different fuel source is used. The fuel property observer outputs an estimate of laminar flame speed for an arbitrary fuel based on the burn-rate difference to a baseline case, using an inverse quasi-dimensional turbulent flame entrainment model with in-cylinder pressure feedback. A real-time model re-calibration method for laminar flame speed prediction is also proposed. Desired combustion phasing targets were calculated based on an Arrhenius function (auto-ignition correlation) with the virtual octane number sensing of the current fuel source. The two fuel properties sensors of laminar flame speed and octane number ensured the capability of fuel type adaptive closed loop ignition control algorithm.

Inputs to the feed forward combustion model is loosely based on a well-established turbulent flame entrainment model, artificial neural network is used to replace the crank angle resolution combustion process calculations. Optimization on inputs selection and neural network internal structure is focused because of the large influences on network generalization capability. Generalization is the ability of the neural network

to interpolate and extrapolate unseen data which directly reflected in the overall control stability. Evaluation on a neural network not only depends on how well it can interpolate between the training data, but also on if the network can still perform outside the boundary.

The real time engine dynamometer experimental results are presented. It is shown that the semi-physical neural network control algorithm is able to regulate the combustion phasing with steady state and "moving" CA50 target for both gasoline and E85. Laminar flame speed plays an important role to the fuel adaptation ability. It is the only changing parameter that will affect combustion duration if fuel type is altered. The semi-physical approach is able to keep the fuel type sensitive property by taking laminar flame speed as input. Robustness of the neural network is also tested when engine speed is over 3500 RPM. The neural network is constructed with the minimum number of 3 inputs and 5 neurons which aims to decrease the chance of data over fitting and better control stability. Further investigation on the type of training data is also carried out which proved steady-state average training samples produced a better network than the cycle to cycle transient training samples.

VII.2 Significant Conclusions and Findings

Contributions and improvements are realized in three distinct areas; (1) non-linear laminar flame speed observer, (2) desired combustion phasing target based on knock prediction with virtual octane sensing, and (3) the development of a semi-physical artificial neural network combustion model to predict combustion duration over the wide

operating range that is intended for real-time engine control. Significant findings in each category are described separately in the following sections.

VII.2.1 NON-LINEAR LAMINAR FLAME SPEED OBSERVER

Multi fuel adaptive SI engines not only aim to take gasoline and E85 as inputs but also adapt to several other bio fuel sources that are capable of generating a large range of laminar flame speeds. It is very important to estimate the laminar flame speed for the current fuel blend because it is a critical input for combustion duration prediction. It is assumed that if a different fuel source is used laminar flame speed is the only fuel property that will alter combustion duration. Several laminar flame speed experimental measurement methods are available based on high speed combustion imaging. The semi-empirical model will be re-fitted based on the experimental results. This method works for getting a research grade laminar flame speed for a specific type of fuel source, however, it is not practical if large numbers of fuel types are blended together. For real time control purpose, first, only the 'fuel behavior' is needed to observe instead of the actual fuel types; second, the allowable error margins can be larger than the research grade results. Therefore, an observer by comparing the burn rates difference to a base line data and output virtual fuel behavior (laminar flame speed) is successfully investigated. Then, a real time laminar flame speed model self re-calibration method is also proposed for feed forward ignition control. The study is carried out only with gasoline and E85 because of the limitation of test cell capability, it is proved:

- The virtual fuel property sensor (observer) is able to calculate laminar flame speed for a wide range of operating conditions with RMSD of 1.27 (cm/s) for gasoline and 2.17 (cm/s) for E85.
- Re-calibration of the feed forward laminar flame speed prediction model with 5 constants has been investigated for accuracy and response time. Using 40 distinct engine operating points as feedback for re-calibrating the 5 unknown constants is able to reproduce laminar flame speed for wide range of operating conditions with RMSD of 2.73 (m/s). This represents less than 5% error to well-known values.

VII.2.2 DESIRED COMBUSTION PHASING TARGET

Model-based ignition timing strategies require a target combustion phasing for proper calibration, generally defined by the crank angle location where fifty percent of the air/fuel mixture is burned (CA50). When fuel type is altered the target CA50 must be updated in the 'knock region' to avoid engine damage while maintaining the highest possible efficiency. This process is particularly important when switching between gasoline and E85 because they have vastly different octane ratings. A semi-physical virtual octane sensor, based on an Arrhenius function combined with a quasi-dimensional turbulent flame entrainment combustion model, is described that identifies the size of the knock region for a given fuel. The combustion model is used to calculate cylinder pressure and temperature which are analyzed with an Arrhenius knock prediction model that accounts for the negative temperature coefficient and air/fuel ratio. An algorithm is developed to identify the "best achievable" combustion phasing and update the target

desired combustion phasing accordingly. The algorithm operates off-line once the fuel octane number is observed to have changed, and then revised combustion phasing targets are calculated throughout the knock region. Experimental measurements and simulations are used to correlate and validate the algorithm with both gasoline and E85.

Octane rating of different fuel sources is also critical to the closed loop ignition timing control algorithm. It will not affect the actual combustion burn rates but will significantly change the achievable combustion phasing target by changing the knock characteristic of the unburned mixture. Again, there can be many combination of different fuel sources blended together per customers' usage. A virtual octane sensor is developed aiming to update the entire achievable combustion phasing target by several knocking events.

Cylinder pressure is assumed to be able to accurately predict from a combustion model or available cylinder pressure sensor data. Unburned gas temperature found to be most difficult parameter but contribute significant amount of accuracy to the auto-ignition prediction routine. It will be even more difficult especially in the advanced high degree of freedom engines when residual gas level can be altered in a wide range by external EGR or variable valve actuation. The hot or cold EGR will greatly affect the unburned mixture temperature hence the overall unburned mixture auto-ignition characteristics.

VII.2.3 COMBUSTION DURATION MODEL DEVELOPMENT

Quasi dimensional turbulent flame entrainment combustion model is agreed to be the most practical solutions for physics model based ignition timing control. The model should be able to account for a wide range of engine technologies/fuel sources because it is based on fundamental spark ignition engine combustion principles. However, the model accuracy highly depends on each sub-input on crank angle basis, such as turbulent intensity, laminar flame speed, flame front area, residual gas fraction etc. Some of the inputs are possible to accurately calculate before combustion without intensive computational power, such as laminar flame speed, residual gas fraction etc. because the in-cylinder pressure and temperature are still able to predict with polytrophic compression and ideal gas law. Lots of thermal and fluid dynamics as well as chemical kinetics are introduced when combustion started, modeling of each of the inputs becomes even more complicated. For example the in-cylinder turbulence which is a typical chaos phenomenon, the simplified flame front area model is still highly depends on the combustion chamber geometry. Therefore, the tradeoff between the model accuracy and required computational power need to be carefully considered.

However, the crank angle resolution equations described the detail heat release reactions is not fully needed for spark timing control, instead only few critical combustion phasing need to know before the control algorithm can make a right decision. Specifically the most important information is the duration from spark to CA50. This inspires the mean value modeling method and therefore neural network is introduced. Combined the gas preparation property inputs semi-physical neural network is formulated. Structure of the network is studied and optimized. Conclusion from the

theoretical analysis indicates: 1) increasing number of inputs will generally require larger size network; 2) large networks need more training samples to produce satisfactory output results; 3) adding one extra input will increase the training time by the order of 2. Study also carried out on the input selection of a linear associative network. Semi-physical approach has been demonstrated to be able to increase the network generalization capability. Physical models also help to increase the correlation of inputs and output(s), hence reduce the required network size.

VII.3 FUTURE WORK

Future research on several key areas could improve the robustness and predictive capability of the combustion phasing control algorithm discussed in this thesis. A list of suggested areas of improvement is as follows:

- Development of physical sub models for high degree of freedom engines including residual gas fraction, turbulence intensity, unburned gas temperature, flame front area etc. The newly developed models should be able to account for advanced engine technologies without tremendous of computational power. Ultimately, this could lead to utilization of pure physics based combustion models for real time feed forward ignition timing control.
- Experimentally utilize several other types of bio fuel sources for further investigation on the fuel type sensitive combustion model, laminar flame speed and octane number observers.
- Study fast combustion phasing feedback determination methods for cylinder pressure sensors which account for combustion cycle to cycle variation.

REFERENCES

[1] International Energy Agency, “2011 World Energy Outlook”.2011

[2] United States Energy Policy Act, Public Law 109-58, August 8, 2005

[3] United States Energy Independence and Security Act, Public Law 110-140, December 19, 2007.

[4] Zoran Filipi, “Frontiers in Advanced Vehicle Propulsion and the Role of Systems Approach to Research and Development,” Seminar at Clemson University ICAR, March 31st, 2011.

[5] U.S. Energy Information Administration, “Annual Energy Review 2009,” Report No. DOE/EIA-0384, 2009.

[6] Guzzella, L., Onder, C., “Introduction to Modeling and Control of Internal Combustion Engine Systems,” Springer-Verlag Berlin Heidelberg, Berlin, 2004.

[7] K. Ahn, A.G. Stefanopoulou and M. Jankovic, “Estimation of Ethanol Content in Flex-Fuel Vehicles Using an Exhaust Gas Oxygen Sensor: Model, Tuning and Sensitivity,” In proceedings of ASME 2008 Dynamic Systems and Control Conference, October, 2008, Ann Arbor, MI, USA.

[8] Jiang, S., and Nutter, D., “Implementation of Model-Based Calibration for a Gasoline Engine”, SAE 2012-01-0722, 2012

[9] Guerrier, M. and Cawsey, P., “The Development of Model Based Methodologies for Gasoline IC Engine Calibration,” SAE Technical Paper 2004-01-1466, 2004

[10] Schlosser, A., Kinoo, B., Salber, W., Werner, S. et al., “Accelerated Powertrain Development Through Model Based Calibration,” SAE Technical Paper 2006-01-0858, 2006

[11] Vibe, I.I., "Semi-empirical expression for combustion rate in engines", Proceedings of Conference on piston engines, USSR Academy of sciences, Moscow, pp. 186-191, 1956.

[12] Wiebe I.I., "Brennverlauf und Kreisprozeb von Ver-brennungsmotoren". In VEB-Verlag Technik, Berlin, 1970.

[13] Lindström, F., Ångström, H., Kalghatgi, G., and Möller, C., "An Empirical SI Combustion Model Using Laminar Burning Velocity Correlations," SAE Technical Paper, 2005-01-2106, 2005.

[14] Longwic, R., "Modelling the Combustion Process in the Diesel Engine with the Use of Neural Networks," SAE Technical Paper 2008-01-2446, 2008, doi:10.4271/2008-01-2446.

[15] Maass, B., Deng, J., and Stobart, R., "In-Cylinder Pressure Modelling with Artificial Neural Networks," SAE Technical Paper 2011-01-1417, 2011, doi:10.4271/2011-01-1417.

[16] Perhinschi, M., Wayne, W., Clark, N., and Lyons, D., "Neural Network Modeling of Emissions from Medium-Duty Vehicles Operating on Fisher-Tropsch Synthetic Fuel," SAE Technical Paper 2007-01-1080, 2007.

[17] De Cesare, M. and Covassin, F., "Neural Network Based Models for Virtual NOx Sensing of Compression Ignition Engines," SAE Technical Paper 2011-24-0157, 2011, doi:10.4271/2011-24-0157.

[18] Xiao B., Wang S. and Prucka R., "A Semi-Physical Artificial Neural Network for Feed Forward Ignition Timing Control of Multi-Fuel SI Engines", SAE 2013-01-0324

[19] Cavina N. and Suglia R., "Spark Advance Control based on a Grey Box Model of the Combustion Process", SAE 2005-01-3760, 2005

[20] N. C. Blizard and J. C. Keck, "Experimental and Theoretical Investigation of Turbulent Burning Model for Internal Combustion Engines", SAE Paper 740191.

[21] Keck J. C., Heywood J. B. and Noske G., "Early Flame Development and Burning Rates in Spark Ignition Engines", SAE 870164, 1987

[22] Heywood J. B., "Internal Combustion Engines Fundamentals", McGraw and Hill, 1988

[23] Boiarciuc A. and Floch A., "Evaluation of a 0D Phenomenological SI Combustion Model", SAE 2011-01-1894, 2011

[24] Prucka R., "An Experimental Characterization of a High Degree of Freedom Spark-Ignition Engine to Achieve Optimized Ignition Timing Control", Dissertation for the degree of Doctor of Philosophy,2008

[25] Liu, C., Jiang, D., and Obokata, T., "A Simplified Turbulence Model for In-cylinder Gas Flow in Quasi-dimensional Turbulence Combustion Model for Spark-ignition Engines," SAE Technical Paper 2000-01-2803.

[26] Schmid, A., Grill, M., Berner, H., Bargende, M. et al., "Development of a Quasi-Dimensional Combustion Model for Stratified SI-Engines," SAE Int. J. Engines 2(2):48-57, 2010

[27] Rakopoulos, C., Michos, C., and Giakoumis, E., "Thermodynamic Analysis of SI Engine Operation on Variable Composition Biogas-Hydrogen Blends Using a Quasi-Dimensional, Multi-Zone Combustion Model,"SAE Int. J. Engines 2(1):880-910, 2009

[28] Lafossas, F., Colin, O., Le Berr, F., and Menegazzi, P., "Application of a New 1D Combustion Model to Gasoline Transient Engine Operation," SAE Technical Paper 2005-01-2107

[29] Shi X., Li G. and Zhou L., "DI Diesel Engine Combustion Modeling Based on ECFM-3Z Model", SAE 2007-01-4138, 2007

[30] D.B. Spalding, Mixing and chemical reaction in steady confined turbulent flames Original Research Article Symposium (International) on Combustion, Volume 13, Issue 1, Pages649-657, 1971.

[31] Abraham, J., Bracco, F. V., and Reitz, R. D., Comparisons of Computed and Measured Premixed Charge Engine Combustion, Combust. Flame, 60, pp. 309 ̈C322, 1985.

[32] S. B. Pope, PDF Methods for Turbulent Reactive Flows, Prog. Energy Combust. Sci. 1985, Vol. 11, pp. 119-192, 1985.

[33] Bray, K. N. C. and Moss, J. B., A unified statistical model of premixed turbulent flame. Acta Astronaut. 4:291-319, 1977

[34] Marble, F. E. and Broadwell, J. E., The Coherent Flame Model of Non-premixed Turbulent Combustion, Report: TRW-9-PU, 1977

[35] Williams, F. A. 1985 Turbulent Combustion. The Mathematics of Combustion, J.Buckmaster, Ed. 97-131.

[36] Peters, J. A., Turbulent Combustion. Cambridge University Press, 2000.

[37] Tan, Z. and Reitz, R., "Modeling Ignition and Combustion in Spark-ignition Engines Using a Level Set Method," SAE Technical Paper 2003-01-0722, 2003.

[38] Chopp, D. L. and Sethian, J. A., Flow under curvature: Singularity formation, minimal surfaces, and geodesics, Journal of Experimental Mathematics, 2(4):235-255, 1993.

[39] Tan, Z. and Reitz, R., "Development of a Universal Turbulent Combustion Model for Premixed and Direct Injection Spark/Compression Ignition Engines," SAE Technical Paper 2004-01-0102, 2004.

[40] Sethian, J. A., Level Set Methods: Evolving Interfaces in Geometry, Fluid Mechanics, Computer Vision and Materials Sciences , Cambridge University Press, 1996.

[41] Naoumov, V., Demin, A., and Sokolov, A., "Three - Zone Model of Combustion and Chemical Non-Equilibrium Ionization in the SI Engine," SAE Technical Paper 2004-01-0622, 2004.

[42] McCulloch W S and Pitts W. A logical calculus of the ideas immanent in nervous activity. Bull. Math. Biophy., vol. 5, pp. 115-133, 1943.

[43] Hebb D O. The Organization of Behaviour: A Neuropsychological Theory. New York: Wiley, 1949.

[44] Minsky M L. Theory of neural-analog reinforcement systems and its application to the brain-model problem. PhD thesis, Princeton University, Princeton, NJ, 1954.

[45] Rosenblatt F. The perceptron: A probabilistic model for information storage and organization in the brain. Psychological Review, vol. 65, pp. 386-408, 1958.

[46] Minsky M L and Papert S A. Perceptrons, Cambridge. MA: MIT Press, 1969.

[47] Widrow B and Hoff M E. Adaptive switching circuits. IRE WESCON Convention Record, vol. 4, pp. 96-104, Aug. 1960.

[48] Hopfield J J. Neural networks and physical systems with emergent collective computational capabilities. In Proceedings of the National Academy of Sciences (US&, vol. 79, pp. 2554-2558, Nov. 1982.

[49] Hopfield J J. Neurons with graded respons 9s have collective computational properties like those of two-state neurons. In Proceedings of the National Academy of Sciences (USA), vol. 81, pp. 3088-3092, 1984.

[50] Rumelhart D E, Hinton G E and Williams R J. Learning internal representations by error propagation. In Parallel Distributed Processing: Explorations in the Microstructure of Cognition, vol. 1 (D.E. Rumelhart, J.L. McClelland, a* the PDP Research Group, eds.), Cambridge, MA: MIT Press, pp. 318-362, 1986a.

[51] Ackley D H, Hinton G E and Sejnowski T J. A learning algorithm for Boltzmann machines. Cognitive Sci., vol. 9, pp. 147-169, 1985.

[52] Grossberg S. Studies of Mind and Brain: Neural Principles of Learning, Perception, Development, Cognitron and Motor Control. Boston, MA: Reidel, 1982.

[53] Ravichandran A and Yegnanarayana B. Studies on object recognition from degraded images using neural networks. Neural Networks, vol. 8, no. 3, pp. 481-488, 1995.

[54] Rangarajan A and Chellappa R. Markov random field models in image processing. The Handbook of Brain Theory and Neural Networks (M.A. Arbib, ed.), Cambridge, MA. MIT Press, pp. 564-567, 1995.

[55] Daugman J G. Complete discrete 2-D Gabor transforms by neural network for image analysis and compression. IEEE nuns. Acoust., Speech, Signal Processing, vol. 36, pp. 1169-1179, July 1988.

[56] McClelland J L and Rumelhart D E. Explorations in Parallel Distributed Processing. Cambridge MA: MIT Press, 1988.

[57] Cherkassky V and Vassilas N. Performance of back propagation netwarks for associative database retrieval. In Proceedings of International Joint Conference on Neural Networks, Washington D.C., vol. I, pp. 77-84, 1989.

[58] Mhaswade P K. A neural network approach for information retrieval from spelled names. Master's thesis, Department of Computer Science and Engineering, Indian Institute of Technology, Madras, Jan. 1997.

[59] Kohonen T. Self-Organizing Maps. 2nd ed., Berlin: Springer Verlag, 1997.

[60] Peterson C and Soderberg B. Neural optimizationn, in The Handbook of Brain Theory and Neural Networks (M.A. Arbib, ed.). Cambridge, MA: MIT Press, pp. 617-621, 1995.

[61] Hertz J A, Krogh A and Palmer R G. Introduction to the Theory of Neural Computation. New York: Addison-Wesley, 1991.

[62] Muller B and Reinhardt J. Neural Networks: An Introduction, Physics of Neural Networks. New York: Springer-Verlag, 1991.

[63] Yuille A L. Constrained optimization and the elastic net. in The Handbook of Brain Theory and Neural Networks (M.A. Arbib, ed.), Cambridge, MA. MTT Press, pp. 250-255, 1995.

[64] Peterson C and Soderberg B. A new method of mapping optimization problems onto neural networks. Znt. J. Neural Systems, vol. 1, pp. 3-22, April 1989.

[65] Wilson G Y and Pawley G S. On the stability of the travelling salesman problem algorithm of Hopfield and Tank. Biol. Cybernet., vol. 58, pp. 63-70, 1988.

[66] Gray R M. Vector Quantization. IEEE ASSP Magazine, vol. 1, pp. 4-29, Apr. 1984.

[67] Nasrabadi N M and King R A. Image coding using Vector Quantization: A Revie. ZEEE Bans. Communications, VO~. 36, pp. 957-971, 1988.

[68] Zurada J M. Introduction to Artificial Neural Systems. Singapore: Info Access and Distribution, 1992.

[69] Ronald K J. Electronic Engine Control Technologies, 2nd edition. Society of Automotive Engineers, Warrendale, PA, 2004.

[70] Narendra K S and Parthasarathy K. Identification and control of dynamical systems using neural networks. IEEE Duns. Neural Networks, vol. 1, no. 1, pp. 4-27, 1990.

[71] Nguyen D H and Widrow B. Neural networks for self-learning control systems. ZEEE Control Systems Magazine, pp. 18-23, Apr. 1990.

[72] Hunt K J, Sbarbaro D, Zbikowski R, et al. Neural networks for control systems-A survey. Automatica, VO~. 28, pp. 1083-1112, 1992.

[73] Narendra K S and Mukhopadhyay S. Intelligent control using neural networks. IEEE Control Systems Magazine, vol. 12, no. 2, pp. 11-18, 1992.

[74] Marko K A, James J, Dosdall J, et al. Automotive control system diagnostics using neural nets for rapid pattern classification of large data sets. In Proceedings of the International Joint Conference on Neural Networks (IJCNN) 1989, vol. 2, pp. 13-16, Washington, DC, July 1989.

[75] Puskorius G V and Feldkamp L A. Neurocontrol of nonlinear dynamical systems with Kalman filter trained recurrent network. IEEE Transactions on Neural Networks, vol. 5, no. 2, pp. 279–297, 1994.

[76] Antanaitis D, Nisonger R and Riefe M. Prediction of Brake System Performance during Race Track/High Energy Driving Conditions with Integrated Vehicle Dynamics and Neural-Network Subsystem Models. SAE paper 2009-01-0860, 2009.

[77] Woerner D, Ranganathan R and Butler A. Developing an Artificial Neural Network for Modeling Heavy Vehicle Rollover. SAE paper 2000-01-3418, 2000.

[78] Leser C, Renner T and Salmon D. Accurate Shock Absorber Load Modeling in an All Terrain Vehicle using Black Box Neural Network Techniques. SAE paper 2002-01-0581, 2002.

[79] James J G, Boehringer F and Burnham K J. Adaptive driver model using a neural network. Artificial Life and Robotics, volume 7, issue 4, pp 170-176, 2004.

[80] Solaymani R S. Modeling Drivers' Behavior During Panic Braking for Brake Assist Application, Using Neural Networks and Logistic Regression and a Comparison. SAE paper 2011-01-2384, 2011.

[81] Moon K, Osborne M, Kuykendall D, and et al. Modeling of Human Response From Vehicle Performance Characteristics Using Artificial Neural Networks. SAE paper 2002-01-1570, 2002.

[82] Brusca S, Lanzafame R and Messina M. A Combustion Model for ICE by Means of Neural Network. SAE paper 2005-01-2110, 2005.

[83] Longwic R. Modelling the Combustion Process in the Diesel Engine with the Use of Neural Networks. SAE paper 2008-01-2446, 2008.

[84] Wu B, Prucka R, Filipi Z, and et al. Cam-phasing Optimization Using Artificial Neural Networks as Surrogate Models-Fuel Consumption and NOx Emissions. SAE paper 2006-01-1512, 2006.

[85] Chi J. Application of Artificial Neural Networks to Aftertreatment Thermal Modeling. SAE paper 2012-01-1302, 2012.

[86] Arsie I, Pianese C and Sorrentino M. Development and Real-Time Implementation of RecurrentNeural Networks for AFR Prediction and Control. SAE Int. J. Passeng. Cars - Electron. Electr. Syst.1(1):403-412, 2009.

[87] Arsie I, Pianese C and Sorrentino M. Nonlinear Recurrent Neural Networks for Air Fuel Ratio Control in SI Engines. SAE paper 2004-01-1364, 2004.

[88] Hellring M, Munther T, Rögnvaldsson T, et al. Robust AFR Estimation Using the Ion Current and Neural Networks. SAE paper 1999-01-1161, 1999.

[89] De Cesare M and Covassin F. Neural Network Based Models for Virtual NOx Sensing of Compression Ignition Engines. SAE paper 2011-24-0157, 2011.

[90] Subramaniam M, Tomazic D, Tatur M, et al. An Artificial Neural Network-based Approach for Virtual NOx Sensing. SAE paper 2008-01-0753, 2008.

[91] Wu B, Filipi Z, Kramer D, et al. Using Neural Networks to Compensate Altitude Effects on the Air Flow Rate in Variable Valve Timing Engines. SAE paper 2005-01-0066, 2005.

[92] Wu B, Filipi Z, Assanis D, et al. Using Artificial Neural Networks for Representing the Air Flow Rate through a 2.4 Liter VVT Engine. SAE paper 2004-01-3054, 2004.

[93] Thomas W M III, Richard S S and Paul J W. Neural Networks for Control. Cambridge, MA: MIT, 1990.

[94] Narendra K S. Neural networks for control: theory and practice. In proceedings of the IEEE, vol. 84, no. 10, pp. 1385 C1406, 1996.

[95] Suykens J, Vandewalle J and De Moor B. Artificial Neural Networks for Modeling and Control of Non-Linear Systems. Boston: Kluwer, 1996.

[96] Hrycej T. Neurocontrol: Towards an Industrial Control Methodology. New York: Wiley, 1997.

[97] Nørgaard M, Ravn O, Poulsen N L, et al. Hansen. Neural Networks for Modeling and Control of Dynamic Systems. London: Springer, 2000.

[98] Yang H, Liu L and Wasacz B. Neural Network Based Feedforward Control for Electronic Throttles. SAE paper 2002-01-1149, 2002.

[99] Al-Assadi S. Neural Network-Based Model Reference Adaptive Control for Electronic Throttle Systems. SAE paper 2007-01-1628, 2007.

[100] Tsuchiya T, Morishita S, Enomoto T, et al. Revolution Control of Generator Diesel Engine byNeural Network Controller. SAE paper 2003-01-0365, 2003.

[101] Khatri D and Kumar B. Feasibility Study Of Neural Network Approach In Engine Management System In S.I. Engine. SAE paper 2000-01-1426, 2000.

[102] Müller R and Schneider B. Approximation and Control of the Engine Torque Using Neural Networks. SAE paper 2000-01-0929, 2000.

[103] Rogers S. Adaptive Neural Network Control of Engine RPM. SAE paper 2004-01-2680, 2004.

[104] Zhenhai G and Bo Z. Vehicle Lane Keeping Single Neural Network Control with Driver Behavior. SAE paper 2004-01-2108, 2004.

[105] Kiencke U., Nielsen L., "Automotive Control Systems", Springer Verlag, Berlin, 2000.

[106] Zhu, G., Haskara, I., and Winkelman, J., "Stochastic Limit Control and Its Application to Knock Limit Control Using Ionization Feedback," SAE 2005-01-0018, 2005.

[107] Yoshiaki, K., Mamoru, S., Hiroshi, S., Nobutaka, T., and Masahiro, I., "MBT control through individual cylinder pressure detection", SAE paper 881779, 1988.

[108] Westbrook, C.K., Warnatz, J., and Pitz, W.J., "A detailed chemical kinetic reaction mechanism for the oxidation of iso-octane and n-heptane over an extended temperature range and its application to analysis of engine knock.", Twenty-second Symposium (Int.) on Combustion, The Combustion Institute, p.893-901, (1988).

[109] Livengood, J. C., Wu, P. C., "Correlation Of Auto-ignition Phenomena In Internal Combustion Engines And Rapid Compression Machines", 5th Symp. (Int.) on Combustion, p. 347, Reinhold Publishing Corp. (1955).

[110] Glassman, I., "Combustion", Academic Press, 1977.

[111] Kasseris, E., "Knock Limits in Spark Ignited Direct Injected Engines Using Gasoline/Ethanol Blends", PhD dissertation, Massachusetts Institute of Technology, 2011.

[112] Wang, S., Lin, Y., Resendiz, N.H., Granados, L., Rodriguez, H., "Ethanol Concentration Sensor," SAE Paper No. 2008-01-2452.

[113] Snyder, D., Adi, G., Bunce, M., Satkoski, C., Shaver, G., "Fuel Blend Fraction Estimation for Fuel-Flexible Combustion Control: Uncertainty Analysis," Control Engineering Practice, Vol. 18, pp. 418-432, 2010.

[114] Theunissen, F., "Percent Ethanol Estimation on Sensorless Multi Fuel Systems; Advantages and Limitations," SAE Paper No. 2003-01-3562, 2003.

[115] Ahn, K., Yilmaz, H., Stefanopoulou, A., Jiang, L., "Ethanol Content Estimation in Flex Fuel Direct Injection Engines Using In-Cylinder Pressure Measurements," SAE Paper No. 2010-01-0166, 2010.

[116] Powell. D, "Engine Control using cylinder pressure: Past, present and future." Journal of Dynamic Systems, Measurement and Control, 115:343-350, 1990.

[117] Sellnau M. C., Matekunas F. A., Battiston P. A., and Chang C. F., "Cylinder-Pressure-Based Engine Control Using Pressure-Ratio-Management and Low-Cost Non-Intrusive Cylinder Pressure Sensors," SAE Paper No. 2000-01-0932, 2000.

[118] Andrie M. J., "Non-Intrusive Low Cost Cylinder Pressure Transducer for Internal Combustion Engine Monitoring and Control," SAE Paper No. 2009-01-0245, 2009.

[119] Yoon, P., Park, S., Sunwoo, M., Ohm, I., Yoon, K., "Closed-Loop Control of Spark Advance and Air-Fuel Ratio in SI Engines Using Cylinder Pressure," SAE Paper No. 2000-01-0933, 2000.

[120] Shimasaki, Y., Maki, H., Sakaguchi, J., Nishizawa, K., Kato, A., Suzuki, H., Kondo, N., Yamada, T., "Study on Combustion Monitoring System for Formula One Engines Using Ionic Current Measurement," SAE Paper No. 2004-01-1921, 2004.

[121] Zhu, G., Daniels, C., Winkelman, J., "MBT Timing Detection and its Closed-Loop Control Using In-Cylinder Pressure Signal," SAE Paper No. 2003-01-3266, 2003.

[122] Wang, W., Chirwa, E., Zhou, E., Holmes, K., Nwagboso, C., "Fuzzy Ignition Timing Control for a Spark Ignition Engine," Proc Instn Mech Engrs, Vol 214, pp 297-306, 2000.

[123] Eriksson. L, et al. "Closed Loop Ignition Control by Ionization Current Interpretation." SAE Paper No. 970854, 1997.

[124] Hellring. M, Munther. T, Rognvaldsson. T, Wickstrom. N, Carlsson. C, Larsson. M and Nytomt. J, "Spark advance control using the ion current and neutral soft sensors." SAE Paper No. 1999-01-1162, 1999.

[125] Guoming G. Zhu, Ibrahim Haskara, and Jim Winkelman, "Closed-Loop Ignition Timing Control for SI Engines Using Ionization Current Feedback," IEEE Trans. on Control System Tech., Vol. 15, No. 3. May 2007.

[126] Giglio, V., Iorio, B., Police, G., Rispoli, N., "In-Cylinder Pressure Measurement for Control and Diagnostics in Spark Ignition Engines," SAE Paper No. 2005-24-062, 2005.

[127] Zhu, G., Haskara, I., Winkelman, J., "Closed-Loop Ignition Timing Control for SI Engines Using Ionization Current Feedback," IEEE Transactions on Control Systems Technology, Vol. 15, No. 3, 2007.

[128] Patterson, G., Davis, R., "Geometric and Topological Considerations to Maximize Remotely Mounted Cylinder Pressure Transducer Data Quality," SAE Paper No. 2009-01-0644, 2009.

[129] Poulos, S., Heywood, J., "The Effect of Chamber Geometry on Spark-Ignition Engine Combustion," SAE Paper No. 830334, 1983.

[130] Prucka, R., Lee, T., Filipi, Z., Assanis, D., "Turbulence Intensity Calculation from Cylinder Pressure Data in a High Degree of Freedom Spark-Ignition Engine," SAE Paper No. 2010-01-0175, 2010.

[131] Syed, I., Mukherjee, A.M., Naber, J., Michalek, D., "Numerical Investigation of Laminar Flame Speed fo Gasoline – Ethanol / Air Mixtures with Varying Pressure, Temperature and Dilution," SAE Paper No. 2010-01-0620, 2010.

[132] Box, G. E. P.; Hunter, W. G.; Hunter, J. S., “Statistics for experimenters” John Wiley and Sons, New York, 1978

[133] Xiao, B., Prucka, R., “Non-Linear Observer of Laminar Flame Speed for Multi-Fuel Adaptive Spark-Ignited Engines”, International Journal of Powertrains No. 36399, In Review.

[134] Pischinger, S.: "Effects of Spark Plug Design Parameters on Ignition and Flame Development in an SI-Engine", Ph. D. thesis, M.I.T., 1989

[135] Hinze P.C. : “Cycle-to-cycle combustion variations in a spark-ignition engine operating at idle” Ph.D thesis”, M.I.T., 1997

[136] Jeonghoon S. and Myoungho S.: “A Modeling and Experimental Study of Initial Flame Kernel Development and Propagation in SI Engines “, SAE paper 2000-01-0960, 2001.

[137] Li Fan and Rolf D. Reitz: “Development of an Ignition and Combustion Model for Spark-Ignition Engines”, SAE paper 2000-01-2809, 2001.

[138] Ahmed E. H. and Keshav S.: “A Study of The Flame Development and Rapid Burn Durations In A Lean-Burn Fuel Injected Natural Gas S.I. Engine “, SAE paper 981384, 1998.

[139] Assanis D. N., Filipi Z. S., Fiveland S. B., Syrimis M., ‘A predictive ignition delay correlation under steady-state and transient operation of a direct injection diesel engine.’ J. Engng Gas Turbines Power 125 (2003): 450–457

[140] Douaud, A. M., Eyzat P., “Four Octane Number Method for Predicting the Anti-Knock Behaviour of Fuels and Engines” SAE 780080, (1978).

[141] Westbrook, C. K., Curran, H. J., Pitz, W. J., Griffiths, J., , Mohamed, and Wo, S. K., “The Effects of Pressure, Temperature and Concentration on the Reactivity of Alkanes: Experiments and Modeling in a Rapid Compression Machine” 27th International Symposium on Combustion, University of Colorado at Boulder, September 2-7,1998

[142] Kee, R. J.; Rupley, F. M.; Miller, J. A. “CHEMKIN-II: A Fortran Chemical Kinetics Package for the Analysis of Gas Phase Chemical Kinetics”; Sandia Report no. SAND 89-8009B; Sandia National Laboratories, (1989).

[143] Viljoen, C., Yates, A., Swarts, A., Balfour, G., and Möller, K., “An Investigation of the Ignition Delay Character of Different Fuel Components and an Assessment of Various Auto-ignition Modeling Approaches”, SAE 2005-01-2084, 2005.

[144] Yates, A., and Viljoen, C., "An Improved Empirical Model for Describing Auto-ignition", SAE 2008-01-1629, 2008.

[145] Yates, A., Swarts, A., and Viljoen, C., "Correlating Auto-ignition Delays And Knock-Limited Spark-Advance Data For Different Types Of Fuel", SAE 2005-01-2083, 2005.

[146] National Automobile Dealers Association "Economic Impact of America's New-Car and New-Truck Dealers: A Dealership and Industry Review," Data Report 2009.

[147] US Department of Energy, Energy Efficiency & Renewable Energy, Vehicle Technologies Program Report "Flexible Fuel Vehicles: Providing a Renewable Fuel Choice," March 2010.

[148] Rousseau, A., Sharer, P., "Comparing Apples to Apples: Well-to-Wheel Analysis of Current ICE and Fuel Cell Vehicle Technologies," Presentation for SAE Paper 2004-01-1302, 2004.

[149] Franklin, M., Kittelson, D., Leuer, R., Pipho, M., "Synchronous, Simultaneous Optimization of Ignition Timing and Air-Fuel Ratio in a Gas-Fueled Spark Ignition Engine," SAE Paper No. 940547, 1994.

[150] Blizard, N., Keck, J., "Experimental and Theoretical Investigation of Turbulent Burning Model for Internal Combustion Engines," SAE Paper No. 740191, SAE Transactions 86, 1974.

[151] Tabaczynski, R., Ferguson, C., Radhakrishnan, K., "A Turbulent Entrainment Model for Spark-Ignition Engine Combustion," SAE Paper No. 770647, 1977.

[152] Tabaczynski, R., Trinker, F., Shannon, B., "Further Refinement and Validation of a Turbulent Flame Propagation Model for Spark Ignition Engines," Combustion and Flame, 39, 111-121, 1980.

[153] Fox, J., Cheng, W., Heywood, J., "A Model for Predicting Residual Gas Fraction in Spark-Ignition Engines," SAE Paper No. 931025, 1993.

[154] Wong, V., Hoult, D., "Rapid Distortion Theory Applied to Turbulent Combustion", SAE Paper Mp. 790357, 1979.

[155] Hillion, M., Chauvin, J., Petit, N., "Open-Loop Combustion Timing Control of a Spark-Ignited Engine," Proceedings of the 47th IEEE Conference on Decision and Control, pp 5635-5642, 2008.

[156] Woschni, G., "A Universally Applicable Equation for the Instantaneous Heat Transfer Coefficient in the Internal Combustion Engine," SAE Technical Paper 670931, 1967, doi:10.4271/670931.

[157] Taskin Kavzoglu, “Determining Optimum Structure for Artificial Neural Networks”, In Proceedings of the 25th Annual Technical Conference and Exhibition of the Remote Sensing Society, Cardiff, UK, pp. 675-682, 8-10 September, 1999.

[158] Atkinson, P.M., and Tantnall, A. R. L., “Neural Networks In Remote Sensing”, International Journal of Remote Sensing, 18, 699-709, 1997.

[159] Bebis, G. and Georgiopoulos, M., “Feed-forward neural networks: why network size is so important”, IEEE Potentials, October/November, pp. 27-31, 1999.

[160] Hirose, Y., Yamashita, K., and Hijiya, S., “Back-propagation algorithm which varies the number of hidden units”, Neural Networks, 4, pp. 61-66, 1991,

[161] Kavzoglu, T., and Mather, P.M., “Assessing artificial neural network pruning algorithm”, Proceedings of the 24th Annual Conference and Exhibition of the Remote Sensing Society (RSS'98), pp. 603-609, 1998